SIMULATION OF GROUNDWATER FLOW DYNAMICS FOR SUSTAINABLE GROUNDWATER MANAGEMENT IN ARID, UNCONFINED AND CONFINED REGIONAL AQUIFERS

By

BENJAMIN NANA OSEI KUFFOUR

A dissertation submitted in partial fulfillment of
the requirements for the degree of

DOCTOR OF PHILOSOPHY

WASHINGTON STATE UNIVERSITY
Department of Civil and Environmental Engineering

DECEMBER 2021

To the Faculty of Washington State University:

The members of the Committee appointed to examine the dissertation of BENJAMIN NANA OSEI KUFFOUR, find it satisfactory and recommend that it be accepted.

_____

Nicholas B. Engdahl, Ph.D., Chair

_____

Jan Boll, Ph.D.

_____

Jennifer Adam, Ph.D.

_____

Kent C. Keller, Ph.D.

ACKNOWLEDGMENT

My appreciation goes to the Palouse Basin Aquifer Committee, Idaho and the U.S. Department of Energy, Office of Science (Subsurface Biogeochemical Research), Award number DE-SC0019123 for providing funding for this project.

The author would like to thank the personnel from the Walla Walla Basin Watershed Council and the Washington State Department of Ecology (DOE) who dedicated time and effort to make available some of the field data used in this project. The personnel include Marie Cobb of the Walla Walla Watershed Council, and Darnell Richard and Casey Swenson of the DOE.

The author would also like to express his profound gratitude to the graduate committee members: Dr. Jan Boll, Dr. Jennifer Adam, Dr. Kent Keller and in particular, my major advisor Dr. Nick Engdahl. Their guidance and reviews stimulate my learning and always give my best.

CONTRIBUTION OF AUTHORS

I would like to recognize the efforts and contributions of all the people who were part of the success of this research. The review conducted on ParFlow (Chapter 2) was a collaborative effort of the author and other five researchers. The following list provides the names of the researchers and their contributions to the review project.

Nicholas B. Engdahl: Supervised and edited the entire review project.

Carol S. Woodward: Wrote Section 3 of the review manuscript on ParFlow model.

Laura E. Condon: Edited the entire manuscript.

Stefan Kollet: Edited the entire manuscript.

Reed M. Maxwell: Edited the entire manuscript.

SIMULATION OF GROUNDWATER FLOW DYNAMICS FOR SUSTAINABLE GROUNDWATER MANAGEMENT IN ARID, UNCONFINED AND CONFINED REGIONAL AQUIFERS

Abstract

by Benjamin Nana Osei Kuffour, PhD
Washington State University
December 2021

Chair: Nicholas B. Engdahl

This document provides details of three research projects. First, a review was conducted on the hydrologic model, ParFlow v3.5.0, to provide information on ParFlow in a format that targets a broader community than a user manual or articles describing specific applications of the model. The history of ParFlow's development, core functionality, model equation discretization and solvers, parallel scaling and performance efficiency, and coupling capabilities of ParFlow with atmospheric, land surface, and subsurface models were discussed. The second project used ParFlow to simulate hydrogeologic conditions of the Walla Walla River Basin (WWRB), southeast Washington and northeast Oregon. Specifically, numerical simulations were performed to test the response of the unconfined aquifer system of the WWRB to supplemental managed aquifer recharge (MAR) scenarios, given a required minimum in-stream flows (ISFs) in the WWR over a 100-year period. The simulations indicated that maintaining minimum ISFs in the WWR and relocating some of the MAR sites downgradient could lead to balanced benefits to all users. The final research project focused on the creation of a three-dimensional groundwater flow model for the Pullman-Moscow Basin, north-central Idaho and southeastern Washington with MODFLOW-

2005. The model was used to evaluate alternative water management scenarios to find long-term solutions to aquifer depletion. Model creation and calibration were done using existing hydrogeologic conditions and parameters estimated from previous studies in the basin, and suggestions of future updates to limit model assumptions and uncertainties were provided. Simulation results indicated that pumping less than 25 percent of historic rates (1983-2018) would stabilize/improve groundwater levels in Pullman and Moscow areas.

TABLE OF CONTENTS

LIST OF TABLES

LIST OF FIGURES

LIST OF FIGURES (*Continued*)

LIST OF FIGURES (*Continued*)

Dedication

This work is dedicated to my sister, Rosina Osei Wiafe whose support encourages me to achieve greater heights. Thank you, Sis, for believing in me!

CHAPTER ONE

1. General Introduction

1.1 Summary of Projects

This project focuses on three different but related research areas: a) an extensive review of a contemporary and widely used integrated hydrologic model called ParFlow, b) the application of the ParFlow model to solving groundwater flow problems in the Walla Walla River Basin (WWRB) located within the inland northwest of the United States, and c) simulation of groundwater flow dynamics along the Moscow-Pullman corridor, within southeastern Washington and north-central Idaho using MODFLOW-2005. The specific research topics evaluated in the project include 1) simulating coupled surface-subsurface flows with ParFlow v3.5.0: capabilities, applications, and ongoing development of an open-source, massively parallel, integrated hydrologic model, 2) sustainable and equitable groundwater management using natural and artificial recharge in an arid, unconfined, regional aquifer, and 3) simulation of regional groundwater flow dynamics in the Moscow-Pullman Basin and its response to alternative management schemes.

Chapter 2 provides an overview of the functions, capabilities, and ongoing development of one of the open-source integrated models, ParFlow, which are presented in a format that is more

accessible to a broad audience than a user manual or articles detailing specific applications of the model. ParFlow is a parallel, integrated, hydrologic model that simulates surface and subsurface flows. ParFlow solves Richards' equation for three-dimensional variably saturated groundwater flow and the two-dimensional kinematic wave approximation of the shallow water equations for overland flow. Specific discussions were made on the core functionality of the model including equations solved and grid types, equation discretization and solvers, parallel scaling and performance efficiency of ParFlow, and coupling capabilities of ParFlow with other atmospheric, land surface, and subsurface models. This paper has already been published and can be found at: "Kuffour, B. N. O., Engdahl, N. B., Woodward, C. S., Condon, L. E., Kollet, S., and Maxwell, R. M.: Simulating coupled surface–subsurface flows with ParFlow v3.5.0: capabilities, applications, and ongoing development of an open-source, massively parallel, integrated hydrologic model, Geosci. Model Dev., 13, 1373–1397, https://doi.org/10.5194/gmd-13-1373-2020, 2020".

Chapter 3 investigates how river flows and artificial recharge systems can be integrated to manage groundwater resources sustainably and equitably in the unconfined aquifers of the WWRB. River flows and groundwater levels had declined in the basin due to excessive pumping. Managed aquifer recharge (MAR) basins and galleries were installed to halt the groundwater level declines and improve in-stream flows (ISFs), but the system has not provided equal benefits to all users across the basin. The core challenge of Chapter 3 was to determine the volume of water that needs to be added to the system to maintain minimum ISFs in the Walla Walla River (WWR) and

stop or reverse groundwater declines, while considering equal benefits to all users. The hydrologic model ParFlow was used to perform numerical simulations to test the response of the aquifer to nine MAR scenarios, given a required minimum ISFs in the WWR over a 100-year period. The key questions are how much water must be added to the WWR to maintain ISFs for a given amount of MAR and how equally distributed are these benefits across the basin. Results indicate that maintaining minimum ISFs in the WWR could stabilize the system, but aquifer levels would continue to decline under current MAR conditions and disproportionately impact downgradient users. A more balanced solution is to relocate some of the MAR sites downgradient from their current locations, which could stabilize the aquifer levels across the basin and augment ISFs in the WWR. MAR practice is growing worldwide, and the findings from this study indicate that it is vital not to focus only on the net mass balance of MAR in a basin, but how recharge is redistributed for the benefit of all users.

In Chapter 4, simulation of groundwater flow dynamics in the Moscow-Pullman Basin and its response to alternative management schemes were performed. There is a growing depletion of the groundwater resource within the Moscow-Pullman Basin due to overexploitation of the aquifer system. The likelihood is that the aquifer may be lost if long-term solutions are not provided to manage water use or groundwater pumping in the region. Long-term remedies require understanding of the hydrogeologic system of the region, which is best studied with groundwater flow models. However, no active groundwater flow model exists today that characterizes the

current groundwater flow system which could be used to evaluate water level dynamics in the region. MODFLOW-2005 was used to create a new groundwater flow model based on the hydrogeologic conditions of the South Fork of the Palouse River Basin (SFPB). The model was calibrated and used to evaluate the impacts of eight (8) pumping scenarios on aquifer levels to identify ways to manage groundwater pumping. Results show that aquifer level declines would persist if pumping stayed equal to the pumping rates from 1983-2018. Average drawdown of 0.05 and 0.1 m per year could occur in Moscow and Pullman areas, respectively over the next four decades. Pumping less than 25 percent of historic rates could lead to stabilized aquifer levels in the Pullman area, but slight declines (less than 0.02 m per year) in the Moscow region. However, aquifer levels could increase by 0.1 and 0.09 m per year in Pullman and Moscow, respectively if pumping was completely halted. The model and results of the pumping scenarios would increase our understanding of the hydrogeologic characteristics and planning future water management alternatives. It will be important for others to be able to use the model in the future so its parameterization can be updated as more knowledge is gained, so all model files are openly and freely available per permission of the Palouse Basin Aquifer Committee (PBAC).

1.2 Format of Dissertation

Chapter 2 was published in the journal of Geoscientific Model Development, so the article format or structure used by the journal is maintained in this dissertation. The version included here is the final accepted version after peer-review. Chapter 3 is prepared to be submitted for publication in the journal of hydrology, as such, the required article structure for the journal of hydrology is used in Chapter 3. Chapter 4 will be converted into a technical report to be given to the funding agency (PBAC) for the Moscow-Pullman Basin model, so it is included using the dissertation formatting requirements prescribed by the Graduate School, Washington State University.

CHAPTER TWO

SIMULATING COUPLED SURFACE-SUBSURFACE FLOWS WITH PARFLOW V3.5.0: CAPABILITIES, APPLICATIONS, AND ONGOING DEVELOPMENT OF AN OPEN-SOURCE, MASSIVELY PARALLEL, INTEGRATED HYDROLOGIC MODEL

Benjamin N. O. Kuffour[1,*], Nicholas B. Engdahl[1], Carol S. Woodward[2],

Laura E. Condon[3], Stefan Kollet[4,5], and Reed M. Maxwell[6]

Published in Geoscientific Model Development Journal:

Citation: Kuffour, B. N., N. Engdahl, C. Woodward, L. Condon, S. Kollet, and R. Maxwell (2020), Simulating Coupled Surface-Subsurface Flows with ParFlow v3.5.0: Capabilities, applications, and ongoing development of an open-source, massively parallel, integrated hydrologic model, Geosci. Model Dev. Discuss., 13(3), 1–66, doi:10.5194/gmd-2019-190.

Abstract

Surface and subsurface flow constitute a naturally linked hydrologic continuum that has not traditionally been simulated in an integrated fashion. Recognizing the interactions between these systems has encouraged the development of integrated hydrologic models (IHMs) capable of treating surface and subsurface systems as a single integrated resource. IHMs is dynamically evolving with improvement in technology and the extent of their current capabilities are often only known to the developers and not general users. This article provides an overview of the core functionality, capability, applications, and ongoing development of one open-source IHM, ParFlow. ParFlow is a parallel, integrated, hydrologic model that simulates surface and subsurface flows. ParFlow solves Richards' equation for three-dimensional variably saturated groundwater flow and the two-dimensional kinematic wave approximation of the shallow water equations for overland flow. The model employs a conservative centered finite difference scheme and a conservative finite volume method for subsurface flow and transport, respectively. ParFlow uses multigrid preconditioned Krylov and Newton-Krylov methods to solve the linear and nonlinear systems within each time step of the flow simulations. The code has demonstrated very efficient parallel solution capabilities. ParFlow has been coupled to geochemical reaction, land surface (e.g., Common Land Model), and atmospheric models to study the interactions among the subsurface, land surface, and the atmosphere systems across different spatial scales. This overview

focuses on the current capabilities of the code, the core simulation engine, and the primary couplings of the subsurface model to other codes, taking a high-level perspective.

2.1 Introduction

Surface and subsurface (unsaturated and saturated zones) water are connected components of a hydrologic continuum (Kumar et al., 2009) . The recognition that flow systems (i.e., surface and subsurface) are a single integrated resource has stimulated the development of integrated hydrologic models (IHMs), which include codes like ParFlow (Ashby and Falgout, 1996; Kollet and Maxwell, 2006) , HydroGeoSphere (Therrien and Sudicky, 1996), PIHM (Kumar, 2009), and CATHY (Camporese et al., 2010) . These codes explicitly simulate different hydrological processes such as feedbacks between processes that affect the timing and rates of evapotranspiration, vadose zone flow, surface runoff and groundwater interactions. That is, IHMs are designed specifically to include the interactions between traditionally incompatible flow domains (e.g., groundwater and land surface flow) (Engdahl and Maxwell, 2015). Most IHMs adopt a similar, physically-based approach to describe watershed dynamics where the governing equations of three–dimensional variably saturated subsurface flow are coupled to shallow water equations for surface runoff. The advantage of the coupled approach is that it allows hydraulically-connected groundwater–surface water systems to evolve dynamically, and for natural feedbacks between the systems to develop (Sulis et al., 2010; Maxwell et al., 2011; Weill et al., 2011; Williams and Maxwell, 2011; Simmer et al., 2015). A large body of literature now exists presenting applications of the various IHMs to solve hydrologic questions. Each model has its own technical documentation, but the individual development, maintenance, and sustainability efforts

differ between tools. Some IHMs represent commercial investments and others are community, open-sourced projects, but all are dynamically evolving as technology improves and new features are added. Consequently, it can be difficult to answer the question of "what exactly can this IHM do today" without navigating dense user documentation. The purpose of this manuscript is to provide a current review of the functions, capabilities, and ongoing development of one of the open-source integrated models, ParFlow, in a format that is more accessible to a broad audience than a user manual or articles detailing specific applications of the model.

ParFlow is a parallel integrated hydrologic model that simulates surface, unsaturated and groundwater flow (Maxwell et al., 2016). ParFlow computes fluxes through the subsurface, as well as interactions with aboveground or surface (overland) flow: all driven by gradients in hydraulic head. Richards' equation is employed to simulate variably saturated three-dimensional groundwater flow (Richards, 1931). Overland flow can be generated by saturation or infiltration excess using a free overland flow boundary condition combined with Manning's equation and the kinematic wave formulations of the dynamic wave equation (Kollet and Maxwell, 2006). ParFlow solves these governing equations employing either a fully coupled or integrated approach where surface and subsurface flows are solved simultaneously using the Richards' equation in three-dimensional form (Gilbert and Maxwell, 2016), or an indirect approach where the different components can be partitioned and flows in only one of the systems (surface or subsurface flows) is solved. The integrated approach allows for dynamic evolution of the interconnectivity between

the surface water and groundwater systems. This interconnection depends only on the properties of the physical system and governing equations. An indirect approach permits partitioning of the flow components i.e., water and mass fluxes between surface and subsurface systems. The flow components can be solved sequentially. For the groundwater flow solution, ParFlow makes use of an implicit backward Euler scheme in time, and a cell-centered finite-difference scheme in space (Woodward, 1998). An upwind finite-volume scheme in space and an implicit backward Euler scheme in time is used for the overland flow component (Maxwell et al., 2007). ParFlow uses Krylov linear solvers with multigrid preconditioners for the flow equations along with a Newton method for the nonlinearities in the variably saturated flow system (Ashby and Falgout, 1996; Jones and Woodward, 2001). ParFlow's physically based approach requires a number of parameterizations e.g., subsurface hydraulic properties, such as porosity, the saturated hydraulic conductivity, and the pressure-saturation relationship parameters (relative permeability). (Kollet and Maxwell, 2008a).

ParFlow is well documented and has been applied to surface and subsurface flow problems including simulating the dynamic nature of groundwater and surface-subsurface interconnectivity in large domains (e.g., over 600 km^2) (Kollet and Maxwell, 2008; Ferguson and Maxwell, 2012; Condon et al., 2013; Condon and Maxwell, 2014), small catchments (e.g., approximately 30 km^2) (Ashby et al., 1994; Kollet and Maxwell, 2006; Engdahl et al., 2016), complex terrain with highly heterogenous subsurface permeability such as the Rocky Mountain National Park, Colorado,

United States (Engdahl and Maxwell, 2015; Kollet et al., 2017), large watersheds (Abu-El-Sha'r and Rihani, 2007; Kollet et al., 2010), continental scale flows (Condon et al., 2015; Maxwell et al., 2015) and even subsurface–surface and –atmospheric coupling (Maxwell et al., 2011; Williams and Maxwell, 2011; Williams et al., 2013; Gasper et al., 2014; Shrestha et al., 2015). Evidence from these studies suggest ParFlow produce accurate results in simulating flows in surface-subsurface systems in watersheds i.e., the code possesses the capability of performing simulations that accurately represent the behaviors of natural systems on which models are based. The rest of the paper is organized as follows: We provide a brief history of ParFlow's development in Sect. 2.1.1. In Sect. 2.2, we describe the core functionality of the code, i.e., the primary functions and the model equations and grid type used by ParFlow. Sect. 2.3 covers equation discretization and solvers (e.g., inexact Newton-Krylov, the ParFlow Multigrid (PFMG) preconditioner, and the Multigrid-Preconditioned Conjugate Gradient (MGCG) method) used in ParFlow. Examples of parallel scaling and performance efficiency of ParFlow are revisited in Sect. 2.4. The coupling capabilities of ParFlow, with other atmospheric, land surface, and subsurface models are shown in Sect. 2.5. We provide a summary and discussion, future directions to the development of ParFlow, and give some concluding remarks in Sect. 2.6.

2.1.1 Development History

ParFlow development commenced as part of an effort to develop an open–source, object–oriented, parallel watershed flow model initiated by scientists from the Center for Applied Scientific Computing (CASC), Environmental Programs, and the Environmental Protection Department at the Lawrence Livermore National Laboratory (LLNL) in the mid–1990s. ParFlow was born out of this effort to address the need for a code that combines fast, nonlinear solution schemes with massively parallel processing power, and its development continues today (e.g. Ashby et al., 1993; Smith et al., 1995; Woodward, 1998; Maxwell and Miller, 2005; Kollet and Maxwell, 2008; Rihani et al., 2010; Simmer et al., 2015). ParFlow, is now a collaborative effort between numerous institutions including Colorado School of Mines, Research Center Jülich, University of Bonn, Washington State University, the University of Arizona, and Lawrence Livermore National Laboratory, and its working base and development community continues to expand.

ParFlow was originally developed for modeling saturated fluid flow and chemical transport in three-dimensional heterogeneous media. Over the past few decades, ParFlow underwent several modifications and expansions (i.e., additional features and capabilities have been implemented) and has seen an exponential growth of applications. For example, a two-dimensional distributed overland flow simulator (surface water component) was implemented into ParFlow (Kollet and

Maxwell, 2006) to simulate interaction between surface and subsurface flows. Such additional implementations have resulted in improved numerical methods in the code. The code's applicability continues to evolve, for example, in recent times, ParFlow has been used in several coupling studies, with subsurface, land surface, and atmospheric models to include physical processes at the land surface (Maxwell and Miller, 2005; Maxwell et al., 2007, 2011; Kollet, 2009; Williams and Maxwell, 2011; Valcke et al., 2012; Valcke, 2013; Shrestha et al., 2014; Beisman et al., 2015) across different spatial scales and resolutions (Kollet and Maxwell, 2008; Condon and Maxwell, 2015; Maxwell et al., 2015). Also, a terrain following mesh formulation has been implemented (Maxwell, 2013) that allows ParFlow to handle problems with fine space discretization near the ground surface that comes with variable vertical discretization flexibility which offer modelers the advantage to increase the resolution of the shallow soil layers (these are discussed in detail below).

2.2 Core Functionality of ParFlow

The core functionality of the ParFlow model is the solution of three-dimensional variably saturated groundwater flow in heterogeneous porous media ranging from simple domains with minimal topography and/or heterogeneity to highly resolved continental-scale catchments (Jones and Woodward, 2001; Maxwell and Miller, 2005; Kollet and Maxwell, 2008; Maxwell, 2013).

Within this range of complexity, the ParFlow model can operate in three different modes: 1). variably saturated; 2.). steady–state saturated; and 3). integrated–watershed flows; however, all these modes share a common sparse coefficient matrix solution framework.

2.2.1 Variably Saturated Flow

ParFlow can operate in variably saturated mode using the well-known, mixed form of Richards' equation (Celia et al., 1990). The mixed form of Richards' equation implemented in ParFlow is:

$$S_s S_w(p) \frac{\partial p}{\partial t} + \phi \frac{\partial (S_w(p))}{\partial t} = \nabla . \boldsymbol{q} + q_s, \qquad (2.1)$$

$$\boldsymbol{q} = -k_s k_r(p) \nabla (p - z), \qquad (2.2)$$

where S_s is the specific storage coefficient $[\mathrm{L}^{-1}]$, S_w is the relative saturation $[-]$ as a function of pressure head p of the fluid/water [L], t is time [T], ϕ is the porosity of the medium $[-]$, $\boldsymbol{q}$ is the specific volumetric (Darcy) flux $[\mathrm{LT}^{-1}]$, k_s is the saturated hydraulic conductivity tensor $[\mathrm{LT}^{-1}]$, k_r is the relative permeability $[-]$ which is a function of pressure head, q_s is the general source/sink term $[\mathrm{T}^{-1}]$ (includes wells and surface fluxes e.g. evaporation and transpiration), and z is depth below the surface [L]. The Richards' equation assumes that the air phase is infinitely mobile (Richards, 1931). ParFlow has been used to numerically simulate river-aquifer exchange (free-surface flow and subsurface flow), (Frei et al., 2009), and highly heterogenous problems under

variably-saturated flow conditions (Woodward, 1998; Jones and Woodward, 2001; Kollet et al., 2010). Under saturated conditions e.g., simulating linear groundwater movement under assumed predevelopment conditions, the steady-state saturated mode can be used.

2.2.2 Steady–State Saturated Flow

The most basic operational mode is the solution of the steady state, fully saturated groundwater flow equation:

$$\nabla . \boldsymbol{q} - q_s = 0, \tag{2.3}$$

where q_s represents a general source/sink term e.g., wells [T^{-1}], $\boldsymbol{q}$ is the Darcy' flux [LT^{-1}] which is usually written as:

$$\boldsymbol{q} = -k_s \nabla P \tag{2.4}$$

where k_s is the saturated hydraulic conductivity [LT^{-1}] and P represents the 3-D hydraulic head-potential [L]. ParFlow does include a direct solution option for the steady state saturated flow that is distinct from the transient solver. For example, ParFlow uses the solver "impes" under single-phase, fully saturated steady state condition relative to the variably saturated, transient mode where Richards' equation solver is used (Maxwell et al., 2016). When studying sophisticated or complex phenomena e.g., simulating fully coupled system (i.e., surface and subsurface flow), an overland flow boundary condition is employed.

2.2.3 Overland Flow

Surface water systems are connected to the subsurface, and these interactions are particularly important for rivers. However, these connections have been historically difficult to represent explicitly in numerical simulations. A common approach has been to use river routing codes, like HEC, and MODFLOW and its River Package to determine head in the river, which is then used as a boundary condition for the subsurface model. This approach prevents feedbacks between the two models, and a better representation of the physical processes in these kinds of problems is one of the motivations for IHMs. Overland flow is implemented in ParFlow as a two–dimensional kinematic wave equation approximation of the shallow water equations. The continuity equation for two-dimensional shallow overland flow is given as;

$$\frac{\partial \psi_s}{\partial t} = \nabla.(\vec{v}\psi_s) + q_s, \qquad (2.5)$$

where $\vec{v}$ is the depth averaged velocity vector [LT^{-1}], ψ_s is the surface ponding depth [L], t is time [T], and q_s is a general source/sink (e.g., precipitation rate) [T^{-1}]. Ignoring the dynamic and diffusion terms results in the momentum equation

$$S_{f,i} = S_{o,i}, \qquad (2.6)$$

which is known as the kinematic wave approximation. The $S_{f,i}$ and $S_{o,i}$ represent the friction $[-]$ and bed slopes (gravity forcing term) $[-]$ respectively, where i indicates $x-$ and $y-$ directions

(also shown in Eq. (2.7) and Eq. (2.8)) (Maxwell et al., 2015). Manning's equation is used to generate a flow depth–discharge relationship:

$$v_x = \frac{\sqrt{S_{f,x}}}{n} \psi_s^{2/3}, \text{ and} \tag{2.7}$$

$$v_y = \frac{\sqrt{S_{f,y}}}{n} \psi_s^{2/3} \tag{2.8}$$

where n is the Manning's roughness coefficient $\left[\mathrm{TL}^{-1/3}\right]$. Flow of water out of the overland flow simulation domain only occurs horizontally at an outlet which is controlled by specifying a type of boundary condition at the edge of the simulation domain. In a natural system, the outlet is usually taken as the region where a river enters another water body such as stream or a lake. ParFlow determines overland flow direction through the D4 flow routing approach. In a simulation domain, the D4 flow routing approach allows for flow to be assigned from a focal cell to only one neighboring cell accessed via the steepest or most vertical slope. The shallow overland flow formulation (Eq. (2.9)) assumes that the flow depth is averaged-vertically and neglects a vertical change in momentum in the column of surface water. To account for vertical flow (from the surface to the subsurface or subsurface to the surface), a formulation that couples the system of equations through a boundary condition at the land surface becomes necessary. Equation (2.5) can be modified to include an exchange rate with the subsurface, q_e, as:

$$\frac{\partial \psi_s}{\partial t} = \nabla . (\vec{v} \psi_s) + q_s + q_e \tag{2.9}$$

which is common in other IHMs. In ParFlow, the overland flow equations are coupled directly to Richards' equation at the top boundary cell under saturated conditions. Conditions of continuity of pressure (i.e., the pressures of the subsurface and surface domains are equal right at the ground surface) and flux at the top cell of the boundary between the subsurface and surface systems are assigned **Fig. 2.1** demonstrates continuity of pressure at the ground surface for flow from the surface into the subsurface. This assignment is done by setting pressure–head, in Eq. (2.1) equal to the vertically–averaged surface pressure, ψ_s;

$$p = \psi_s = \psi, \tag{2.10}$$

and the flux, q_e equal to the specified boundary conditions (e.g., Neumann or Dirichlet type). For example, if Neumann type boundary conditions are specified, which are given as;

$$q_{BC} = -k_s k_r \nabla(\psi - z) \tag{2.11}$$

and one solves for the flux term in Eq. (2.10), the result is;

$$q_e = \frac{\partial \|\psi,0\|}{\partial t} - \nabla\vec{v}\|\psi,0\| - q_s \tag{2.12}$$

where the $\|\psi,0\|$ operator is defined as the greater of the quantities, ψ and 0. Substituting Eq. (2.12) for the boundary condition in Eq. (2.11), requiring the aforementioned flux continuity $q_{BC} = q_e$, leads to

$$-k_s k_r \nabla(\psi - z) = \frac{\partial \|\psi,0\|}{\partial t} - \nabla.(\vec{v}\|\psi,0\|) - q_s \tag{2.13}$$

Equation (2.13) shows that the surface water equations are represented as a boundary condition to the Richards' equation. That is, the boundary condition links flow processes in the subsurface

with those at the land surface. This boundary condition eliminates the exchange flux and accounts for the movement of the free surface of ponded water at the land surface (Kollet and Maxwell, 2006; Williams and Maxwell, 2011).

Many IHMs couple subsurface and surface flows making use of the exchange flux, q_e model. The exchange flux between the domains (the surface and the subsurface) depends on hydraulic conductivity and the gradient across some interface where indirect coupling is used (VanderKwaak, 1999; Panday and Huyakorn, 2004). The exchange flux concept gives a general formulation of a single set of coupled surface-subsurface equations. The exchange flux term, q_e may be included in the shallow overland flow continuity equation as the exchange rate term with the subsurface (Eq. (2.9)) in a coupled system (Kollet and Maxwell, 2006).

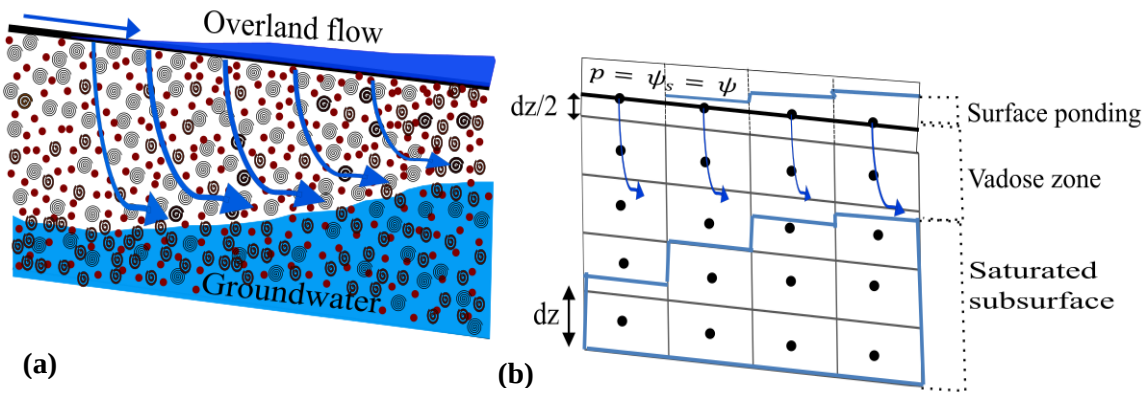

Figure 2.1: Coupled surface and subsurface flow systems. The physical system is represented in **(a)** and a schematic of the overland flow boundary condition (continuity of pressure and flux at

the ground surface) is in **(b)**. The equality, $p = \psi_s = \psi$ in Fig. 2.1 signifies that at the ground surface, the vertically averaged surface pressure and subsurface pressure head are equal, which is the unique overland flow boundary used by ParFlow.

2.2.4 Multi-Phase Flow and Transport Equations

Most applications of the code have reflected ParFlow's core functionality as a single-phase flow solver, but there are also embedded capabilities for multi-phase flow of immiscible fluids and solute transport. Multi–phase systems are distinguished from single–phase systems by the presence of one or more interfaces separating the phases, with boundaries changing between the phases. The flow equations that are solved in multi–phase systems in a porous medium comprise a set of mass balance and momentum equations. The equations are given by:

$$\frac{\partial}{\partial t}(\phi \rho_i S_i) + \nabla.(\phi \rho_i S_i \vec{v}_i) - \rho_i Q_i = 0, \qquad (2.14)$$

$$\phi S_i \vec{v}_i + \lambda_i.(\nabla p_i - \rho_i \vec{g}) = 0, \qquad (2.15)$$

where $i = 1, \dots, n$ denotes a given phase (such as air or water). In these equations, ϕ is the porosity of the medium $[-]$ which explains the fluid capacity of the porous medium, and for each phase, i, $S_i(\vec{x}, t)$ is the relative saturation $[-]$ which indicates the content of phase i in the porous medium, $\vec{v}_i(\vec{x}, t)$ represent Darcy velocity vector $[\mathrm{LT}^{-1}]$, $Q_i(\vec{x}, t)$ stands for source/sink term $[\mathrm{T}^{-1}]$, $p_i(\vec{x}, t)$

is the average pressure $[\mathrm{ML^{-1}T^{-2}}]$, $\rho_i(\vec{x},t)$ is the mass density $[\mathrm{ML^{-3}}]$, λ_i is the mobility $[\mathrm{L^3TM^{-1}}]$, $\vec{g}$ is the gravity vector $[\mathrm{LT^{-2}}]$, $\vec{x}$ and t represent space vector and time, respectively. ParFlow solves for the pressures on a discrete mesh and uses a time-stepping algorithm based on a mass conservative backward Euler scheme and spatial discretization (a finite volume method). ParFlow's multi–phase flow capability has not been applied in major studies, however, this capability is also available for testing (Ashby et al., 1993; Tompson et al., 1994; Falgout et al., 1999; Maxwell et al., 2016).

The transport equations included in the ParFlow package describe mass conservation in a convective flow (no diffusion) with degradation effects and adsorption included along with extraction and injection wells (Beisman et al., 2015; Maxwell et al., 2016). The transport equation is defined as follows:

$$\left(\frac{\partial}{\partial t}\left(\phi c_{i,j}\right)+\lambda_j\phi c_{i,j}\right)+\nabla.\left(c_{i,j}\vec{v}\right)=-\left(\frac{\partial}{\partial t}\left((1-\phi)\rho_s F_{i,j}\right)+\lambda_i(1-\phi)\rho_s F_{i,j}\right)+$$

$$\sum_k^{nI}\gamma_k^{I;i}\chi\Omega_k^I\left(c_{i,j}-c_{i,j}^{-k}\right)-\sum_k^{nE}\gamma_k^{E;i}\chi\Omega_k^E c_{i,j} \qquad (2.16)$$

where $c_{i,j}(\vec{x},t)$ represents concentration fraction of contaminant $[-]$, , λ_i is degradation rate $[\mathrm{T^{-1}}]$, $F_i(\vec{x},t)$ is the mass concentration $[\mathrm{L^3M^{-1}}]$, $\rho_s(\vec{x})$ is the density of the solid mass $[ML^{-3}]$, n_I is injection wells $[-]$, $\gamma_k^{I;i}(t)$ is injection rate $[\mathrm{T^{-1}}]$, $\Omega_k^I(\vec{x})$ represent the area of the injection well $[-]$, $c_{i,j}^{-k}(\vec{x},t)$ is the injected concentration fraction $[-]$, n_E is the extraction wells $[-]$, $\gamma_k^{E;i}(t)$ is extraction rate $[\mathrm{T^{-1}}]$, $\Omega_k^E(\vec{x})$ is an extraction well area $[-]$, $i=0,\dots,n_{p-1}\ \left(n_p\ \epsilon\{1,2,3\}\right)$ is the

number of phases, $j = 0, \ldots, n_c - 1$ represents the number of contaminants, $c_{i,j}$ is the concentration of contaminant j in phase i, k is hydraulic conductivity $[\mathrm{LT}^{-1}]$, $\chi\Omega_k^I$ is the characteristic function of an injection well region, and $\chi\Omega_k^E$ is the characteristic function of an extraction well region. The mass concentration term, $F_{i,j}$ is taken to be instantaneous in time and a linear function of contaminant concentration:

$$F_{i,j} = K_{d;j} c_{i,j} \tag{2.17}$$

where $K_{d;j}$ is the distribution coefficient of the component $[\mathrm{L}^3\mathrm{M}^{-1}]$. The transport/advection equation or convective flow calculation performed by ParFlow offers a choice of a first-order explicit upwind scheme or a second-order explicit Godunov scheme. The advection calculations are discretized as boundary value problems for each primary dimension over each computed cell. The discretization is a fully-explicit, forward Euler first-order accurate in time approach. The implementation of a second-order explicit Godunov scheme (second-order advection scheme) minimizes numerical dispersion and presents a more accurate computational process at these time scales than either an implicit or lower-order explicit scheme. Stability issue here is that the simulation timestep is restricted via the courant-Friedrichs-Lewy (CFL) condition, which demands that time steps are chosen small enough to ensure that mass not be transported more than one grid cell in a single timestep in order to maintain stability (Beisman, 2007).

2.2.5 Computational Grids

An accurate numerical approximation of a set of partial differential equations is strongly dependent on the simulation grid. Integrated hydrologic models can use unstructured or structured meshes for the discretization of the governing equations. The choice of grid type to adopt is problem-specific and often a subjective choice since the same domain can be represented in many ways, but there are some clear tradeoffs. For example, structured grid models, such as ParFlow, may be preferred to unstructured grid models because structured grids provide significant advantages in computational simplicity and speed, and are amenable to efficient parallelization (Durbin, 2002; Kumar et al., 2009; Osei-Kuffuor et al., 2014). ParFlow adopts a regular, structured grid specifically for its parallel performance. There are currently two regular grid formulations included in ParFlow, an orthogonal grid and a terrain-following formulation (TFG); both allow for variable vertical discretization (thickness over an entire layer) over the domain.

2.2.5.1 Orthogonal Grid

Orthogonal grids have many advantages, and many approaches are available to transform an irregular grid into an orthogonal grid such as conformal mapping. This mapping defines a transformed set of partial differential equations using an elliptical system with “control functions”

determined in such a way that the generated grid would be either orthogonal or nearly orthogonal. However, conformal mapping may not allow flexibility in the control of the grid node distribution, which diminishes its usefulness with complex geometries (Mobley and Stewart, 1980; Haussling and Coleman, 1981; Visbal and Knight, 1982; Ryskin and Leal, 1983; Allievi and Calisal, 1992; Eca, 1996).

A Cartesian, regular, orthogonal grid formulation is implemented by default in ParFlow, though some adaptive meshing capabilities are still included in the source code. For example, layers within a simulation domain can be made to have varying thickness. The upper portion of **Fig. 2.2** shows the standard way topography or any other non-rectangular domain boundaries are represented in ParFlow. The domain limits, and any other internal boundaries, can be defined using grid-independent triangulated irregular network (TIN) files that define a geometry, or a gridded indicator file can be used to define geometric elements. ParFlow uses the octree space partitioning algorithm (a grid-based algorithm or mesh generators filled with structured grids) (Maxwell, 2013) to depict complex structures/land surface representations (e.g., topography, watershed boundaries, and different hydrologic facies) in three-dimensional space (Kollet et al., 2010). These land surface features are mapped onto the orthogonal grid, and looping structures that encompass these irregular shapes are constructed (Ashby et al., 1997). The grid cells above ground surface are inactive (shown in upper region of **Fig. 2.2**) and are stored in the solution vector but not included in the solution.

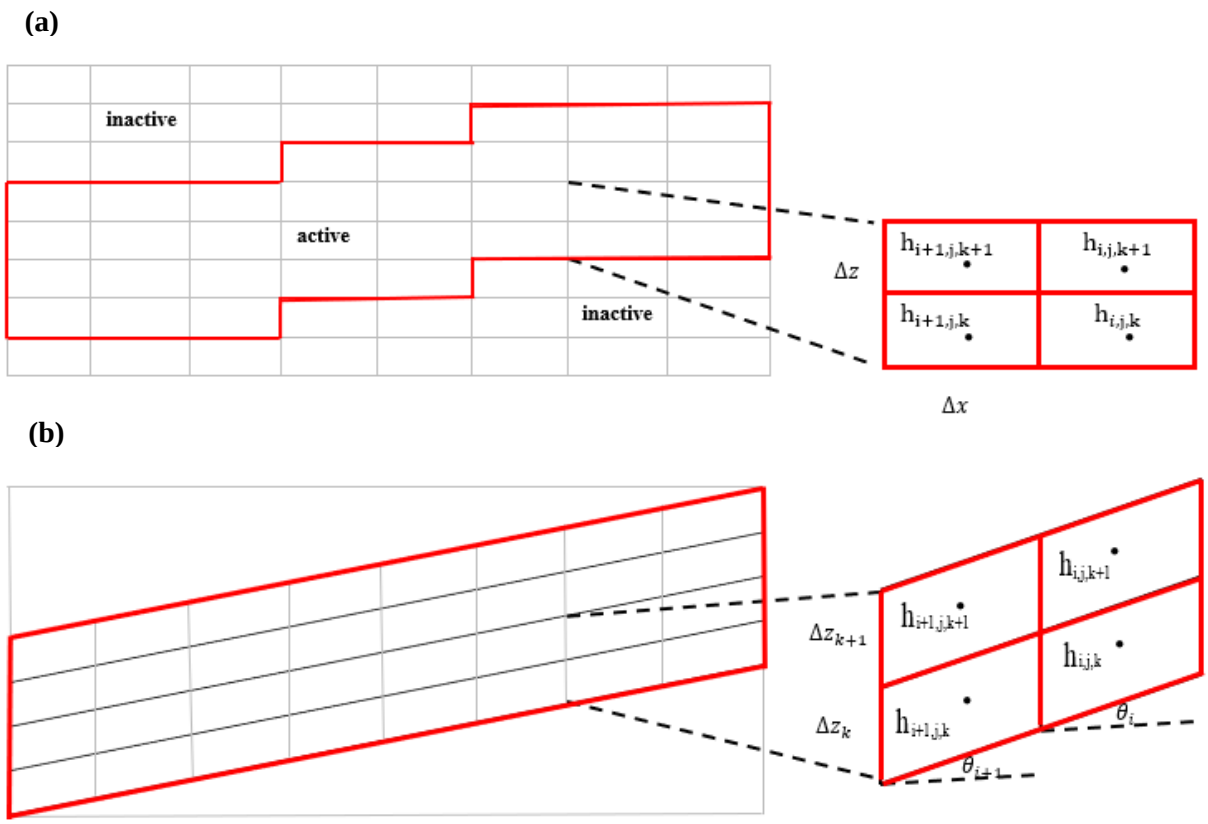

Figure 2.2: Representation of orthogonal **(a)** and the terrain following **(b)** grid formulations and schematics of the associated finite difference dependences (right). The i, j, and k are the x, y, and z cell indices.

2.2.5.2 Terrain Following Grid

The inactive portion of a watershed defined with an orthogonal grid can be quite large in complex watersheds with high-relief. In these cases, it is advantageous to use a grid that allows these regions to be omitted. ParFlow's structured grid conforms to the topography via transformation by the terrain following grid formulation. This transform alters the form of Darcy's law to incorporate a topographic slope component. For example, subsurface fluxes are computed separately in both x and y directions making use of the terrain following grid transform as:

$$q_x = K \sin(\theta_x) + K \frac{\partial p}{\partial x} \cos(\theta_x), \text{ and}$$

$$q_y = K \sin(\theta_y) + K \frac{\partial p}{\partial y} \cos(\theta_y) \qquad (2.18)$$

where q_x and q_y represent source/sink terms, such as fluxes, that include potential recharge flux at the ground surface $[\mathrm{LT}^{-1}]$, p is the pressure head [L]; K is the saturated hydraulic conductivity tensor , $[\mathrm{LT}^{-1}]$ (e.g., K_x, K_y, or K_Z), θ is the local angle $[-]$ of topographic slope, S_x and S_y in the x and y directions and may be presented as $\theta_x = \tan^{-1} S_x$ and $\theta_y = \tan^{-1} S_y$ respectively (Weill et al., 2009). The terrain following grid formulation comes in handy when solving coupled surface and subsurface flows (Maxwell, 2013). The terrain following grid formulation uses the same surface slopes specified for overland flow to transform the grid, whereas the slopes specified in the orthogonal grid are only used for 2-D overland flow routing and do not impact the subsurface

formulation (see **Fig. 2.2**). Note that TIN files can still be used to deactivate portions of the transformed domain.

2.3 Equation Discretization and Solvers

The core of the ParFlow code is its library of numerical solvers. As noted above, in most cases, the temporal discretization of the governing equations uses an implicit (backward Euler) scheme; with cell-centered finite differences in spatial dimensions. Different components of this solution framework have been developed for the various operational modes of ParFlow including an inexact Newton-Krylov nonlinear solver (Sect. 2.3.1), a multigrid algorithm (Sect. 2.3.2), and a multigrid-preconditioned conjugate gradient (MGCG) solver in (Sect. 2.3.3). The conditions, requirements, and constraints on the solvers depend on the specifics of the problem being solved, and some solvers tend to be more efficient (faster overall convergence) than others for a given problem. The core structure of these solvers and some of their implementation details are given below, with an emphasis on the main concepts behind each solver.

2.3.1 Newton–Krylov solver for Variably Saturated Flow

The cell-centered fully-implicit discretization scheme applied to Richards' equation leads to a set of coupled discrete nonlinear equations that need to be solved at each time step, and, for

variably saturated subsurface flow, ParFlow does this with the inexact Newton-Krylov method implemented in the KINSOL package (Hindmarsh et al., 2005; Collier et al., 2015). Newton-Krylov methods were initially utilized in the context of partial differential equations by (Brown and Saad, 1990). In the approach, coupled nonlinear system as a result of discretization of the partial differential equation is solved iteratively. Within each iteration, the nonlinear system is linearized via a Taylor expansion. After linearization, an iterative Krylov method is used to solve the resulting linear Jacobian system (Woodward, 1998; Osei-Kuffuor et al., 2014). For variably saturated subsurface flow, ParFlow uses the GMRES Krylov method (Saad and Schultz, 1986). Figure 3.3 is a flow chart of the solution technique ParFlow uses to provide approximate solutions to systems of nonlinear equations.

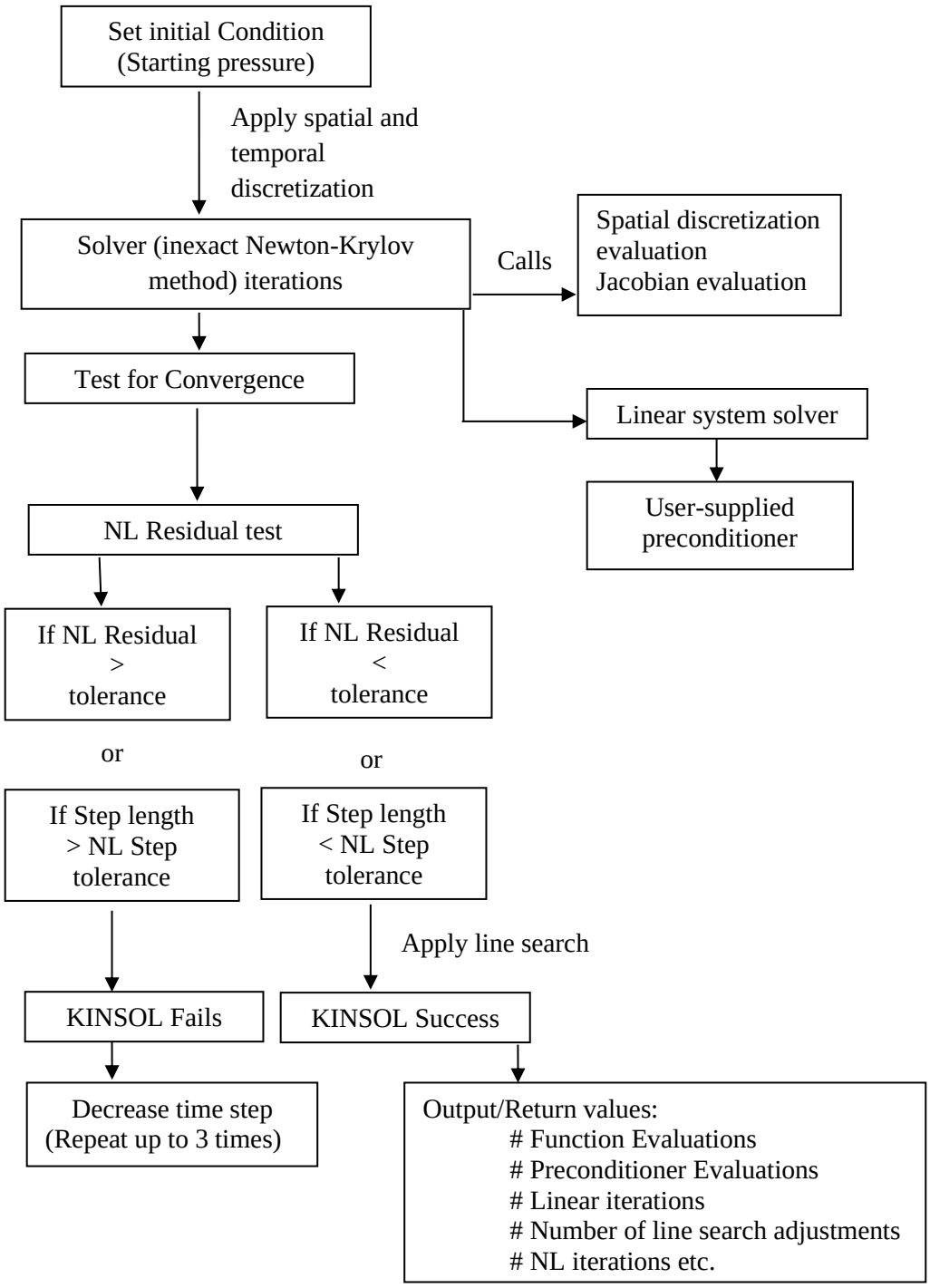
Set initial Condition
(Starting pressure)
Apply spatial and
temporal
discretization
Solver (inexact Newton-Krylov
method) iterations
Calls
Spatial discretization
evaluation
Jacobian evaluation
Test for Convergence
Linear system solver
User-supplied
preconditioner
NL Residual test
If NL Residual
>
tolerance
If NL Residual
<
tolerance
or
or
If Step length
> NL Step
tolerance
If Step length
< NL Step
tolerance
Apply line search
KINSOL Fails
KINSOL Success
Decrease time step
(Repeat up to 3 times)
Output/Return values:
Function Evaluations
Preconditioner Evaluations
Linear iterations
Number of line search adjustments
NL iterations etc.

Figure 2.3: Working flow chart of ParFlow's solver for linear and non-linear system solution.

The benefit of this Newton-Krylov method is that the Krylov linear solver requires only matrix-vector products. Because the system matrix is the Jacobian of the nonlinear function, these matrix-vector products may be approximated by taking directional derivatives of the nonlinear function in the direction of the vector to be multiplied. This approximation is the main advantage of the Newton-Krylov approach as it removes the requirement for matrix entries in the linear solver. An inexact Newton method is derived from a Newton method by using an approximate linear solver at each nonlinear iteration, as is done in the Newton-Krylov method (Dembo et al., 1982; Dennis and Schabel, 1996). This approach takes advantage of the fact that when the nonlinear system is far from converged, the linear model used to update the solution is a poor approximation. Thus, the convergence criteria of an early linear system solve are relaxed. The tolerance required for solution of the linear system is decreased as the nonlinear function residuals approach zero. The convergence rate of the resulting nonlinear solver can be linear or quadratic, depending on the algorithm used. Through the KINSOL package, ParFlow can either use a constant tolerance factor or ones from Eisenstat and Walker, (1996). Krylov methods can be very robust, but they can be slow to converge. As a result, it is often necessary to implement a preconditioner, or accelerator, for these solvers.

2.3.2 Multigrid Solver

Multigrid (MG) methods constitute a class of techniques or algorithms for solving differential equations (system of equations) using a hierarchy of discretization (Volker, 1987; Briggs et al., 2000). Multigrid algorithms are applied primarily to solve linear and nonlinear boundary value problems and can be used as either preconditioners or solvers. The most efficient method for preconditioning the linear systems in ParFlow is the ParFlow Multigrid algorithm (PFMG) (Ashby and Falgout, 1996; Jones and Woodward, 2001). Multigrid algorithms arise from discretization of elliptic partial differential equations (Briggs et al., 2000), and, in ideal cases, have convergence rates that do not depend on the problem size. In these cases, the number of iterations remains constant even as problems sizes grow large. Thus, the algorithm is algorithmically scalable. However, it may take longer to evaluate each iteration as problem sizes increase. As a result, ParFlow utilizes the highly efficient implementation of PFMG in the hypre library (Falgout and Yang, 2002).

For variably saturated subsurface flow, ParFlow uses the Newton-Krylov method coupled with a multigrid preconditioner to accurately solve for the water pressure (hydraulic head) in the subsurface and diagnoses the saturation field (which is used in determining the water table). (Woodward, 1998; Jones and Woodward, 2000, 2001; Kollet et al., 2010). The water table is calculated for computational cells having hydraulic heads above the bottom of the cells. Generally,

a cell is saturated if the hydraulic head in the cell is above the node elevation (cell center) or the cell is unsaturated if the hydraulic head in the cell is below the node elevation. For saturated flow, ParFlow uses the conjugate gradient method also coupled with a multigrid method. It is important to note that subsurface flow systems are usually much larger radially than they are thick, so it is common for the computational grids to have highly anisotropic cell aspect ratios to balance the lateral and vertical discretization. Combined with anisotropy in the permeability field, these high aspect ratios produce numerical anisotropy in the problem, which can cause the multigrid algorithms to converge slowly (Jones and Woodward, 2001). To correct this problem, a semi-coarsening strategy or algorithm is employed, whereby the grid is coarsened in one direction at a time. The direction chosen is the one with the smallest grid spacing i.e., the tightest coupling. In an instance where more than one direction has the same minimum spacing, then the algorithm chooses the direction in the order of x, followed by y, and then z. To decide on how and when to terminate the coarsening algorithm, Ashby and Falgout (1996) determined that a semi-coarsening down to a $(1 \times 1 \times 1)$ grid is ideal for groundwater problems.

2.3.3 Multigrid-Preconditioned Conjugate Gradient (MGCG)

ParFlow uses the multigrid-preconditioned conjugate gradient (CG) solver to solve the groundwater equations under steady-state, and fully saturated flow conditions (Ashby and Falgout,

1996). These problems are symmetric and positive definite, two properties for which the CG method was designed to target. While CG lends itself to efficient implementations, the number of iterations required to solve a system such as results from discretization of the saturated flow equation increases as the problem size grows. The PFMG multigrid algorithm is used as a preconditioner to combat this growth and results in an algorithm for which the number of iterations required to solve the system grows only minimally. See Ashby and Falgout (1996) for a detailed description of these solvers and the parallel implementation of the multigrid preconditioned CG method in ParFlow (Gasper et al., 2014; Osei-Kuffuor et al., 2014).

2.3.4 Preconditioned Newton-Krylov for Coupled Subsurface – Surface Flows

As discussed above, coupling between subsurface and surface or overland flow in ParFlow is activated by specifying an overland boundary condition at the top surface of the computational domain, but this mode of coupling allows for activation and deactivation of the overland boundary condition during simulations where ponding or drying occur. Thus, surface-subsurface coupling can occur anywhere in the domain during a simulation, and it can change dynamically during the simulation. Overland flow may occur by the Dunne or Horton mechanism depending on local dynamics. Dunne overland flow occurs when infiltration capacity of the surface soil exceeds the rainfall rate. The rainfall rate exceeds the infiltration capacity of the surface soil in Horton overland

flow. Overland flow routing is enabled when the subsurface cells are fully saturated. In ParFlow the coupling between the subsurface and surface flows is handled implicitly. ParFlow solves this implicit system with the inexact Newton-Krylov method described above. However, in this case, the preconditioning matrix is adjusted to include terms from the surface coupling. In the standard saturated or variably saturated case, the multigrid method is given the linear system matrix, or a symmetric version, resulting from discretization of the subsurface model. Because ParFlow uses a structured mesh, these matrices have a defined structure making their evaluation and application of multigrid straightforward. Due to varying topographic height of the surface boundary, where the surface coupling is enforced, the surface effects add non-structured entries in the linear system matrices. These entries increase complexity of the matrix entry evaluations and reduce effectiveness of the multigrid preconditioner. In this case, the matrix-vector products are most effectively performed through computation of the linear system entries, rather than the finite difference approximation to the directional derivative. For the preconditioning, surface couplings are only included if they model flow between cells at the same vertical height i.e., in situations where overland flow boundary conditions are imposed or activated. This restriction maintains the structured property of the preconditioning matrix while still including much of the surface coupling in the preconditioner. Both these adjustments led to considerable speedup in coupled simulations (Osei-Kuffuor et al., 2014).

2.4 Parallel Performance Efficiency

Scaling efficiency metrics offer a quantitative method for evaluating the performance of any parallel model. Good scaling generally means that the efficiency of the code is maintained as the solution of the system of equations is distributed onto more processors or as the problem resolution is refined and processing resources are added. Scalability can depend on the problem size, the processor number, the computing environment, and the inherent capabilities of the computational platform used e.g., choice of a solver. The performance of ParFlow (or any parallel code) is typically determined through weak and strong scaling (Gustafson, 1988). Weak scaling involves the measurement of code's efficiency in solving problems of increasing size (i.e., describes how the solution time change with change in the number of processors for a fixed problem size per processor). In weak scaling, the simulation time should remain constant, as the size of the problem and number of processing elements grow such that the same amount of work is conducted on each processing element. Following Gustafson (1988), scaled parallel efficiency is given by:

$$E(n,p) = \frac{T(n,1)}{T(pn,p)} \tag{2.19}$$

where $E(n,p)$ denotes parallel efficiency, T represents the run time as a function of the problem size n, which is spread across several processors p. Parallel code is said to be perfectly efficient if $E(n,p) = 1$, and the efficiency decreases as $E(n,p)$ approaches 0. Generally, parallel efficiency

decreases with increasing processor number as communication overhead between nodes/processors becomes the limiting factor.

Strong scaling describes the measurement of how much the simulation or solution time changes with the number of processors for a given problem of fixed total size (Amdahl, 1967). In strong scaling, a fixed size task is solved on a growing number of processors, and the associated time needed for the model to compute the solution is determined (Woodward, 1998; Jones and Woodward, 2000). If the computational time decreases linearly with the processor number, a perfect parallel efficiency ($E = 1$) results. The value of E is determined using Eq. (2.19). ParFlow has been shown to have excellent parallel performance efficiency, even for large problem sizes and processor counts (see Table 2.1) (Ashby and Falgout, 1996; Kollet and Maxwell, 2006). In situations where ParFlow works in conjunction with or coupled to other subsurface, land surface or atmospheric models (see Sect. 2.5) i.e., increased computational complexity by adding different components or processes, improved computational time may not only depend on ParFlow. The computational cost of such an integrated model is extremely difficult to predict because of the nonlinear nature of the system. The solution time may depend on number of factors including the number of degrees of freedom, the heterogeneity of the parameters, which processes are active (e.g., snow accumulation compared to nonlinear snowmelt processes in land surface model or the switching on or off of the overland flow routing in ParFlow). The only way to know how fast a specific problem will run is to try that problem. Many of the studies presented in Table 2.1 include

computational times for problems with different complexities where ParFlow was used. In a scaling study with ParFlow, Maxwell (2013) examined the relative performance of preconditioning the coupled variably saturated subsurface and surface flow system with the symmetric portion or full matrix for the system. Both options use ParFlow's multigrid preconditioner. Solver performance was demonstrated by combining the analytical Jacobian and the non-symmetric linear preconditioner. The study showed that the non-symmetric linear preconditioner presents faster computational times and efficient scaling. A section of the study results is reproduced in Table 2.1, in addition to other scaling studies demonstrating ParFlow's parallel efficiency. This tradeoff was also examined in Jones and Woodward (2000).

It is worth noting that large and/or complex problem sizes (e.g., simulating a large heterogenous domain size with over 8.1 billion unknowns) will always take time to solve directly, but the approach for setting up a problem depends on the specific problem being modeled. Even for one specific kind of model there may be multiple workflows and how to model such complexity becomes sole responsibility of the modeler. The studies involving ParFlow outlined in Table 2.1 provide a wealth of knowledge regarding domain setup for problems of different complexities. Since these are all specific applications, their information will likely be very useful to modelers trying to build a new domain during the setup and planning phases.

2.5 Coupling

Different integrated models including atmospheric or weather prediction models (e.g., Weather Research Forecasting Model, Advanced Regional Prediction System, Consortium for Small-Scale Modeling), land surface models (e.g., Common Land Model, Noah Land Surface Model), and a subsurface model (e.g., CruchFlow) have been coupled with ParFlow to simulate a variety of coupled earth system effects (see Figure 2.4(a)). Coupling between ParFlow and other integrated models was performed to better understand the physical processes that occur at the interfaces between the deeper subsurface and ground surface, and between the ground surface and the atmosphere. None of the individual models can achieve this on their own because ParFlow cannot account for land surface processes (e.g. evaporation), and atmospheric and land surface models generally do not simulate deeper subsurface flows (Ren and Xue, 2004; Chow et al., 2006; Beisman, 2007; Maxwell et al., 2007; Shi et al., 2014). Model coupling can be achieved either via "offline coupling" where models involved in the coupling process are run sequentially and interactions between them is one–way (i.e. information is only transmitted from one model to the other) or "online" where they interact and feedback mechanisms among components are represented (Meehl et al., 2005; Valcke et al., 2009). Each of the coupled models uses its own solver for the physical system it is solving, then information is passed between the models. As long as each model exhibits good parallel performance, this approach still allows for simulations at very high resolution, with a large number of processes (Beven, 2004; Ferguson and Maxwell,

2010; Shen and Phanikumar, 2010; Shi et al., 2014). This section focuses on the major couplings between ParFlow and other codes. We point out specific functions of the individual models as stand–alone codes that are relevant to the coupling process. In addition, information about the role or contribution of each model at the coupling interface (see Fig. 2.4(b)) that connects with ParFlow are presented (Fig. 2.5 shows the communication network of the coupled models). We discuss couplings between ParFlow and its land surface model (a modified version of the original Common Land Model introduced by Dai et al., (2003)), Consortium for Small-Scale Modeling (COSMO), Weather Research Forecasting Model, Advanced Regional Prediction System, and CrunchFlow in sections 2.5.1, 2.5.2, 2.5.3, 2.5.4, and 2.5.5 respectively.

Table 2.1: Details for the various scaling studies conducted using ParFlow.

Simulation Case	**Computer System**	**Processor Number**	**Jacobian/ Numerical Method**	**Preconditioner**	**Computation time (seconds)**	**Problem Size (cell Number)**	**Parallel Efficiency (%)**	**Study**
Surface processes and variably saturated flow (ParFlow and CLM)	JUGENE (IBM Blue-Gene Super-computer)	16,384	Finite difference	ParFlow Multigrid	10,920	486,000	58.00	(Kollet et al., 2010)
Terrain Following Grid	JUGENE (IBM Blue-Gene Super-computer)	4,096	Analytical	Non-Symmetric	1,130.50	2,048,000,000	80.91	(Maxwell, 2013)
Overland flow	Intel Xeon Tightly coupled Linux Cluster	100	Finite difference	–	10,800	50,000	82.00	(Kollet and Maxwell, 2006)
Excess infiltration produced runoff	Intel Xeon Tightly coupled Linux Cluster	100	Finite difference	–	10,800	50,000	72.00	(Kollet and Maxwell, 2006)

Terrain Following Grid	JUGENE (IBM Blue-Gene Super-computer)	16,384	Finite difference	Symmetric	2,100.81	8,192,000,000	50.60	(Maxwell, 2013)
Subsurface and Overland flow coupling	IBM BGQ architecture	1,024	Analytical /Finite difference	ParFlow Multigrid	7,200	150,000	50.00	(Osei-Kuffuor et al., 2014)
Fully coupling terrestrial systems modeling platform	IBM BGQ system JUQUEEN	4,096	–	–	–	38,880	82.00	(Gasper et al., 2014)
Performance evaluation of ParFlow code (modified version of ParFlow)	(IBM Blue-Gene Super-computer) JUQUEEN	458,752	Finite difference	–	–	10,569,646,080	–	(Burstedde et al., 2018)

a: The hyphen "– "shows that information was not provided by the appropriate study

2.5.1 ParFlow–Common Land Model (PF.CLM)

The Common Land Model (CLM) is a land surface model designed to complete land-water-energy balance at the land surface (Dai et al., 2003). CLM parameterizes the moisture, energy and momentum balances at the land surface and includes a variety of customizable land surface characteristics and modules, including land surface type (land cover type, soil texture, and soil color), vegetation and soil properties (e.g. canopy roughness, zero-plane displacement, leaf dimension, rooting depths, specific heat capacity of dry soil, thermal conductivity of dry soil, porosity), optical properties (e.g. albedos of thick canopy), and physiological properties related to the functioning of the photosynthesis-conductance model (e.g. green leaf area, dead leaf, and stem area indices). A combination of numerical schemes is employed to solve the governing equations. CLM uses a time integration scheme which proceeds by a split-hybrid approach, where the solution procedure is split into "energy balance" and "water balance" phases in a very modularized structure (Mikkelson et al., 2013; Steiner et al., 2005, 2009). The CLM described here and as incorporated in ParFlow is a modified version of the original CLM introduced by Dai et al., (2003), though the original version was coupled to ParFlow in previous model applications (e.g. Maxwell and Miller, 2005). The current coupled model, PF.CLM consist of ParFlow incorporated with land surface model Jefferson et al. (2015), (2017), and Jefferson and Maxwell (2015). The modified CLM is composed of a series of land surface modules that are called as a subroutine within ParFlow to

compute energy and water fluxes (e.g., evaporation and transpiration) to and out of the soil. For example, the modified CLM computes bare ground surface evaporative flux, E_{gr} as

$$E_{gr} = -\beta \rho_a u_* q_* \tag{2.20}$$

where β (dimensionless) denotes soil resistance factor, ρ_a represents air density [ML^{-3}], u_* represents friction velocity [LT^{-1}], and q_* (dimensionless) stands for humidity scaling parameter (Jefferson and Maxwell, 2015). Evapotranspiration for vegetated land surface, E_{veg} is computed as

$$E_{veg} = \left[R_{pp,dry} + L_w\right] L_{SAI} \left[\frac{\rho_a}{r_b}\left(q_{sat} - q_{af}\right)\right] \tag{2.21}$$

where r_b is the air density boundary resistance factor [LT^{-1}], q_{sat} (dimensionless) is saturated humidity at the land surface, and q_{af} (dimensionless) is the canopy humidity. Combination of q_{sat} and q_{af} forms the potential evapotranspiration. The potential evapotranspiration is divided into transpiration $R_{pp,dry}$ (dimensionless) which depends on the dry fraction of the canopy, and evaporation from foliage covered by water L_w (dimensionless). L_{SAI} (dimensionless) is summation of the leaf and stem area indices which estimates the total surface from which evaporation can occur. A detailed description of the equations CLM of PF.CLM uses can be found in Jefferson et al. (2015), (2017), and Jefferson and Maxwell (2015).

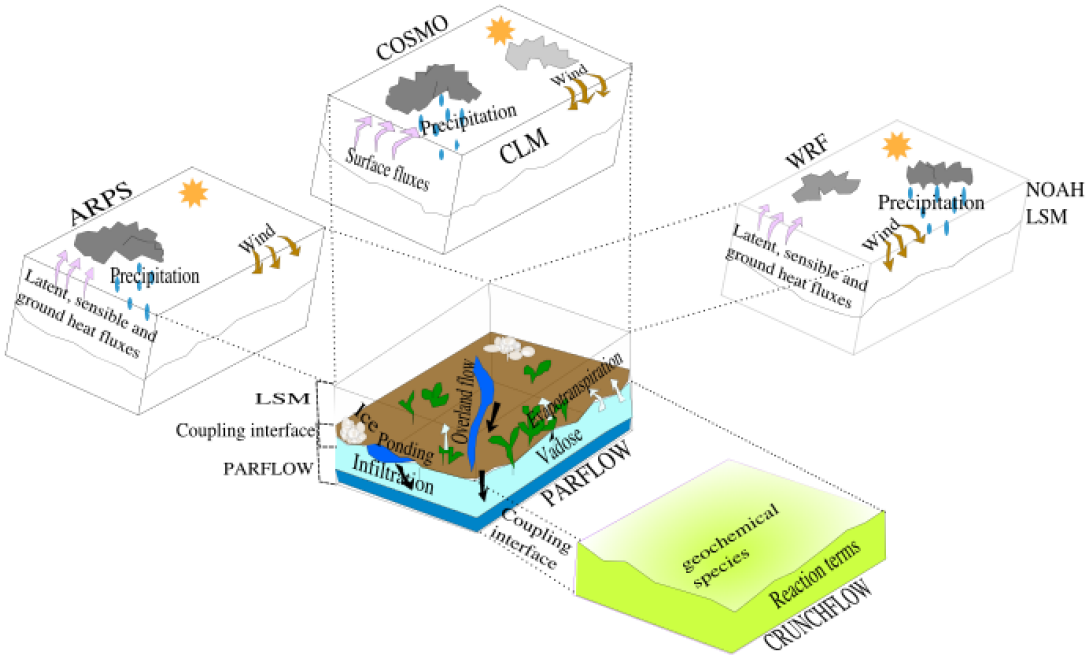

Figure 2.4(a): A pictorial description of the relevant physical environmental features and model coupling. CLM represents the Community Land Model, a stand-alone Land Surface Model (LSM) via which ParFlow couples' COSMO. The modified version of CLM by Dai et al., (2003) and is not shown in Fig. 2.4(a) because it is a module only for ParFlow, not really a stand-alone LSM any longer. The core model (ParFlow) always solves the variably saturated 3-D groundwater flow problem, but the various couplings add additional capabilities.

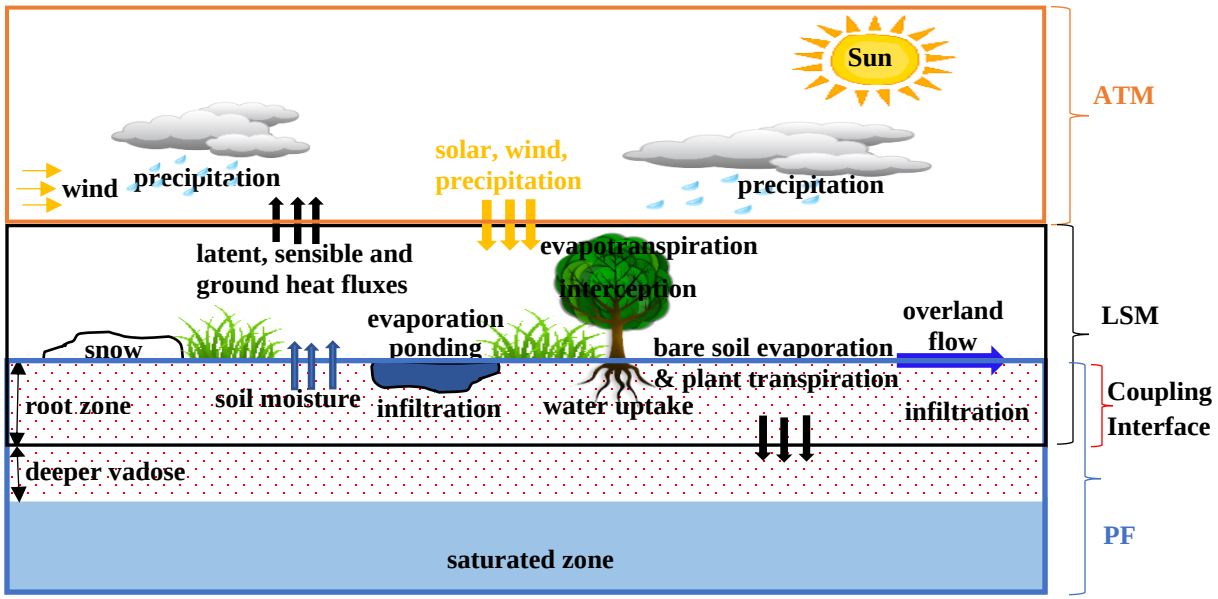

Figure 2.4(b): Schematic showing information transmission at the coupling interface. PF, LSM, and ATM indicate the portions of the physical system simulated by ParFlow, Land Surface Models, and Atmospheric Models respectively. The downward and upward arrows indicate the directions of information transmission between adjacent models. Note: Coupling between ParFlow and CrunchFlow (not shown) occur within the subsurface.

PF.CLM simulates variably saturated subsurface flow, surface or overland flow, and above-ground processes. PF.CLM was developed prior to the current community land model (see Sect. 2.5.2), and the module structure of the current and early versions are different. PF.CLM has been updated over the years to improve its capabilities. PF.CLM was first done in the early 2000's,

as an undiversified, a column proof-of-concept model, where data or message was transmitted between the coupled models via input/output files (Maxwell and Miller, 2005). Later, PF.CLM was presented in a distributed or diversified approach with a parallel input/output file structure where CLM is called as a set sequence of steps within ParFlow (Kollet and Maxwell, 2008a). These modifications, for example, were done to incorporate subsurface pressure values from ParFlow into chosen computations (Jefferson and Maxwell, 2015). These, to some extent differentiate the modified version (PF.CLM) from the original CLM by Dai et al. (2003). Within the coupled PF.CLM, ParFlow solves the governing equations for overland and subsurface flow systems and the CLM modules add the energy balance and mass fluxes from the soil, canopy, and root zone that can occur (i.e. interception, evapotranspiration etc.) (Jefferson and Maxwell, 2015).

At the coupling interface where the models overlap and undergo online communication (Fig. 2.4(b)), ParFlow calculates and passes soil moisture as well as pressure heads of the subsurface to CLM, and CLM calculates and transmits transpiration from plants, canopy and ground surface evaporation, snow accumulation and melt, and infiltration from precipitation to ParFlow (Ferguson et al., 2016). In short, CLM does all canopy water balances and snow, but once the water through falls to the ground, or snow melts, ParFlow takes over and estimates the water balances via the nonlinear Richards' equation. The coupled model, PF.CLM, has been shown to more accurately predict root-depth soil moisture compared to the uncoupled model i.e., stand-alone land surface model (CLM) with capability of computing near surface soil moisture. This increased accuracy

results from the coupling of soil saturations determined by ParFlow and their impacts on other processes including runoff and infiltration (Kollet, 2009; Shrestha et al., 2014; Gebler et al., 2015; Gilbert and Maxwell, 2016). For example, Maxwell and Miller (2005) found that simulations of deeper soil saturation (more than 40cm) vary between PF.CLM and uncoupled models, with PF.CLM simulations closely matching the observed data. Table 2.2 contains summaries of studies conducted with ParFlow coupled to either the original version of CLM by Dai et al. (2003) or modified CLM (ParFlow with land surface model).

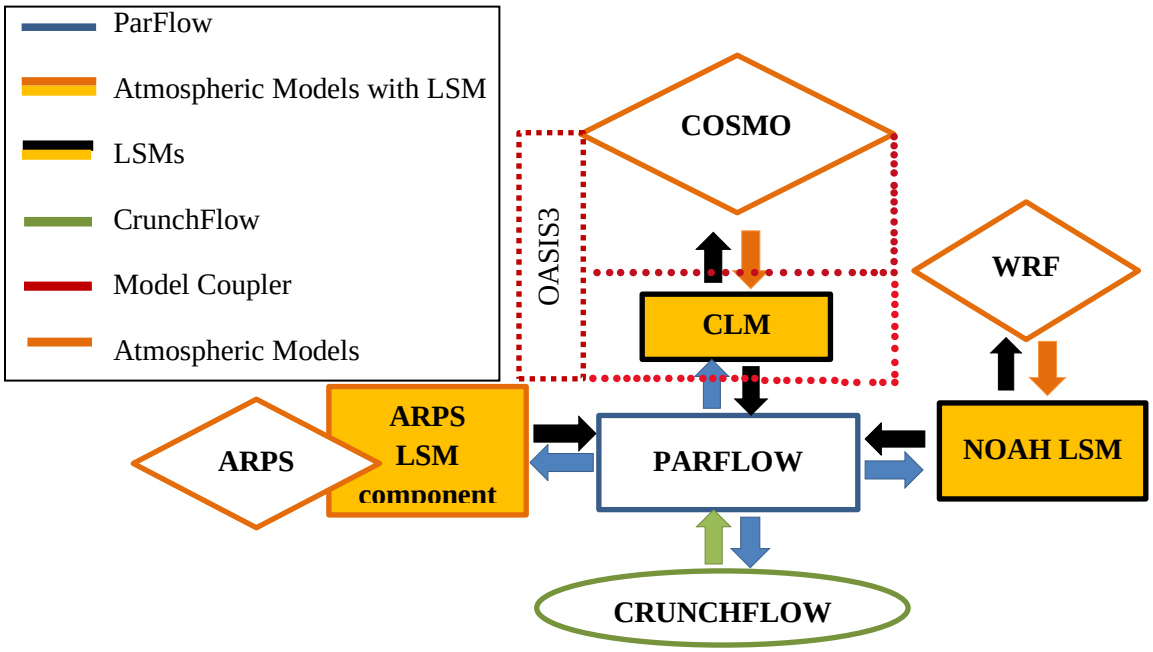

Figure 2.5: Schematic of the communication structure of the coupled models. Note: CLM represents a stand-alone Community Land Model. The modified version of Common Land Model by Dai et al., (2003) is not shown here because it is a module only for ParFlow, not really a stand-alone LSM any longer.

2.5.1.1. ParFlowE–Common Land Model (ParFlowE[CLM])

It is well established that ParFlow in conjunction with CLM performs well in estimating all canopy water and subsurface water balances (Maxwell and Miller, 2005; Mikkelson et al., 2013; Ferguson et al., 2016). ParFlow, as a component of the coupled model has been modified into a

new parallel numerical model, ParFlowE to incorporate the more complete heat equation coupled to variably saturated flow. ParFlowE simulates coupling of terrestrial hydrologic and energy cycles i.e., coupled moisture, heat, and vapor transport in the subsurface. ParFlowE is based on the original version of ParFlow having identical solution schemes and coupling approach with CLM. A coupled three-dimensional subsurface heat transport equation is implemented in ParFlowE using a cell-centered finite difference scheme in space and an implicit backward Euler differencing scheme in time. However, the solution algorithm employed in ParFlow is fully exploited in ParFlowE where the solution vector of the Newton-Krylov method was extended to two dimensions (Kollet et al., 2009). In some integrated and climate models, the convection term of subsurface heat flux and the effect of soil moisture on energy transport is neglected due to simplified parameterizations and computational limitations. However, both convection and conduction terms are considered in ParFlowE (Khorsandi et al., 2014). In ParFlowE, functional relationships (i.e., equations of state) are performed to relate density and viscosity to temperature and pressure, and thermal conductivity to saturation. That is, modeling thermal flows by relating these parameterizations in simulating heat flow is an essential component of ParFlowE. In coupling between ParFlowE and CLM, ParFlowE[CLM], the one-dimensional subsurface heat transport in the CLM is replaced by the three-dimensional heat transport equation including the process of convection of ParFlowE. CLM computes mass and energy balances at ground surface that lead to moisture fluxes and pass these fluxes to the subsurface moisture algorithm of

ParFlowE[CLM]. These fluxes are used in computing subsurface moisture and temperature fields which are then passed back to the CLM.

Table 2.2: Selected coupling studies involving application of ParFlow and atmospheric, land surface, and subsurface models

Application	**Coupled Model**	**Simulation Scale and Size (*x*, *y*, and *z* dimensions)**	**Model Development**	**Model Calibration**	**Study**
Surface heterogeneity, surface energy budget	CLM	Watershed (30m x 30m x 84m)			(Reyes et al., 2016)
Sensitivity analysis (evaporation parameterization)	CLM (modified)	Column (1m x 1m x 10m)			(Jefferson and Maxwell, 2015)
Sensitivity of photosynthesis and stomatal resistivity parameters	CLM (modified)	Column (2m x 2m x 10m)			(Jefferson et al., 2017)
Active subspaces; dimension reduction; energy fluxes	CLM (modified)	Hillslope (300m x 300m x 10m)			(Jefferson et al., 2015)
Spin-up behavior; initial conditions watershed	CLM	Regional (75km x 75km x 200m)			(Seck et al., 2015)
Urban processes	CLM	Regional (500m x 500m x 5m)		Yes	(Bhaskar et al., 2015)
Global sensitivity	CLM	Watershed (84km x 75km x 144m)		Yes	(Srivastava et al., 2014)
Entropy production optimization and inference principles	CLM	Hillslope (100m x 100m x 5m)			(Kollet, 2015)
Soil moisture dynamics	CLM	Catchment (1180m x 74m x 1.6m)		Yes	(Zhufeng et al., 2015)

Dual-boundary forcing concept	CLM	Catchment (49km x 49km x 50m)		(Rahman et al., 2015)
Initial conditions; Spin-up	CLM	Catchment; Watershed (28km x 20km x 400m)		(Ajami et al., 2014, 2015)
Groundwater-fed irrigation impacts of natural systems; optimization water allocation algorithm	CLM	Watershed; Sub-watershed (41km x 41km x 100m)		(Condon and Maxwell, 2013, 2014)
Subsurface heterogeneity (land surface fluxes)	CLM	Watershed (209km x 268km x 3502m)		(Condon et al., 2013)
Mountain Pine Beetle	CLM	Hillslope (500m x 1000m x 12.5m)		(Mikkelson et al., 2013)
Groundwater-land surface-atmosphere feedbacks	CLM	Watershed (32km x 45km x 128m)		(Ferguson and Maxwell, 2010, 2011, 2012)
Subsurface heterogeneity (land surface processes)	CLM	Hillslope (250m x 250m x 4.5m)		(Atchley and Maxwell, 2011)
Computational scaling	CLM	Hillslope (150m x 150m x 240m)		(Kollet et al., 2010)
Subsurface heterogeneity (infiltration in arid environment)	CLM	Hillslope (32km x 45km x 128m)		(Maxwell, 2010)
Subsurface heterogeneity (land energy fluxes)	CLM	Hillslope (5km x 0.1km x 310m)		(Rihani et al., 2010)
Heat and subsurface energy transport (ParFlowE)	CLM	Column (1m x 1m x 10m)	Yes	(Kollet et al., 2009)

Subsurface heterogeneity on evapotranspiration	CLM	Column, Hillslope (32m x 45m x 128m)			(Kollet, 2009)
Subsurface heterogeneity (land-energy fluxes; runoff)	CLM	Watershed; Hillslope (3km x 3km x 30m)			(Kollet and Maxwell, 2008)
Climate change (land-energy feedbacks to groundwater)	CLM	Watershed (3000m x 3000m x 30m)			(Maxwell and Kollet, 2008)
Model development experiment	CLM	Column	Yes		(Maxwell and Miller, 2005)
Subsurface transport	CLM	Aquifer (30m x 15m x 0.6m)			(Tompson et al., 1998, 1999; Maxwell et al., 2003)
Model development (TerrSysMP)	COSMO	Watershed (64km x 64km x 30m)	Yes		(Shrestha et al., 2014)
Implementation and Scaling (TerrSysMP)	COSMO	Continental	Yes		(Gasper et al., 2014)
Groundwater response to ground surface-atmosphere feedbacks	COSMO	Continental (436m x 424m x 103m)	Yes		(Keune et al., 2016)
Atmosphere, DART, data assimilation	WRF	Watershed (15km x 15km x 5m)	Yes		(Williams et al., 2013)
Coupled model development (Atmosphere)	WRF	Watershed (15km x 15km x 5m)	Yes		(Maxwell et al., 2011)
Subsurface heterogeneity (runoff generation)	WRF	Hillslope (3km x 3km x 30m)			(Meyerhoff and Maxwell, 2010)
Subsurface uncertainty to the atmosphere	WRF	Watershed (15km x 15km x 5m)	Yes		(Williams and Maxwell, 2011)
Subsurface transport	ARPS	Watershed (17m x 10.2m x 3.8m)		Yes	(Maxwell et al., 2007)
Terrain and soil moisture heterogeneity on atmosphere	ARPS	Hillslope (5km x 2.5km x 80m)			(Rihani et al., 2015)

Risk Assessment of CO leakage	CRUNCHFLOW	Aquifer (84km x 75km x 144m)	Yes	(Atchley et al., 2013)
Reactive transport heterogeneous saturated subsurface environment	CRUNCHFLOW	Aquifer (120m x 120m x 120m)		(Beisman et al., 2015)

b: “CLM” show that coupling with ParFlow was by the original Common Land Model or Community Land Model. “CLM (modified)” show that the modified version of Common Land Model by (Dai et al., 2003) was a module for ParFlow.

2.5.2 ParFlow in the Terrestrial Systems Modeling Platform, TerrSysMP

ParFlow is part of the Terrestrial System Modeling Platform TerrSysMP, which comprise the nonhydrostatic fully compressible limited-area atmospheric prediction model, COSMO, designed for both operational numerical weather prediction and various scientific applications on the meso–β (horizontal scales of 20–200km) and meso–γ (horizontal scales of 2–20km) (Duniec and Mazur, 2011; Levis and Jaeger, 2011; Bettems et al., 2015), and CLM version 3.5 (CLM3.5). Currently, it is used in direct simulations of severe weather events triggered by deep moist convection, including intense mesoscale convective complexes, prefrontal squall–line storms, supercell thunderstorms, and heavy snowfall from wintertime mesocyclones. COSMO solves nonhydrostatic, fully compressible hydro–thermodynamical equations in advection form using the traditional finite difference method (Vogel et al., 2009; Mironov et al., 2010; Baldauf et el., 2011; Wagner et al., 2016).

An online coupling between ParFlow and the COSMO model is performed via CLM3.5 (Gasper et al., 2014; Shrestha et al., 2014; Keune et al., 2016). Similar to the Common Land Model (Dai et al., 2003), CLM3.5 modules account for surface moisture, carbon, and energy fluxes between the shallow or near-surface soil (discretized/specified top soil layer), snow, and the atmosphere (Oleson et al., 2008). The model components of a fully coupled system consisting of COSMO, CLM3.5, and ParFlow are assembled by making use of the multiple–executable approach (e.g., with OASIS3-MCT model coupler). The OASIS3-MCT coupler employs communication strategies based on the message passing interface standards, MPI1/MPI2 and the Project for Integrated Earth System Modeling, PRISM, Model Interface Library (PSMILe) for

parallel communication of two–dimensional arrays between OASIS3-MCT coupler and the coupling models (Valcke et al., 2012; Valcke, 2013). The OASIS3-MCT specifies the series of coupling, frequency of the couplings, the coupling fields, the spatial grid of the coupling fields, transformation type of the (two–dimensional) coupled fields, and simulation time management and integration.

At the coupling interface, the OASIS3-MCT interface interchanges the atmospheric forcing terms and the surface fluxes in serial mode. The lowest level and current time step of the atmospheric state of COSMO is used as the forcing term for CLM3.5. CLM3.5 then computes and returns the surface energy and momentum fluxes, outgoing longwave radiation, and albedo to COSMO (Baldauf et al., 2011). The air temperature, wind speed, specific humidity, convective and grid-scale precipitation, pressure, incoming shortwave (direct and diffuse) and longwave radiation, and measurement height are sent from COSMO to CLM3.5. In CLM3.5, a mosaic/tilling approach may be used to represent the subgrid-scale variability of land surface characteristics, which considers a certain number of patches/tiles within a grid cell. The surface fluxes and surface state variables are first calculated for each tile and then spatially averaged over the whole grid cell (Shrestha et al., 2014) . As with PF.CLM3.5, the one–dimensional soil column moisture predicted by CLM3.5 gets replaced by ParFlow's variably saturated flow solver, so ParFlow is responsible for all calculations relating soil moisture redistribution and groundwater flow. Within the OASIS3-MCT ParFlow sends the calculated pressure and relative saturation for the coupled region soil layers to CLM3.5. The CLM3.5 also transmits depth-differentiated source and sink terms for soil moisture including soil moisture flux e.g., precipitation, and soil evapotranspiration for the coupled region soil layers to ParFlow. Applications of TerrSysMP in fully coupled mode from saturated

subsurface across the ground surface into the atmosphere include a study on the impact of groundwater on the European heat wave 2003 and the influence of anthropogenic water use on the robustness of the continental sink for atmospheric moisture content (Keune et al., 2016).

2.5.3 ParFlow–Weather Research Forecasting models (PF.WRF)

The Weather Research and Forecast (WRF) is a mesoscale numerical weather prediction system designed to be flexible and efficient in a massively parallel computing architecture. WRF is a widely used model that provides a common framework for idealized dynamical studies, full physics numerical weather prediction, air-quality simulations, and regional climate simulations (Michalakes et al., 1999, 2001; Skamarock et al., 2005). The model contains numerous mesoscale physics options such as microphysics parameterizations (including explicitly resolved water vapor, cloud, and precipitation processes), surface layer physics, shortwave radiation, longwave radiation, land surface, planetary boundary layer, data assimilation, and other physics and dynamics alternatives suitable for both large-eddy and global-scale simulations. Similar to COSMO, the WRF model is a fully compressible, conservative-form, non-hydrostatic atmospheric model which uses time-splitting integration techniques (discussed below) to efficiently integrate the Euler equations (Skamarock and Klemp, 2007).

The online ParFlow WRF coupling (PF.WRF) extends the WRF platform down to bedrock by including highly resolved three-dimensional groundwater and variably saturated shallow or deep vadose zone flows, and a fully integrated lateral flow above ground surface (Molders and Ruhaak, 2002; Seuffert et al., 2002; Anyah et al., 2008; Maxwell et al., 2011). The land surface model portion that links ParFlow to WRF is supplied by WRF through its land surface component,

the Noah Land Surface Model (Ek et al., 2003); the standalone version of WRF has no explicit model of subsurface flow. Energy and moisture fluxes from the land surface are transmitted between the two models via the Noah LSM which accounts for the coupling interface, and which is conceptually identical to the coupling in PF-COSMO. The three-dimensional variably saturated subsurface and two-dimensional overland flow equations, and the three-dimensional atmospheric equations given by ParFlow and WRF are simultaneously solved by the individual model solvers. Land surface processes, such as evapotranspiration, are determined in the Noah LSM as a function of potential evaporation and vegetation fraction. This effect is calculated with the formulation:

$$E(x) = F^{fx}(1 - f_{avg})E_{pot} \qquad (2.22)$$

where $E(x)$ stands for rate of soil evapotranspiration (length per unit time), fx represents empirical coefficient, f_{avg} denotes vegetation fraction, and E_{pot} is potential evaporation, determined that depends on atmospheric conditions from the WRF boundary layer parameterization (Ek et al., 2003). The vegetation fraction is zero over bare soils (i.e., only soil evaporation), so Eq. 2.22 becomes:

$$E(x) = F^{fx}E_{pot} \qquad (2.23)$$

The quantity F is parameterized as follows:

$$F = \frac{\phi S_w - \phi S_{res}}{\phi - \phi S_{res}}, \qquad (2.24)$$

where ϕ is the porosity of the medium, S_w and S_{res} are relative saturation and residual saturation respectively, from van Genuchten relationships (Van Genuchten, 1980; Williams and Maxwell, 2011). Basically, F refers to the parameterization of the interrelationship between evaporation and

near-ground soil water content and provides one of the connections between Noah LSM and ParFlow, and thus WRF.

In the presence of a vegetation layer, plant transpiration (length per unit time) is determined as follows:

$$T = G(z)C_{plant}f_{veg}E_{pot}, \qquad (2.25)$$

where $C_{plant}(-)$ represents a constant coefficient between 0 and 1, which depends on vegetation species, and the $G(z)$ function represents soil moisture which provides other connection between the coupled models (i.e., ParFlow, Noah, and WRF). The solution procedure of PF.WRF uses an operator–splitting approach where both model components use the same time step. WRF soil moisture information including runoff, surface ponding effects, unsaturated and saturated flow, which includes an explicitly resolved water table are calculated and sent directly to the Noah LSM within WRF by ParFlow and utilized by the Noah LSM in the next time step. WRF supplies ParFlow with evapotranspiration rates and precipitation via the Noah LSM (Jiang et al., 2009). The interdependence between energy and mass balance of the subsurface, ground surface, and lower atmosphere can be studied fully with this coupling approach. The coupled PF.WRF via the Noah-LSM has been used to simulate explicit water storage and precipitation within basins, to simulate surface runoff and to simulate the land-atmosphere feedbacks and wind patterns as a results of subsurface heterogeneity (Maxwell et al., 2011; Williams and Maxwell, 2011). Studies with coupled model PF.WRF are highlighted in Table 2.2.

2.5.4 ParFlow–Advanced Regional Prediction System (PF. ARPS).

The Advanced Regional Prediction System (ARPS) composed of a parallel mesoscale atmospheric model was created to explicitly predict convective storms and weather systems. The ARPS platform aids in effectively investigating the changes and predictability of storm-scale weather in both idealized and more realistic settings. The model deals with the three dimensional, fully compressible, non-hydrostatic, spatially filtered Navier-Stokes equations (Rihani et al., 2015). The governing equations include conservation of momentum, mass, water, heat or thermodynamic, turbulent kinetic energy, and the equation of state of moist air making use of a terrain-following curvilinear coordinate system (Xue et al., 2000). The governing equations presented in a coordinate system with z as the vertical coordinate are given as

$$\frac{dv}{dt} = -2\Omega \times v - \frac{1}{\rho}\nabla P + g + F \qquad (2.26)$$

$$\frac{d\rho}{dt} = -\rho\nabla . v \qquad (2.27)$$

$$\frac{dT}{dt} = -\frac{RT}{C_v}\nabla . v + \frac{Q}{C_v} \qquad (2.28)$$

$$P = \rho RT \qquad (2.29)$$

Equations (2.26) to (2.29) are momentum, continuity, thermodynamic and equation of state, respectively. The material (total) derivative d/dt is defined as

$$\frac{d}{dt} = \frac{\partial}{\partial t} + \nabla . v \qquad (2.30)$$

The variables v, ρ, T, P, g, F, Q in Eq. (2.26) to (2.29) represent velocity [LT^{-1}], density [ML^{-3}], temperature [K], pressure [$ML^{-1}T^{-2}$], gravity [LT^{-2}], frictional force [MLT^{-2}], and the diabatic heat source [$ML^{-2}T^{-2}$], respectively (Xu et al., 1991). The ARPS model employs high-order monotonic advection technique for scalar transport and fourth-order advection for other variables e.g., mass density and mass mixing ratio. A split-explicit time advancement scheme is utilized with leapfrog on the large time steps, and an explicit and implicit scheme for the smaller time steps is used to inculcate the acoustic terms in the equations (Rihani et al., 2015).

The PF.ARPS forms a fully–coupled model that simulates spatial variations in above ground processes and feedbacks, forced by physical processes in the atmosphere and the below the ground surface. In the online coupling process, ARPS land surface model forms the interface between ParFlow and ARPS to transmit information (i.e., surface moisture fluxes) between the coupled models. ParFlow as a component of the coupled model replaces the subsurface hydrology in the ARPS land surface model. Thus, ARPS is integrated into ParFlow as a subroutine to create a numerical overlay at the coupling interphase (specified layers of soil within the land surface model in ARPS) with the same number of soil layers at the ground surface within ParFlow. The solution approach employed is an operator-splitting that allows ParFlow to match the ARPS internal timesteps. ParFlow calculates the subsurface moisture field at each timestep of a simulation and passes the information to ARPS land surface model, which is used in each subsequent timestep. At the beginning of each time step, the surface fluxes from ARPS that are important to ParFlow include evapotranspiration rate and spatially–variable precipitation (Maxwell et al., 2007). PF. ARPS has been applied to investigate the effects of soil moisture

heterogeneity on atmospheric boundary layer processes. PF.ARPS keeps a realistic soil moisture that is topographically-driven distribution and shows spatiotemporal relationship between water depth, land surface and lower atmospheric variables (Maxwell et al., 2007; Rihani et al., 2015). A summary of current studies involving PF. ARPS is included in Table 2.2.

2.5.5 ParFlow–CrunchFlow (ParCrunchFlow)

CrunchFlow is a software package developed to simulate multicomponent multi-dimensional reactive flow and transport in porous and/or fluid media (Steefel, 2009). Systems of chemical reactions that can be solved by the code include kinetically controlled homogenous and heterogeneous mineral dissolution reactions, equilibrium–controlled homogeneous reactions, thermodynamically controlled reactions, and biologically–mediated reactions (Steefel and Lasaga, 1994; Steefel and Yabusaki, 2000). In CrunchFlow, discretization of the governing coupled partial differential equations which connect subsurface kinetic reactions and multicomponent equilibrium, flow and solute transport is based on finite volume (Li et al., 2007; Li et al., 2010). Coupling of reactions and transport in CrunchFlow that are available at runtimes are performed using two approaches. These are briefly discussed below.

First, a global implicit or one–step method approach is based on a backwards Euler time discretization, with a global solution of the coupled reactive transport equations using Newton's method. This global implicit scheme solves the transport and reaction terms simultaneously (up to two-dimensional) (Kirkner and Reeves, 1988; Steefel, 2009). Second, a time or operator splitting

of the reaction and transport terms which is based on an explicit forward Euler method; the sequential non-iterative approach, SNIA (in which the transport and reaction terms are solved) (Steefel and Van Cappellen, 1990; Navarre-Sitchler et al., 2011). The stability criteria associated with the explicit approach is that the simulation timestep is restricted via the courant-Friedrichs-Lewy (CFL) condition, under the circumstance that the transportation of mass does not occur over multiple grid cell, but a single grid cell in a timestep. Thus, a small-time step must be used to ensure this condition holds. This small step size may lead to simulations that will demand much time to solve Beisman, (2007), so more processors are used, in order to decrease the processor workload and decrease solution time of the simulation. Coupling of fully saturated flow to the reactive transport calculations and coupling between a partially saturated flow and transport (flow and diffusion) can be done successively. However, these simulations require calculations of the flow and liquid saturation fields with a different model.

ParCrunchFlow is a parallel reactive transport model developed by combining ParFlow with CrunchFlow. ParCrunchFlow was designed to be only applicable for subsurface simulation. The coupled model relies on ParFlow's robustness ability to efficiently represent heterogeneous domains and simulate complex flow to provide a more realistic representation of the interactions between biogeochemical processes and non-uniform flow fields in the subsurface than the uncoupled model. ParFlow provides solution of Richards' equation to ParCrunchFlow, which is not present in the biogeochemical code CrunchFlow. ParCrunchFlow employs operator-splitting method to reactive transport, in which the transport and reaction terms are decoupled and calculated independently. Online coupling between the models is achieved through a sequential non-iterative approach, where the reaction terms in CrunchFlow's operator-splitting solver gets

connected to ParFlow's advection terms. ParCrunchFlow takes advanatage of multidimensional advection capability of ParFlow instead of CrunchFlow's advective-dispersive transport capabilities (up to two-dimensional). A steady state governing differential equation for reaction and advection (with no dispersion and diffusion terms) in a single-phase system is given by

$$\frac{\partial C_i}{\partial t} + \nabla.(vC_i) - R_i = 0\,, \quad (i = 1,\ N_{tot}\ ) \tag{2.31}$$

where C_i is the concentration of species i, v represents velocity of flow, R_i indicates total reaction rate of species i, and N_{tot} represents total species number. In the coupling process, the advection terms are calculated by ParFlow's transport solver through a first-order explicit upwind scheme or a second-order explicit Godunov scheme. Low-order upwind weighting schemes can introduce numerical dispersion, which can impact the simulated reactions, and a comparison of several upwinding schemes can be found in (Benson et al., 2017). CrunchFlow calculates the reaction terms using the Newton-Raphson method. For example, in the coupled–model ParCrunchFlow, ParFlow code assigns all hydrological parameters, undertakes the functions relating to parallelization including domain decomposition and message transmission, and solves for pressure and flow fields. The CrunchFlow module is then used to evaluate all reaction terms and conversions between mobile and immobile concentrations. Sequence of simulations of a floodplain aquifer, comprising biologically mediated reduction of nitrate have been performed with ParCrunchFlow. The simulations demonstrate that ParCrunchFlow realistically represents the changes in chemical concentrations seen in most field scale systems than CrunchFlow alone (summarized in Table 2) (Beisman, 2007; Beisman et al., 2015).

2.6 Discussion and Summary

IHMs constitute classes of simulation tools ranging from simple lumped parameter models to comprehensive deterministic, distributed and physically-based modeling systems for simulation of multiple hydrological processes (LaBolle et al., 2003; Castronova et al., 2013). They are indispensable in studying the interactions between surface and subsurface systems. IHMs that calculate surface and subsurface flow equations in a single matrix (Maxwell et al., 2015), scaling from the beginning parts to the mouth of continental river basins at high-resolutions are essential (Wood, 2009) in understanding and modeling surface-subsurface systems. IHMs have been used to address surface and subsurface science and applied questions. For example, evaluating the effects of groundwater pumping on streamflow and groundwater resources (Markstrom et al., 2008), evaluating relationship between topography and groundwater (Condon and Maxwell, 2015), coupling water flow and transport (Sudicky et al., 2008; Weill et al., 2011) and assessing the resilience of water resources to human stressors or interventions and related variations (Maxwell et al., 2015) over large spatial extents at high resolution. Modeling or simulation at large spatial extents e.g., regional and continental scales and resolution e.g., $1km^2$ (**Fig. 2.6**), and even small spatial scale (**Fig. 2.7**) comes with the associated computational load even on massively parallel computing architectures. IHMs, such as ParFlow have overcome the computational burden of simulating or resolving questions (e.g., involving approximating variably saturated and overland flow equations) beyond such levels of higher spatial scales and resolutions. This capability may not be associated with more conceptually based models which, for example, may not simulate lateral groundwater flow or resolve surface and subsurface flow by specifying zones of groundwater network of stream before performing a simulation (Maxwell et al., 2015) For cross-

comparison of ParFlow with other contemporary IHMs, more comprehensive model testing and analyses have recently been done and readers can access these resources at Maxwell et al. (2014), Koch et al. (2016) and Kollet et al. (2017).

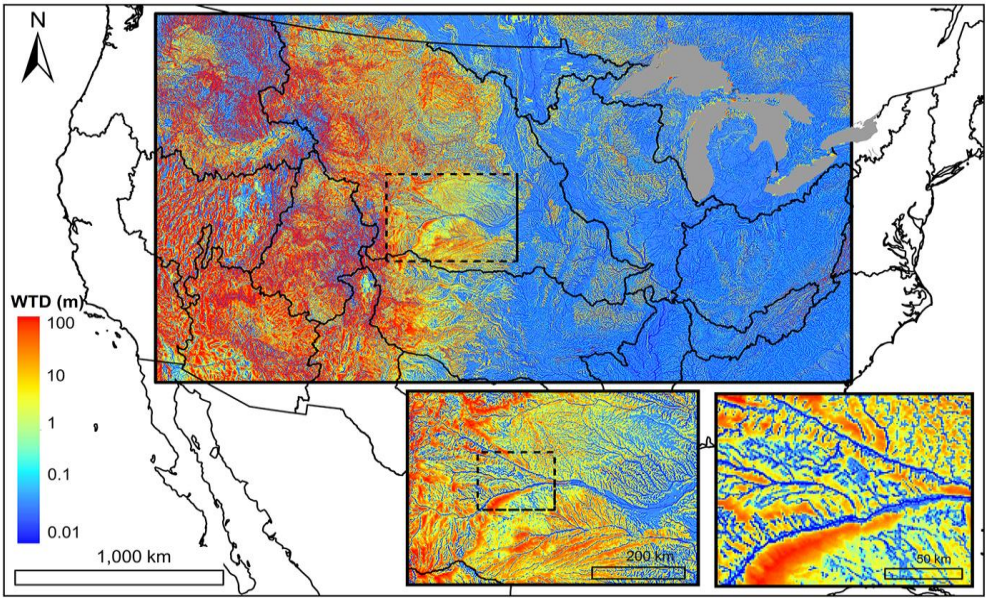

Figure 2.6: Map of water table depth (m) over the simulation domain with two insets zooming into the North and South Platte River basin, headwaters to the Mississippi River. Colors represent depth in log scale (from 0.01 to 100 m) (reproduced from Maxwell et al., 2015). The domain uses 1km^2 grid cells and represents one of the largest, and highest resolution domains simulated by integrated models to date.

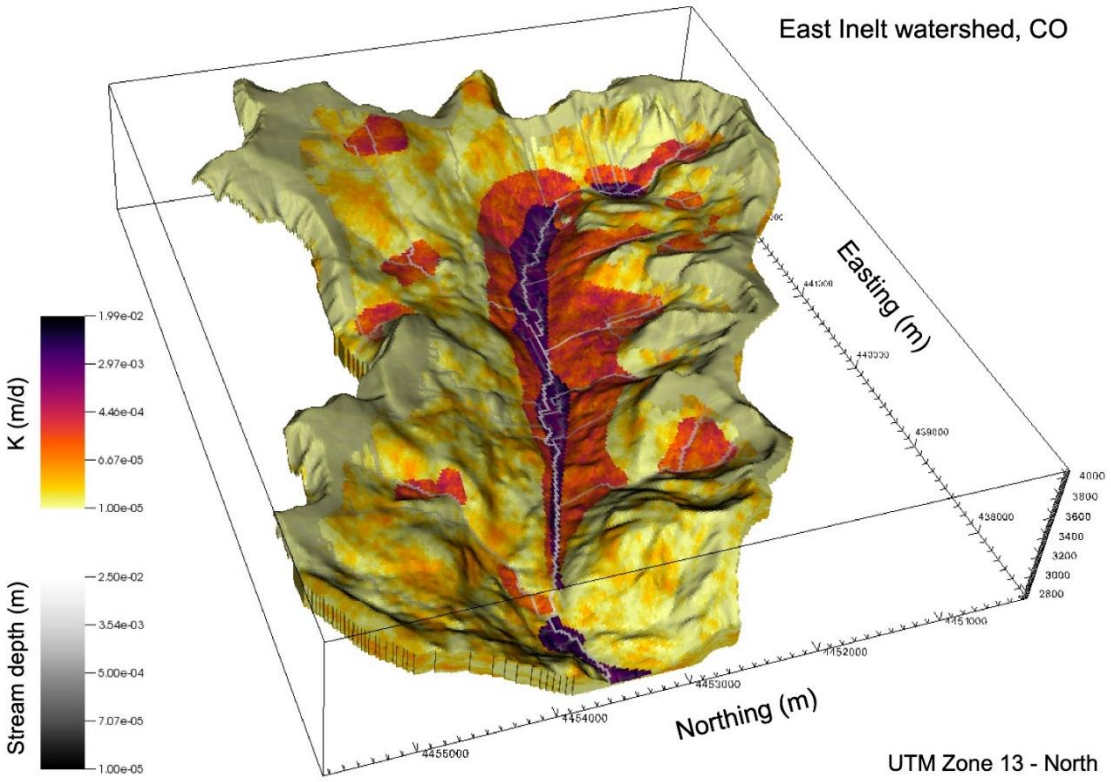

Figure 2.7: Map of hydraulic conductivity (K) and stream depth in the East Inlet watershed in Colorado (Engdahl and Maxwell, 2015). This domain covers 30km^2 using 3.1 million lateral grid cells. The springs emanating from within the hillslopes highlight the realism afforded by integrated modeling at small scales.

ParFlow is based on efficient parallelism (high performance efficiency) and robust hydrologic capabilities. The model solvers and numerical methods used are powerful, fast, robust, and stable, which has contributed to the code's excellent parallel efficiency. As stated earlier, ParFlow is very capable of simulating flows under saturated and variably saturated conditions i.e., surface, vadose, and groundwater flows, even in highly heterogeneous environments. For example,

in simulation of surface flows (i.e. solving the kinematic wave overland flow equations), ParFlow possesses the ability to accurately solve streamflow (channelized flow) by using parameterized river routing subroutines (Maxwell and Miller, 2005; Maxwell et al., 2007, 2011). ParFlow includes coupling capabilities with a flexible coupling interface which has been utilized extensively in resolving many hydrologic problems. The interface-based and process-level coupling used by ParFlow is an example for enabling high-resolution, realistic modeling. However, based on the applications, it would be worthwhile to create one, or several, generic coupling interfaces within ParFlow to make it easier to use its surface/subsurface capabilities in other simulations. Nonetheless, ParFlow has been used in coupling studies in simulating different processes and/or systems including simulating energy and water budgets of the surface and subsurface (Rihani et al., 2010; Mikkelson et al., 2013), surface water and groundwater flows and transport (Kollet and Maxwell, 2006; Beisman, 2007; Beisman et al., 2015; Maxwell et al., 2015), and subsurface, surface, and atmospheric mass and energy balance (Maxwell and Miller, 2005; Maxwell et al., 2011; Shrestha et al., 2014; Sulis et al., 2017). Undoubtedly, such coupled-model simulations come with computational burden and ParFlow performs well in overcoming such problems, even at high spatial scale and resolutions. This capability of ParFlow (coupling with other models) is continuously being exploited by hydrologic modelers, and new couplings are consistently being established. For example, via model coupling, the entire transpiration process could be investigated i.e., from carbon dioxide sequestration from the atmosphere by plants, subsurface moisture dynamics and impacts, to oxygen production by plants. Likewise, land cover change effects on mountain pine beetles may be investigated via coupling of integrated models. But these projected research advances can only be achieved if the scientific community keeps

advancing code performance by developing, revising, updating, and rigorously testing these models' capabilities.

Presently, ParFlow's open-source model and open developer community is fully transparent, and this openness is a major difference between it and other models that has enabled ParFlow to continue evolving. The user community is growing daily across the globe. Code developers have made available, aside from the ParFlow working manual, an active and frequently-updated blog (current blog: "http://parflow.blogspot.com/") and other sources including "https://www.parflow.org" and "https://github.com/parflow" where code developers and experienced users provide great information and suggestions that help in fixing bugs and ease frustrations of other users. Over the years, these easily accessible resources have proven to be helpful. The code is constantly updated through release of new versions with modifications designed to meet varying hydrologic challenges and directions for applications across different scales and fields. Each ParFlow package (version) comes with verified simulation test cases with directions that simulate different real systems and idealized cases. These serve as great resource where additional code modifications have been tested in every release of the code. ParFlow has a clear, rigorous verification procedure to make sure that any changes checked in do not "break" previous developments. This ensures numerical accuracy and backwards compatibility. Moreover, the full suite of test cases is automatically re-run before any submitted change can even be considered for merging with the master branch of the code. The number of branches/forks cannot be controlled in any open source (or community) code, but any contributions to the master branch are exhaustively vetted before being pushed out to users. Further, there is a software development and sustainability plan to improve the capabilities of ParFlow such as incorporation of new

formulations of both kinematic and diffusive wave approximations, and advanced parallelization support (GPU's and heterogeneous compute architectures). ParFlow works very well on different computing architectures and operating systems from "Laptops to Supercomputers" (single CPU, Linux clusters, highly scalable systems including IBM Blue Gene) with the same source code and input on all platforms. The code can use significant computational power and runs efficiently on supercomputing environments (e.g., Edison, Cori, JUQUEEN, and Yellowstone). Through ParFlow hydrologic modelers have available a very efficient yet still growing integrated hydrologic model to simulate and understand surface-subsurface flows.

Code availability

ParFlow is an open–source, object–oriented, parallel watershed flow model developed by community of scientists from the Environmental Protection Department at the Lawrence Livermore National Laboratory (LLNL), Colorado School of Mines and F-Z Jülich with supporting scientists from several other institutions. The current version of ParFlow is available at: https://github.com/parflow/parflow/releases/tag/v3.6.0. The version of ParFlow described in this manuscript is archived on zenodo: https://doi.org/10.5281/zenodo.3555297.

Competing Interest

We declare that no conflict of interest exists whatsoever between any of the authors and the editors or the referees.

CHAPTER THREE

SUSTAINABLE AND EQUITABLE GROUNDWATER MANAGEMENT USING NATURAL AND ARTIFICIAL RECHARGE IN AN ARID, UNCONFINED, REGIONAL AQUIFER

Benjamin N. O. Kuffour[1*] and Nicholas B. Engdahl[1]

This chapter is prepared to be submitted to Journal of Hydrology for Publication. The writing style presented here follows the Journal's prescribed writing format.

Abstract

Many river-dependent aquifers in arid and semi-arid environments are stressed by excessive groundwater abstraction that has led to declining groundwater levels and reduced river flows. One water management strategy has been the use of managed aquifer recharge (MAR) to offset impacts of groundwater pumping on aquifer levels and improve stream flows. The Walla Walla River Basin (WWRB) within the inland northwest of the United States is where excessive pumping has resulted in groundwater level declines and reduced in-stream flows (ISFs). MAR have been established to prevent loss of water, but aquifer levels keep declining across the basin. Studies have suggested additional MAR installations, but because the aquifers are recharged mainly by the WWR, an integrated approach is proposed that includes minimum ISFs requirements to manage the water resources. The core challenge is to estimate how much water must be added to the system to maintain minimum ISFs and reverse groundwater declines, while considering equal benefits to all users. The hydrologic model ParFlow was used to perform numerical simulations to test the response of the aquifer to supplemental MAR scenarios, given required minimum ISFs in the WWR over a 100-year period. The key questions are how much water must be added to the WWR to maintain ISFs for a given amount of MAR and how evenly these benefits are distributed across the basin. Simulation results suggest that maintaining minimum ISFs in the WWR could stabilize the system, but groundwater declines would continue under current MAR conditions. A more balanced solution is to relocate some of the MAR sites downgradient relative to the current sites, which could stabilize the aquifer levels and improve ISFs in the WWR. The results of these simulations show clearly that it is important not just to look at net mass balance

for MAR scenarios but also the likely flow paths that will distribute benefits more evenly to all users.

3.1 Introduction

Groundwater overdraft is one of the most significant problems faced by many of the arid and semi-arid regions of the world today. These water-starved regions are extracting water at unsustainable rates and corrective action is needed to ensure water security and prevent long-term storage loss [*Zinn and Konikow*, 2007; *Konikow*, 2011; *van der Gun*, 2012]. One such region of concern is the inland northwest of the United States (US), where groundwater pumping has resulted in mean annual water level decline of 0.5 m over the last 6 decades [*Russo and Lall*, 2017]. The decreasing water levels from groundwater overdraft have widespread impacts including diminished spring creek flows and reduced baseflow [*Petrides*, 2012], both of which threaten aquatic and riparian environments [*Scherberg et al.*, 2018]. A less obvious problem is that excessive pumping could impair groundwater quality and accelerate salinization [*Bouwer*, 2002], resulting in an unusable aquifer. These and other concerns have motivated efforts to try to mitigate the declining water levels in the region. For example, changes have been made to short-term and long-term water management practices including reduced deliveries to junior water rights holders, reduced river diversions at low stream flows, and the use of engineered systems to artificially add water to the subsurface [*Morris*, 1956; *Mary and Coombs*, 2002; *Scherberg et al.*, 2005; *Fontaine*, 2007; *Scherberg*, 2012; *Petrides et al.*, 2015]. However, the limited extents of these efforts have resulted in minimal impacts at the basin scale; water levels continue to decline in response to excessive pumping, so remedial action is necessary to prevent aquifer extinction.

One of the most direct strategies to mitigate the impacts of overdraft is the use of managed aquifer recharge (MAR) [*Bekele et al.*, 2011; *Petrides*, 2012; *Cahill et al.*, 2015; *Mirlas et al.*,

2015; *Xanke et al.*, 2015]. MAR takes many forms, but it simply means an intentional addition of water to the subsurface in excess of natural recharge to directly support the aquifers, and this is a key difference between MAR and other sources like agricultural irrigation recharge. Options for adding MAR water may include surface water percolation (infiltration) basins, ditches, injection wells, and induced bank infiltration, among many others. All of these options can improve groundwater levels, enhance baseflow to rivers, improve water quality, or have other environmental benefits [*Bouwer*, 2002; *Cey et al.*, 2008; *Racz et al.*, 2012; *Ringleb et al.*, 2016]. In the inland northwest, MAR applications have generally been small or volume relative to the magnitude of pumping, often as mere pilot projects [*Gibson and Campana*, 2014; *Gibson et al.*, 2018]. The limited size means most of the benefits have likely not been fully realized, but there is also the lesser mentioned issue of stakeholders benefitting unevenly [*Barber et al.*, 2009; *Petrides*, 2012; *Pagel*, 2016; *Patten*, 2017]. For example, users pumping too far away from MAR sites might not see improvements in their water levels [*Scherberg, et al.*, , 2005; *Scherberg*, 2012; *Scherberg et al.*, 2018], or specific benefits may take precedence over others, like prioritizing in-stream flows over agricultural users' needs. This implies that factors beyond the total net recharge volumes can have profound influence on the perceived success of a MAR system and that a more holistic view is necessary to achieve a reasonable balance.

The Walla Walla River Basin (WWRB) (**Fig. 3.1**) is a place where these challenges are exposed in plain sight because it is a highly productive region of irrigated agriculture that suffers from long-term aquifer declines and has seen reductions in stream flows. The Walla Walla River (WWR) is hydraulically connected to the aquifer and the prolonged pumping has, causing several periods where flows have fallen below the minimum required ISFs of 0.71 m^3/s [*Mahoney et al.*,

2009; *Scherberg et al.*, 2014, 2018]. This is especially concerning because the aquifers are believed to be recharged mainly by the WWR, supplemented by snowmelt from surrounding highlands [*Bower and Lindsey*, 2010]. The WWRB has attempted over a dozen pilot and full-scale studies to artificially recharge the groundwater system using infiltration basins and galleries [*Bower and Lindsey*, 2010; *Bower et al.*, 2011; *Gibson and Campana*, 2014; *Scherberg et al.*, 2014; *Petrides et al.*, 2015; *Patten*, 2017; *Gibson et al.*, 2018]; however, most of these were limited to short-term tests or persist with recharge volumes far below those being extracted. Consequently, previous MAR efforts have not managed to stop the declining water levels or restore the river to a sustainable level. Furthermore, the recharge projects that were implemented have not provided downgradient users with the same benefits as those closer to the MAR sites. This imbalance in the distribution of benefits from the applied water in the basin have caused irrigated agriculture activity (e.g., Gardena Farms spring alfalfa growers) further downstream to rely almost entirely on winter soil moisture storage using water supplied from the WWR to meet their water needs. The concern is that if these diversions are halted due to low flows in the WWR, groundwater may have already dropped too far to be an economically viable alternative and these downgradient users will lose their livelihoods instead of benefitting from MAR [*Patten*, 2014, 2017; *GeoSystems Analysis Inc.*, 2015].

Because the WWR and its underlying aquifer are hydraulically connected, aquifer declines will increase river loss, so a holistic management approach needs to be adopted to sustain both the aquifer and the WWR. The difficult question presented by the WWRB is, how to maintain minimum ISFs requirements year-round while providing sufficient MAR to halt or reverse groundwater declines across the entire basin? A conventional approach would be to explore

options for adding MAR sites throughout the basin to balance out declines [*Scherberg et al.*, 2014, 2018]. Each MAR site comes with a cost meaning that it is usually desirable to put in the minimum number of sites that can add the large volumes of water; however, this can only be effective if MAR sites have broad areas of influence. Topography and flow paths in the WWRB mean that its MAR sites tend to have narrow, localized regions of influence, only compounding as the recharge nears the river, so the number of dedicated MAR sites needed to cover the basin evenly would be vast and costly. Recognizing the profound role the river plays in this system, and its ISFs requirements, we suggest that an alternative approach might be feasible that reduces the number of MAR sites yet provides nearly equal benefits to all users. The central hypothesis is that the WWRB aquifer can be stabilized simply by maintaining at least the minimum ISFs in the WWR; in other words, add water to the river and it naturally provides a large, distributed body for MAR. However, the topography of the basin clearly implies that this will not achieve uniform benefits to all stakeholders and would force some to drill deeper to access what will have become a much deeper aquifer. To minimize the loss of water to stakeholders (either by loss of access or economic infeasibility), we suggest a more balanced approach is to add some recharge water to the river and some at targeted locations within the basin to provide water more evenly to stakeholders. We use numerical models of the WWRB to simulate how the system will respond, assuming minimum ISFs are maintained, and how the aquifer is impacted by several supplementary MAR scenarios. The metrics used to assess these scenarios over a 100-year simulation period are basin wide water levels, the uniformity of water levels and water level changes, which determines how water users across the basin would benefit in each scenario, and the flux from the river, which dictates the

volume of water that must be added to the river to maintain the minimum ISFs and how to balance additions between in-basin MAR sites and supplemental river flows.

The results of the simulations show that maintaining minimum ISFs in the WWR could stabilize the system, but aquifer levels would continue to decline under current MAR conditions. Reducing the number of MAR sites and maintaining minimum ISFs in the WWR would result in mean DTW declines of up to 0.1 m in the downgradient regions of the basin relative to the current MAR conditions, meaning that deeper wells would be needed if a reduced MAR approach is employed. However, aquifer levels generally would stabilize or increase if the minimum ISFs are maintained in the WWR, and some MAR sites are relocated in the basin instead of the current locations. In addition, MAR must be done at maximum recharge volumes for the individual sites to cause the increase in aquifer levels across the basin. The novelty of this study, relative to other MAR studies in the region, is that this study employed an integrated approach where equivalent MAR volumes in the basin were taken and redistributed more evenly across the basin while requiring that minimum ISFs are met for the WWR. The major benefits of this approach are that it provided a way to achieve a more balanced aquifer recharge with improved baseflow to the WWR. The implication for other regions is that basins recharged by losing streams, or streams that become losing under excessive pumping, may be mitigated more effectively by prioritizing the stream, then supplementing that recharge with MAR, instead of focusing on MAR to improve ISFs.

3.1.1 Water Rights and Meeting Minimum ISFs

In 1989, the Washington State legislature passed numerous key provisions that allow the Department of Ecology (DOE) to acquire water rights on voluntary basis and hold that water in trust to improve ISFs to enhance fish migration and provide water for irrigation, municipal and other beneficial uses [*Ebeling et al.*, 2019]. Water right acquisitions have been effective in restoring many streams and river flows, but extreme low flows in some of the state's river basins remain due to water withdrawals, impoundments, and land use changes. In the Walla Walla River Basin (WWRB), water right is over appropriated (i.e., water rights have been issued for more water than is available). This has historically led to seasonal patterns of low ISFs and dry years in the WWR, as irrigators try to meet their demands [*Robinson*, 2016].

Several water acquisitions tools (e.g., water right leasing and purchasing) and innovative measures (e.g., market exchanges or water banking, auctions, source water substitution and drought-year leases) are continually tested and employed to increase ISFs. For example, the threat to Endangered Species Act works towards a more sustainable equilibrium by purchasing water rights from irrigators and placing them into Washington State's Trust Water Right Program to allow a certain ISFs to be protected. Water banking constitutes institutional mechanism that aids the legal transfer and market exchange of surface water, groundwater, and storage entitlements. Specific functions of market exchange may include handling administrative water right transfers, setting prices, matching buyers with sellers, setting rules and criteria for market exchange transactions, and certifying the legality of water rights [*Cronin et al.*, 2012]. The development of water exchanges or markets in the Washington's southeast corner and Oregon has been an

important progress of the long-lasting water right transfer process. The WWRB has water market that provides mitigation exchange credits for any new permit-exempt groundwater uses within the basin.

The market exchange of water to increase ISFs in the basin is limited, despite growing interest and support by local, state, federal, tribal, and private entities in using market-based incentives to find water. One of the most challenging tasks in acquiring water rights to improve ISFs is finding willing sellers [*Adelsman*, 2003]. There are couple of ways that could be useful to meeting the minimum ISFs in the WWR assumed in this work. 1) there needs to be continual advocacy for maintaining ISFs that provides benefits or prioritizes endangered fishes, 2) out-of-stream water right holders should be willing to enter into transaction with interested buyers who prioritizes the ISFs. 3) The alternative could be for the WWRB to purchase water right from the Columbia River to augment ISFs in the WWR or use that water to complete MAR in the basin. However, these efforts may come with the associated challenges such as extent and duration of ISFs problems including drought years and summer low flows, available funding, and acceptance by water right owners or holders and communities of ISFs needs that need to be evaluated by the basin.

3.2 Study Area

3.2.1 Geography and Climate

The WWRB occupies an area of approximately 4,455 km^2 within southeastern Washington and northeastern Oregon, US [*Petrides*, 2008, 2012], but most of the basin (73%) lies within Washington. The WWRB is bordered to the south by the Horse Heaven Hills. The main physiographic features of the basin's landscape include rolling foothills, lightly timbered mountains, incised areas of streams and rivers, lined and unlined canals, and Palouse prairie, which covers most of the land area. The WWR is a perennial tributary of the Columbia River fed by snowmelt from the basin's adjacent highlands i.e., the Blue Mountains. The WWR and its key tributaries including Mill Creek and Touchet River flow a total distance of about 3,949 km along the larger streams and tributaries [*Mendel et al.*, 2005]. The WWR is the main recharge source to the shallow alluvial aquifer and serves as a habitat for several endangered species including salmon fisheries, bull trout, and steelhead [*Schwarzenegger*, 2005; *Petrides*, 2008]. The subarea considered for simulation encompasses 518 km^2 bordered to the south by the Horse Heaven Hills, and from southeast to northeast (46° 00' N 118° 32' W) by the Walla Walla River (WWR), which flows westward. The stretch of the WWR within the simulated area is approximately 48 km (**Fig. 3.1**) [*Mary and Coombs*, 2002; *Scherberg et al.*, 2005].

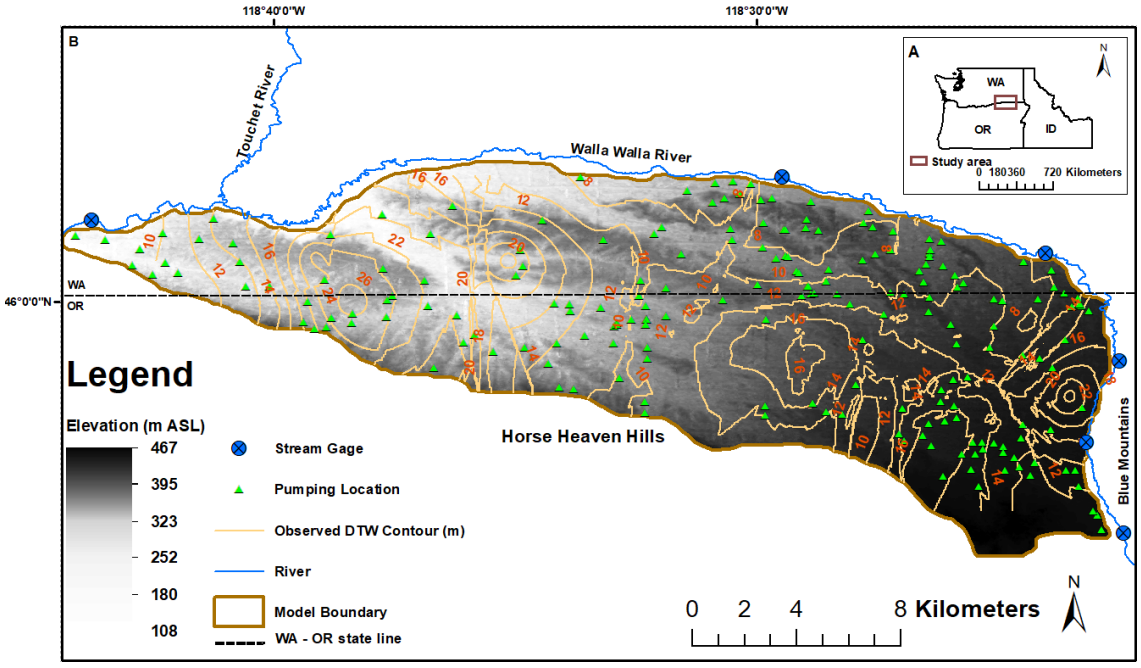

Fig. 3.1: A: Location of the study area within inland Pacific Northwest, B: Location of simulated area within the Walla Walla River Basin showing stream gages on the WWR, digital model elevation (DEM), groundwater pumping wells, and average observed DTW contour in 2020 at the start of the base-case.

Peak flows in the mainstem WWR and the smaller streams on the Blue Mountains are created by seasonal mountain snow peaks, spring runoff and heavy rainfall events [*Petrides*, 2012; *Scherberg et al.*, 2014]. The annual mean flow in the WWR is approximately 16.6 m^3/s, ranging from lows of 4.7 m^3/s to highest flows of 34.3 m^3/s (https://waterdata.usgs.gov/nwis). Precipitation in winter and spring months largely falls as snow with a total annual average of 430 mm. The lowest precipitation occurs in the summer months and cumulative totals from July to September are 38 mm, on average. High temperatures in the basin occur in July and August with an average daily maximum of 32 °C [*Scherberg et al.*, 2014]. About 87% of the precipitation falls within the

non-irrigation seasons, between the months of October and May. [*Schwarzenegger*, 2005; *Petrides*, 2012].

3.2.2 Land Use

Land use in the basin consists of urban areas (i.e., residential, and industrial settlements), irrigated agriculture, and native and riparian vegetation. About 79% of the area is allocated for agricultural activities including crop fields and grazing, with approximately 15% forestland, and the remainder is urban. Large proportions of the agricultural lands are covered by livestock and crops/vegetation such as alfalfa, wheat, peaches, apples, orchids, grapes, native grasses, and pasture. Irrigation water demands in the basin are primarily met by diversions from the WWR, with high amounts of groundwater pumping during low river flows [*Gibson and Campana*, 2014]. The Oregon Department of Water Resources estimated the annual irrigation and domestic water demands across the WWRB to be close to 141 and 2.0 million m^3, respectively. Generally, water demand for anthropogenic uses (e.g., water for both irrigated agriculture and domestic uses) in the basin are supplied with a 53% mixture of surface water diversions and the remaining 47% is pumped from groundwater [*Wozniak*, 2007; *Petrides*, 2008].

3.2.3 Hydrogeology and Geological Setting

Groundwater movement in the basin generally follows the topography. Groundwater flow from east to west, and piezometric contours also suggest northwesterly flow away from the mountain block [*Bower et al.*, 2011; *Patten*, 2017]. Groundwater occurs within two distinct aquifers: a deep

basalt aquifer made from series of lava flows that overlies the basement rocks, and a shallow gravel aquifer made of layers of glacial outwash and alluvial sediments [*Scherberg et al.*, 2014]. The volcanic activity that formed the basaltic material spanned 11 million years between the periods from 17 to 6 Ma, characterized by short periods of intense lava flows and long, dormant periods between flow events [*Vaccaro et al.*, 2015]. The basalt aquifer underlies the entire WWRB and has an estimated thickness ranging from 1 km to more than 10 km [*GSI Water Solutions*, 2007; *Lindsey*, 2007; *Ely et al.*, 2014; *Vaccaro et al.*, 2015]. The widespread basalt aquifer has limited hydraulic connection to surface water sources (e.g., WWR and its tributaries) and the deep recharge supplying the basalt aquifer is thought to be from the mountain blocks. Indirect hydrologic connection exists between portions of the alluvial aquifer and the topmost water-bearing areas of the underlying basalt aquifer where flow of water from the alluvial aquifer to the basalt aquifer is likely to occur [*HDR Engineering Inc.*, 2009; *Petrides*, 2012]. The basalt aquifer is less productive than the shallow alluvial aquifer within the basin, so it has seen little use [*Petrides*, 2008].

The shallow alluvial aquifer is composed of clastic layers that accumulated during the Quaternary and pre-and post-Pleistocene cataclysmic flooding, the Mio-Pliocene, and following the end of the basaltic material volcanism [*Price*, 1960; *GSI Water Solutions*, 2007; *Robinson*, 2016]. The Mio-Pliocene deposits are composed of three units: upper coarse unit (an indurated, weathered, basalt lithic sand, silt, and gravel of up to 185 m thick); fine unit (weakly indurated, micaceous claystone and siltstone with intercalated sand and gravel); and basal coarse unit (an interbedded micaceous sand in indurated siltstone and claystone) which covers the top of the basalt

at different locations in the basin. The 90 m thick Mio-Pliocene basal coarse unit is at the bottom of the 150 m fine unit and a 180 m thick coarse unit lies at the top of the 150 m fine unit. The fine and the laterally discontinuous basal coarse units can provide productive volumes of groundwater but the Mio-Pliocene coarse unit is the main water bearing unit in the basin [*Lindsey*, 2007; *Petrides*, 2012; *Scherberg et al.*, 2014]. The Quaternary deposits comprise a fine unit and a coarse unit. The coarse unit which is composed of uncemented basalt lithic sand and gravel materials that overlay the Mio-Pliocene coarse unit (the Ringold Formation-a sequence of continental clastic sediments). The Quaternary coarse unit is highly conductive and ranges from less than a meter to more than 61 m thick. The top of the coarse unit is usually found within the upper few meters of the alluvial aquifer. The fine-grained Quaternary unit is mainly made up of silts and fine sands, and loess including the Touchet beds deposited by flooding and eolian processes. The unit extends from less than a meter to over 130 m thick forming a substantial part of the vadose zone across the WWRB. The fine unit is unconfined and is generally thought to have hydraulic conductivity values on the order of less than 10^1 m. The fine unit is absent in large parts of the basin and do not form a confining unit, so the coarse unit is thought to be the dominant member of the unconfined aquifer [*Reidel et al.*, 1989; *Lindsey*, 1996, 2007; *Bower and Lindsey*, 2010].

3.2.4 Basin Water Management

Current water management practices in the basin aim to minimize the continuous declines in groundwater levels while meeting established streamflow targets [*Bower et al.*, 2011; *Gibson and Campana*, 2014; *GeoSystems Analysis Inc.*, 2015]. The estimated annual amount of 143 million

m^3 of water are pumped mostly by irrigation districts including the WWR Irrigation District, the Hudson Bay District Improvement Company, and Gardena Farms Irrigation District to meet their crop water demands [*Wozniak*, 2007; *Petrides*, 2008]. Historic data shows that groundwater elevations have declined 4.8 cm/year, on average, between 1950 and 2012 in response to the high pumping rates [*Bower and Lindsey*, 2010; *Petrides et al.*, 2015; *Patten*, 2017; *Gibson et al.*, 2018]. Increasingly common low stream flows and degradation to fish habitat caused local water managers to develop a collaborative program to better manage the water resources in the basin. In 2000, as part of the water management program, stakeholders including the WWR Irrigation District, the Hudson Bay District Improvement Company, and Gardena Farms Irrigation District made an agreement to allow for minimum flows of 0.71 m^3/s (average of 2 m river stage) along the WWR in normal years. During extreme dry seasons, downstream minimum flows in the river were required not to be less than 0.51 m^3/s. The in-stream flow agreement was intended to maintain flows in the river throughout the year [*Mendel et al.*, 2005; *Petrides*, 2008, 2012] but this has not always been the case and mean daily flows have been zero (https://waterdata.usgs.gov/nwis). In 2004, a series of artificial recharge (i.e., MAR) pilot systems were installed to improve aquifer levels and baseflow to the WWR, but the MAR systems have not been able to improve ISFs and reverse the declines in aquifer levels across the basin.

Many studies have explored opportunities to improve the efficiency of the artificial recharge operations to reverse the declining aquifer levels. *Petrides*, [2012] performed field testing with a chemical (Bromide) tracer to evaluate the feasibility of MAR to restore depleted aquifer levels and analyzed groundwater travel time from infiltration basins to groundwater wells and springs within

the basin. The study detected high groundwater flows (i.e., 60 m/day) from the infiltration basins to the targeted springs and groundwater wells in the basin; however, this could be a high estimate if preferential flow paths were encountered. This suggests that a basin-wide implementation of MAR would be efficient in restoring groundwater levels, but large scale MAR could be expensive and with an added requirement to meet minimum in-stream flow a more integrated approach would be beneficial. *Scherberg et al.* [2014] used the Integrated Water Flow Model (IWFM) to compute the basin's shallow groundwater and surface conditions under water management scenarios with varying water use, MAR, and river flows. The study predicted a mean increase of 1.5 m groundwater elevation over a period of 10 years under maximum (additional) MAR implementation compared with no MAR conditions. *Scherberg et al.* [2018] developed a numerical groundwater-surface water model to perform a 10-year simulation of five water management scenarios to predict future water conditions in the basin. The results from *Scherberg et al.* [2018] suggest that converting all canals to pipes and increasing MAR applications (from 11.1 million m^3/year to 29.9 million m^3/year) in the basin relative to the basin's MAR system can allow for increased summer flows in the WWR while stabilizing groundwater storage levels. However, piping the canals with no MAR system would result in low summer flows and declining groundwater storage.

3.3. Methods

3.3.1 Governing Equations and Simulation Tool

The approach herein uses numerical simulation of the WWRB to determine whether or not it is reasonable to expect that the aquifer can be stabilized simply by maintaining at least the minimum ISFs in the WWR, perhaps supplemented by MAR. The physically-based, integrated hydrologic simulation platform ParFlow was chosen for this study [*Ashby and Falgout*, 1996; *Kollet and Maxwell*, 2006]. ParFlow solves the mixed form of Richards' equation for variably saturated flow in three dimensions given as

$$S_s S_w(p) \frac{\partial p}{\partial t} + \phi \frac{\partial (S_w(p))}{\partial t} = \nabla . \boldsymbol{q} + q_s, \qquad (3.1)$$

where S_s is the specific storage coefficient [L^{-1}], S_w is the relative saturation [$-$] as a function of pressure head p of the fluid/water [L], t is time [T], ϕ is the porosity of the medium [$-$], and q_s is the general source/sink term [T^{-1}] (includes wells and surface fluxes e.g., evapotranspiration). A terrain following grid (TFG) transform [*Maxwell*, 2013] was used in this study. A TFG is a simulation grid that conforms to surface topography, which reduces inactive cells above and below a domain to improve performance. The TFG transformation is made within the Darcy flux term, $\boldsymbol{q}$ [LT^{-1}] as:

$$\boldsymbol{q} = -k_s k_r(p)[\nabla(p + z)\cos\theta_i + \sin\theta_i], \qquad (3.2)$$

where k_s is the saturated hydraulic conductivity tensor [LT^{-1}], k_r is the relative permeability [$-$] which is a function of pressure head, z is depth below the surface [L], θ_i denotes the angle [$-$] of topographic slope, and where the subscript i represents the direction of flow x or y. [*Maxwell et*

al., 2015; *Kuffour et al.*, 2020]. ParFlow solves the nonlinear system of equations using a globally implicit approach that employs a parallel, multigrid based Newton-Krylov technique, which allows fully-coupled solution of the surface-subsurface flow systems [*Jones and Woodward*, 2001]. The highly nonlinear functions that characterizes changes in permeability and saturation with pressure i.e. relative permeability and saturation functions may be described, for example, by the *VanGenuchten* [1980] relationships. In this study, the standard Van Genuchten relationships are used to describe the relative saturation and permeability functions, which can be found in [*Kuffour et al.*, 2020].

3.3.2 Model Structure

The CSM for this study describes the aquifer as a system of five layers covering an area of 518 km^2 that extends to a maximum depth of 750 m below land surface. The layers represent the five sedimentary geologic units of the alluvial deposits and extend to the upper water-bearing portions of the basalt aquifer formation. The layer representing the bottom Mio-Pliocene basal coarse unit was extended to include a portion of the basalt deposits to capture the influence the groundwater pumping wells screened in the basalt aquifer have on the simulated region; pumping from the basalts is less than 20% of the total annual pumping which justify the need to include the basalt portion as part of the model. The thickness of each geologic unit was determined using 1,800 driller's logs data prepared by *GSI Water Solutions* [2007]. Inverse distance weighting (IDW) interpolation was used to interpolate each unit's logs data into a laterally continuous surface. IDW was used here instead of semi-variogram based (i.e., kriging) or other geostatistical methods

because the dataset is large and well-distributed throughout the basin, and the units are thought to be, generally, laterally extensive because of their lacustrine-like origins.

3.3.3 Numerical Model Boundary Condition

The basic assumption behind the proposed management strategy is that the minimum ISFs in the WWR must be maintained. Flows will be higher at times during the year, so this assumption represents the minimum amount of expected river flow gain/loss to the aquifer. As such our results will represent a "worst case" scenario estimate based on meeting the minimum legal requirements but is also a reasonable starting point from a numerical standpoint given the lack of information about fluxes into and out of the WWR along the simulated area. The WWR is represented along the northern and eastern boundaries of the numerical model domain (**Fig. 3.1**). A constant head 2m below the land surface was set along the river boundary based on the average observed head in the WWR for the numerical model under the minimum ISFs depth. The WWR flows in an incised channel, so it is below the land surface; land surface elevation is used as the top of the simulation domain, hence the recessed boundary. The constant head (Dirichlet) boundary was defined in the model to ensure that the average river stage in the WWR was captured in the numerical model. **Table 3.1** provides a summary of all model geometry, boundary conditions, and hydraulic properties in the model.

Table 3.1: Model Geometry, Boundary Conditions, and Basin Hydraulic Parameters used in the Model.

Model Geometry		
Lateral extensions in x and y	37 km and 14 km	
Vertical extension in z	750 m below land surface	
Lateral and Vertical resolutions	dx:100 m, dy: 100 m, and dz: 150 m	
Boundary	**Boundary Condition**	**Value**
Subsurface Top Boundary	Constant Flux	5.86×10^{-5} m/d
Subsurface Bottom Boundary	No Flow	Zero
North and East (River Boundary)	Constant Head	2 m river head
South (Mountain front) Boundary	Constant Flux	$0.0045\ \mathrm{m}^3/\mathrm{s}$
West Boundary	General Head Boundary	2 m below land surface
Initial Conditions		
Hydraulic Pressure fields from Calibrated model	Calibrated conditions	
Saturation		
Residual and Saturated saturation	0.14 and 1.0	
Slope and grid type	Topographic slope; Terrain following	
van Genuchten parameters (domain-wide)	$\alpha = 3.548$; $n = 4.162$	
Simulation period	100 years	
Time step size	Week	

The Horse Heaven Hills Mountain block cover a large portion of the WWRB to the south of the simulated area (**Fig. 3.1**). Recharge from the Horse Heaven Hills Mountain block boundary into the model area was specified as a constant flux (Neumann boundary condition). Subsurface inflow of groundwater into the model area from the adjacent mountain block was estimated as a product of the net surface recharge over the mountain block and the surface area of the mountain block at the boundary of the modeled aquifer system. The assumption is that steady-state, piston flow occurs in the mountain block since there is no pumping and no significant withdrawal outside

the low elevations of the basin. This approach provides a reasonable estimate of mountain block recharge considering that no characteristic hydraulic conductivity distributions exist for the mountain block and there are no estimates of modern recharge rates.

The western edge of the model domain was set as a general head boundary and was given a reference head value corresponding to the head in the river external to the model domain (**Fig. 3.1**). Groundwater is believed to flow into and out of the model domain at the western boundary.

The bottom of the model was defined as a no-flow boundary, which is consistent with the conceptual model because the basalt aquifer sits on impermeable bedrock; some leakage into the deeper aquifer is possible but this is not thought to contribute significantly to regional flow dynamics; the permeability contrast between the basalt and alluvial aquifers alone implies that all flow is mostly lateral.

Net surface recharge in the model area was estimated to be the difference between precipitation and evapotranspiration. Long-term projection of the net surface recharge was estimated from *Roderick et al.* [2014]. The net surface recharge was assumed to be spatially constant (uniform) flux at the top layer of the domain.

Seepage from irrigation agriculture in the basin is considered to be minimal because close to 95% of all irrigation canals and ditches in the basin are lined and the Walla Walla Basin Watershed Council (WWBWC) is considering lining all canals in the near future [*Patten*, 2017; *Scherberg et al.*, 2018].

3.3.4 Model Parameterization and Calibration

The simulations started with a spin-up process to obtain equilibrium or steady-state predevelopment conditions, followed by transient flow modeling or calibration to bring the domain closer to modern conditions that includes present day groundwater pumping. The boundary conditions specified above were used throughout the model simulations, but pumping wells were added for the transient model. Initial parameter values including hydraulic parameters (e.g., hydraulic conductivity, specific storage, and porosity) for the steady-state model were based on Soil Survey Geographic Database (SSURGO) classification for soils and *Scherberg et al.* [2018] from the simulated area. The model was then run forward in time until steady state groundwater levels were achieved.

A transient calibration followed the steady-state calibration to estimate the parameters of the transient model. The data for the calibration were the locations and meter readings of yearly withdrawal rates of the 220 wells within the period of 2015 and 2020, which were obtained from the Washington State Department of Ecology (DOE) and Oregon Water Resources Department. A major complication to these efforts was that data on the screened intervals were not part of the archive. As such, screened intervals were estimated based on knowledge of the most conductive hydrogeological units of the aquifers because anthropogenic users are unlikely to complete a well in an unproductive region of the aquifer. Calibration targets were placed in the same locations as the current observation wells in the basin in the estimated screened intervals and wells with available records were used. These water level data were collected and managed by the Walla Walla Basin Watershed Council (https://www.wwbwc.org/monitoring/groundwater). The

transient calibration was performed by manually using Jacobian informed (perturbation) methods to adjust the subsurface flow controlling parameters including the hydraulic conductivities and specific storage coefficients of the geologic units (**Table 3.2**).

Table 3.2: Calibrated model hydraulic parameters used in the model.

Geologic Layers	**Permeability (m/d)**	**Porosity**	**Specific Storage**
Quaternary fine (top layer)	0.29	0.43	4.60×10^{-6}
Quaternary coarse	2.16	0.42	1.00×10^{-4}
Miopliocene coarse	1.05	0.43	6.20×10^{-5}
Miopliocene fine	0.48	0.37	9.50×10^{-6}
Miopliocene basal coarse and water-bearing upper unit of basalt	0.29	0.35	1.00×10^{-5}

Simulations were sequentially updated until the simulated depth to groundwater table closely matched the observed depth to groundwater table from 3,702 weekly observation well data points measured across the simulated area between the years 2015 and 2020. The transient calibrated model showed good agreement to observations as shown in **Fig. 3.2**.

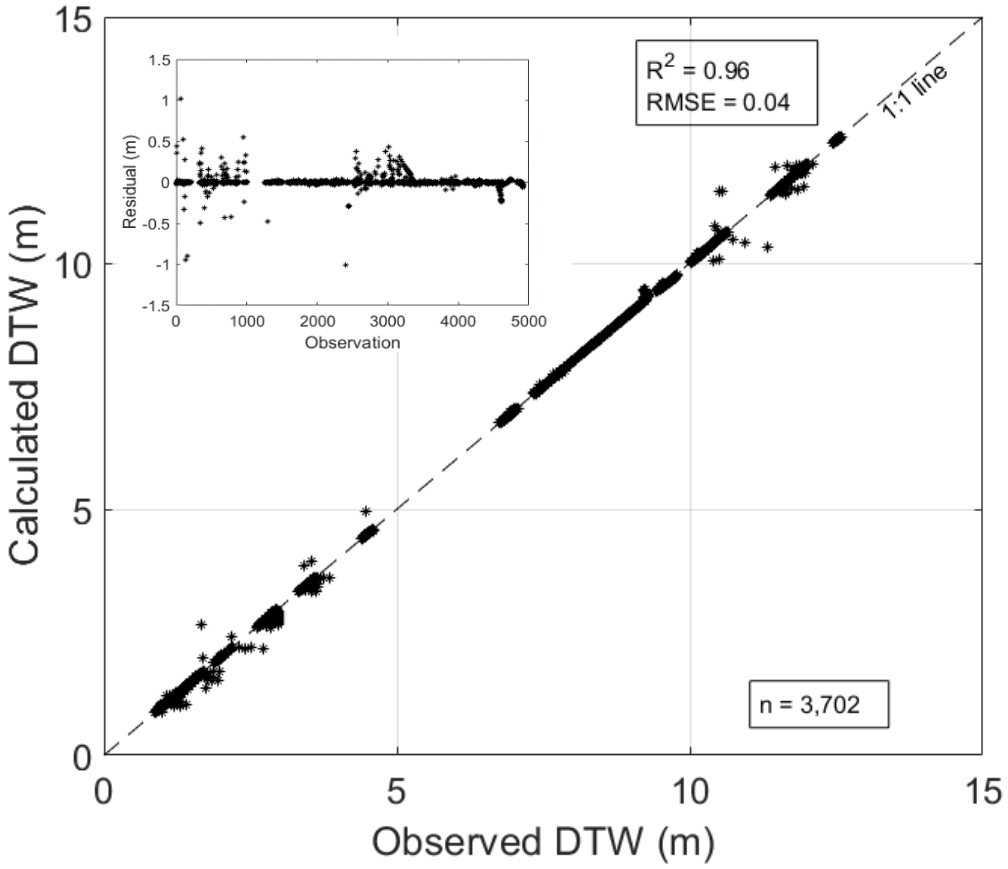

Fig. 3.2: Plot of observed versus calculated depths to groundwater (DTW) from the calibrated model. A total of 3,702 weekly DTW data points (n = 3,702) from observation wells measured from 2015 and 2020 in the simulated area. The insert is a residual plot for the observed and calculated DTW.

3.3.5 MAR

The WWRB managers implemented recharge systems using artificial infiltration basins and buried perforated conduits (galleries) to augment groundwater recharge, stabilize aquifer levels across the basin and improve baseflow to the WWR [*Patten*, 2014; *Scherberg et al.*, 2014]. However, the MAR system as currently implemented has not reversed the declining aquifer levels nor boosted ISFs across the basin, so a more balanced approach is needed that offers equal benefits to all users. The key questions are i). how much water must be imported, ii) and where should it be applied to provide "balanced benefits" (increase aquifer levels across the basin and ISFs in the WWR) to all water users? The options could be to add water to the WWR and supplement that with MAR, to prioritize only the WWR to recharge the aquifer, or to focus exclusively on MAR away from the river. MAR scenarios were designed to test some of the ways these options could be implemented.

The impacts of the MAR were first assessed in terms of basin-wide mass balance. A complete water balance was calculated to quantify the groundwater and surface water flux to identify the flux from the WWR. The global mass balance for the system is:

$$Q_{river} = \frac{dV_{aq}}{dt} - \left(Q_{net\,surf} + Q_{mt} + Q_{mar}\right) + Q_{pump} \qquad (3.3)$$

where Q_{river} [L^3T^{-1}] is the fluxes/recharge from the WWR into the model area, V_{aq} [L^3] is the volume of the aquifer, $Q_{net\,surf}$ [L^3T^{-1}] represents the net surface recharge flux (precipitation minus evapotranspiration) over the simulated area, Q_{mt} [L^3T^{-1}] is adjacent mountain block

recharge, Q_{mar} [L^3T^{-1}] is the flux from the artificial recharge systems, and Q_{pump} [L^3T^{-1}] denotes the groundwater pumping rate. Equation (3.3) is written this way because the fluxes from the WWR must be computed (all other terms are known or easily calculable) and this is also one of the key assessment metrics for the comparative scenarios. The WWR is a Dirichlet boundary so the flux along the boundary will vary over time as groundwater heads change. The flux could be approximated from Darcy's Law, or Richards' equation, but doing so would require approximating gradients and integrating them along the river to produce the net flux. Eq. (3.3) is already based on easily computed or known quantities and is less prone to errors, so it is a simple and effective way to identify the river flux, which is the proxy for how much water would be required to meet the minimum ISFs and will also differentiate gaining/losing conditions.

3.3.5.1 MAR Site Placement

The Walla Walla Basin has 16 existing MAR sites within the simulated area and the base-case model assumes that no additional sites are created. Though not all are currently active, plans exist to put all into use in the near future [*Patten*, 2014, 2017]. MAR sites were implemented in the model using the sites dimensions/sizes and specifications for each MAR site in the basin, as designated by the WWBWC (https://www.wwbwc.org/aquifer-recharge-projects/).

The simulation area was demarcated into five zones to capture how the different regions of the basin respond to the MAR. These zones also provide natural grouping of the basin by geographic regions defined based on physical characteristics, such as near the mountain front (high

elevation areas), near the WWR, massively pumped or irrigation districts (farming zones), and even areas without MAR installations that would yield improved baseflow and stabilized or increased groundwater levels. For example, the westside of the basin with no current MAR sites was considered as Zone 1 (**Fig. 3.3**), which is a farming zone (i.e., Gardena Farms Irrigation District). Zone 1 was useful to further assess the impacts of the WWR and MAR on groundwater levels farther away from each of the current MAR sites in the basin. The MAR sites within each zone were categorized as belonging to that zone during the simulation.

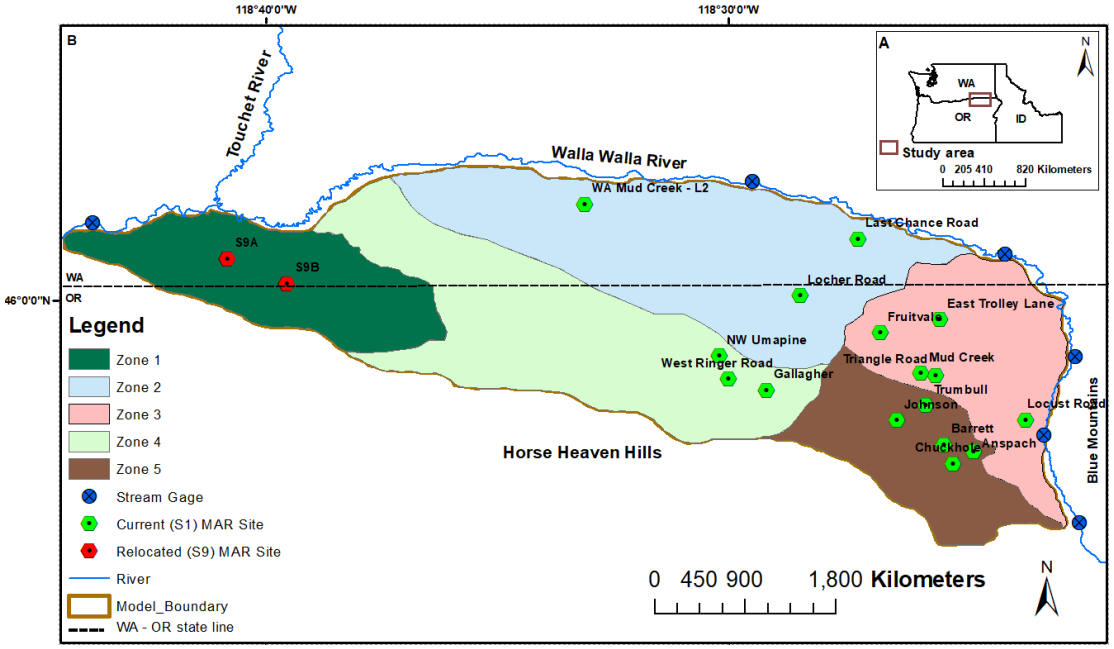

Fig. 3.3: A: Map showing study area within Inland Pacific Northwest United States; B: Locations of the current MAR sites in each of the defined zones and the proposed relocated sites for S9. S1, S2, and S9 have the same number of MAR sites, but Anspach (Zone 5) and Fruitvale (Zone 3) were relocated to form S9A and S9B (Zone 1), respectively for S9 MAR sites. Anspach and Fruitvale sites were relocated to develop the S9 MAR site scenario to evenly distribute recharge

water. The division of the model area into zones were based on physical characteristics that define each zone (as described in section 3.3.5.1), as such, the individual zones were not equally sized.

3.3.5.2. MAR Scenarios

MAR scenarios were specified based on the current number of MAR sites, different combinations of reduced numbers of sites, and relocation of some of the sites relative to the current site locations. The cases where system modifications were imposed are not meant to be an exhaustive optimization and are instead explorations of how a slightly different system could benefit users. For the reduced MAR sites scenarios, MAR sites in each of the zones were paired with one other zone and each of the paired zones constituted a scenario. The zone pairings were selected to estimate which MAR site combinations within the geographic regions or zones would offer a more evenly distributed recharge, even at a reduced numbers of sites relative to the current sites and determine if using a smaller number of sites at specific locations could provide equal spatial distribution of recharge as the current sites. The scenarios allow for focused evaluation of MAR on aquifer levels across the basin. A key motivator for the design of these scenarios is that it is economically advantageous to use the smallest number of MAR sites possible because each site comes with associated costs. A total of nine scenarios were designed; a base-case which represents the current MAR conditions, a maximum recharge or full-scale scenario, a site relocation scenario, and six scenarios where zone pairings were done to simulate the different reduced MAR site options. Detailed description of each of the scenarios are provided below.

Base-case scenario (S1)

A base-case scenario where MAR is currently applied in the basin was considered as Scenario 1 (S1). Current operation of the system is such that the existing 16 MAR sites are activated on an individual basis when resources for recharge are available, so the specific amounts vary from year to year. As such an estimate of the average annual volume added at each of the current active sites was used. An estimated annual total of 638,064 m^3 of water was applied for S1 which was based on available records for 2017 to 2018 water year for the active recharge sites within the simulated area. The recharge was distributed based on specified rates for the sites by the Walla Walla Basin Watershed Council for the recorded year [*Patten*, 2017]. The base-case (S1) is used to evaluate the response of the aquifer to the MAR system based on the current MAR conditions in the basin.

Maximum Recharge (Scenario 2)

Scenario 2 (S2) considers all the MAR sites to be active with a maximum recharge volume based on the maximum recharge amounts that were applied at each site over its history; these are observed values. The distribution of recharge was based on the observed value at each of the sites. A total annual volume of 9.76 million m^3 of water was applied to the sites for S2. The locations of the MAR sites were not changed in this scenario as used in the base-case scenario. Scenario 2 was created to evaluate the response of the system to maximum recharge from the MAR system across the basin.

Scenario 3 (S3)

The eight MAR sites located within Zones 2 and 3 (**Fig. 3.3**) were activated. A total annual volume of 5.73 million m^3 of water was applied at the MAR sites within Zones 2 and 3. The volumes used at the sites were estimated under the assumption that the sites received the maximum recharge. Scenario 3 was designed to evaluate aquifer response if only sites located near the WWR (Zones 2 and 3) were activated. MAR in Zones 2 and 3 were also seen as a support to the WWR by offering increased baseflow, but Zone 3 contains MAR sites within irrigation districts and residential areas with extensive groundwater pumping which could influence flow paths.

Scenario 4 (S4)

All six MAR sites within Zones 2 and 4 were activated which provided annual recharge volumes of 5.61 million m^3. The distribution of recharge was based on the maximum recharge or observed value at each of the sites. Scenario 4 simulated the response of the aquifer to MAR applied within Zones 2 and 4 which were in proximity to both WWR and the mountain to the south of the simulated area, respectively. The conceptual model behind this scenario was that MAR added near the mountain could augment recharge from the mountain block and together with recharge near the WWR could reverse groundwater declines across the basin.

Scenario 5 (S5)

MAR sites within Zones 3 and 4 were activated in this scenario. A total of eight sites were used which provided about 638,943 m^3 of water for recharge. The distribution of recharge was based on the maximum recharge or observed value at each of the sites. This scenario considers a case where relatively small volumes of water were applied near the WWR upgradient of the

simulated area with intense pumping for irrigated agriculture and along the mountain front where the aquifer predominantly gets recharged by the mountain block. This scenario relied mainly on the WWR to recharge the aquifer with little support from the MAR system.

Scenario 6 (S6)

Scenario 6 activates only eight MAR sites within Zones 2 and 5 with an annual total recharge volume of 9.12 million m^3. The distribution of recharge was based on the maximum recharge value at each of the sites. The response of the aquifer was evaluated with MAR applied at high elevation portions of the basin relative to the other zones or sites and near the WWR for Zones 5 and 2, respectively. This scenario used the largest volume of water relative to all the other scenarios where the number of MAR sites was reduced from the base-case MAR sites. The expectations were that the WWR would be supported by baseflow from the nearby MAR sites and large MAR volumes from the elevated regions would be distributed to recharge the aquifer across the basin.

Scenario 7 (S7)

A total of ten MAR sites within Zones 3 and 5 were activated to supply a combined annual total volume of 4.15 million m^3 of water to recharge the aquifer. The distribution of recharge was based on the maximum recharge value at each of the sites. Recharge in this scenario was applied at the upgradient portion of the simulated region i.e., near the WWR and at high elevation to the east and southeast of the basin (**Fig. 3.3**). This scenario prioritized both groundwater outflow to

the WWR and upgradient aquifer recharge that could spread spatially to the downgradient portion over time.

Scenario 8 (S8)

This scenario used the eight MAR sites within Zones 4 and 5 which supplies about 4.02 million m^3 of water annually. The distribution of recharge was based on the maximum recharge value at each of the sites. Both Zones 4 and 5 contained MAR sites near the mountain front and at high elevation areas to the south and southeast of the basin, respectively. MAR served as a supplemental recharge to mountain block recharge to potentially cause rises in aquifer levels along the southern portions of the simulated region. In this case, the WWR was relied upon to recharge the aquifers to the north and east sides of the basin, to offer evenly recharge aquifer across the basin.

Scenario 9 (S9)

This scenario assumes that all MAR sites were active and are receiving maximum recharge volumes as in the case of Scenario 2, but some sites were relocated to the downgradient portions of the basin. Both Fruitvale and Anspach sites were relocated to Zone 1 (**Fig. 3.3**). This was done to evaluate the response of the aquifer system and the WWR to the evenly distributed recharge (from MAR) across the basin. There are infinite ways to optimize Scenario 9, but the modified system employed only takes the same volume of water in a maximum MAR condition and distributes it more evenly to the benefit of all users.

MAR scenarios were simulated by applying water to specific regions within the top layer of the subsurface at varying depths based on the MAR site specifications (e.g., site sizes/dimensions and applied volumes) by the watershed council. MAR water application rates in the basin had no regulated or stipulated time since MAR is done when resources such as surface water are available within the year, so an estimated weekly timestep was used for the simulations. MAR scenarios were simulated using the final state of the calibrated transient model as the initial condition. All scenarios had the same representation of model grid and domain setups as presented in **Table 3.1**. The scenarios were simulated over a 100-year period to capture the long-term variability of the impacts of each scenario on the river and the aquifer levels. The metrics used to evaluate scenarios were average depth to groundwater table (DTW) and the fluxes from or to the WWR for each of the scenarios.

3.4 Results

3.4.1 Base-Case Scenario (S1)

The base-case scenario shows that the simulated WWR loss under the current conditions is approximately 3.0 million m^3 per year. This suggests that the estimated total volume of water added to the system through MAR and fluxes from the WWR under the base-case scenario is about 3.64 million m^3 per year. The WWR is disproportionately supplying recharge (82%) relative to MAR (18%). The indication is that the WWR would remain a losing stream under the status quo conditions, and such high losses would likely reduce ISFs over time if the boundary were modeled

dynamically instead of as a constant Dirichlet boundary. Physically, if additional water is not added to the WWR to meet the ISF it would likely go dry.

The simulated DTW under the base-case scenario indicates that aquifer levels would likely continue to decline across most portions of the basin, even if the minimum ISFs are maintained in the WWR (**Fig. 3.5**), though the system would ultimately stabilize after about 100 years. Groundwater levels within Zones 1, 2, and 4 show declining trends over the simulation period. The aquifer level in Zone 1 declined on average about 0.9 m during the simulation where groundwater recharge is believed to be solely dependent on seepage from the WWR. The declines in groundwater levels were in response to the pumping for irrigated agriculture largely by the Gardena Farm Irrigation District (GFID) within Zone 1.

Recharge from the MAR system was mostly local to the MAR sites especially within the upgradient region of the simulated area where the sites were located. The amount of recharge from the applied water decreases with distance away from the vicinity of the MAR sites. The simulated aquifer levels show that current MAR sites had minimal impact on the groundwater system within Zones 3 and 5 (**Fig. 3.3**). The small increases in DTW in Zone 5 were as a result of the response of the aquifer to MAR within the zone such as the Johnson site which currently receives more than twice the volume of water as the other sites. The WWR contributed greatly to the increase in DTW in Zone 3 due to the proximity of the zone to the WWR. The simulations show clear equity in the distribution of recharge across the basin and imply that even large seepage volumes from the WWR will not stop declines in many parts of the system.

3.4.2 Maximum Recharge (S2)

The maximum recharge scenario, S2, assumed that all MAR sites were active at their historic maximum amounts, and this generally led to increases in water levels near the WWR; the implication being that the WWR would transition to a gaining stream. The WWR gained about 1.0 million m^3 per year after approximately 9.76 million m^3 per year was added to the system through MAR. The results from S2 simulations indicate that the minimum ISFs could be maintained in the WWR under maximum recharge as ISFs would likely be improved by the groundwater system.

Depth to water was observed to increase across the basin under S2 relative to S1 (**Table 3.3**). The minimum and maximum differences in DTW between S2 and S1 were 0.1 and 17.8 m in Zones 1 and 5, respectively; the minimum occurred where no MAR site was situated, and the maximum was in the zone containing most of the high-volume recharge sites. Zone 1 recorded slow but continual declines in DTW (less than a meter) over the duration of simulation under the maximum recharge scenario but increasing trends in DTW were seen in Zones 2, 3, and 4 (**Fig. 3.5**). The aquifer levels increased within Zones 2, 3, and 4 by 0.4, 0.8, and 6.9 m, respectively relative to S1. The S2 simulations indicate that maximum recharge would not provide equal spatial distribution of recharge across the basin, only upgradient users (Zones 2, 3, 4, and 5) could benefit from the increases in aquifer levels.

Table 3.3: Mean depth to groundwater table (DTW) within defined zones for the scenarios over the 100-year simulation period.

Zones	Scenario	Mean DTW (m)	Δ in DTW relative to S1 (m)	Zones	Scenario	Mean DTW (m)	Δ in DTW relative to S1 (m)
	S1	30.6	–		S1	31.4	–
	S2	30.5	0.1		S2	24.5	6.9
	S3	30.5	0.1		S3	24.9	6.5
	S4	30.5	0.1		S4	24.7	6.7
1	S5	30.7	-0.1	**4**	S5	35.8	-4.4
	S6	30.5	0.1		S6	24.8	6.6
	S7	30.7	-0.1		S7	35.8	-4.4
	S8	30.7	-0.1		S8	35.8	-4.4
	S9	10.9	19.6		S9	24.0	7.4
	S1	3.0	–		S1	25.9	–
	S2	2.6	0.4		S2	8.1	17.8
	S3	2.6	0.4		S3	30.8	-4.9
	S4	2.6	0.4		S4	33.7	-7.8
2	S5	3.3	-0.3	**5**	S5	32.8	6.9
	S6	2.6	0.4		S6	12.0	13.9
	S7	3.3	-0.3		S7	13.6	12.3
	S8	3.3	-0.3		S8	17.1	8.8
	S9	2.6	0.4		S9	12.4	13.5
	S1	6.8	–				
	S2	6.0	0.8				
	S3	7.3	-0.5				
	S4	7.3	-0.5				
3	S5	7.3	-0.5				
	S6	6.1	0.7				
	S7	6.1	0.7				
	S8	6.2	0.6				
	S9	6.3	0.5				

Note: Negative value for a change in DTW indicates a decline in water level for the corresponding scenario relative to S1. Positive value for a change in DTW indicates a rise in corresponding scenario relative to S1.

3.4.3 Reduced MAR Scenarios (S3–S8)

Simulation of the reduced MAR scenarios (S3–S8) indicate that operating MAR sites within Zones 2 and 5 (S6) would make the WWR a gaining stream with significantly less water than S2. The volume of water that would be gained by the WWR to help maintain minimum ISFs in the WWR under S6 was about 0.87 million m^3 per year (**Fig 3.4**). It is noteworthy that all other reduced MAR sites scenarios (S3, S4, S5, S7, and S8) created losing conditions for the WWR, and that all of these except S5 provide significant reductions in river flow loss. Scenarios S3, S4, S5, S7, and S8 resulted in 0.61, 0.55, 2.60, 0.69, and 0.55 million m^3 per year, respectively flow of water from the WWR into the groundwater system. In all the reduced MAR site scenarios where the WWR becomes a losing stream, the greatest amount of water moves into the aquifer under S5 where only MAR sites within Zones 3 and 4 were active. This represents the amount of water supplied to the aquifer when minimum ISFs are maintained in the WWR, and likewise dictates the amount of water that would be required to be added to the WWR to improve ISFs when only S5 MAR sites were active. Flow of water from the WWR into the aquifer was at the lowest for the scenario with the least number of MAR sites but had high MAR recharge rates compared with the other reduced MAR site scenarios such as S4 with 6 MAR sites (**Fig. 3.3**). This suggest that the losing rates of the WWR are likely to decline if more water or large volumes of water are imported to the system through MAR. The results of these simulations show that the current MAR system could be effective for limiting or eliminating river flow loss but inspecting the spatial distribution

of water level changes shows that does not necessarily translate to uniform benefits across the basin.

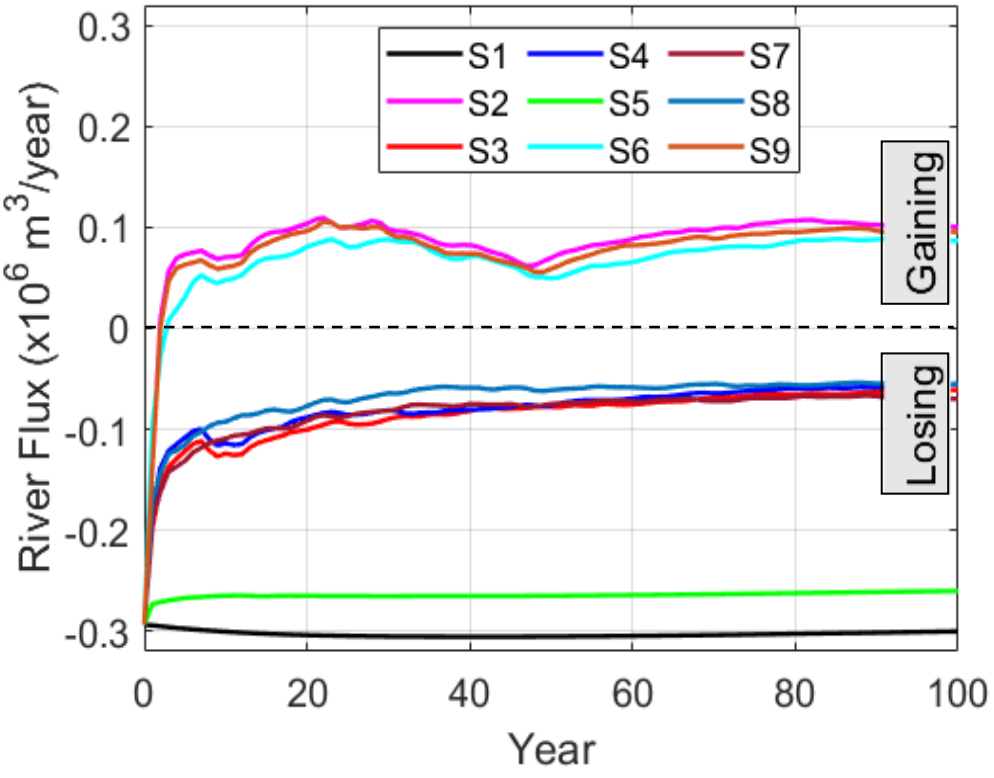

Fig. 3.4: Estimated fluxes from the Walla Walla River (WWR) in each of the simulated scenarios. Positive river flux indicates WWR was a gaining stream and negative indicates WWR was a losing stream. The early times (0-5 years) gaining trends were because recharge went from onset to full at time zero and was not gradually ramped up until after about 5 years. Recharge from the MAR pushed water back into the WWR at the early times, but the fluxes relatively stabilized in response to impacts from pumping until the end of the simulation. Pumping reduced groundwater storage allowing for more water to move from the WWR to recharge the aquifer leading to stabilized

fluxes. Scenarios (S2, S6, and S9) with high recharge rates resulted in the WWR becoming a gaining stream.

Reducing the number of MAR sites resulted in a minimum change in DTW (0 to 0.1 m) in Zone 1 between the base-case and the reduced MAR site scenarios such as S3, S4, and S6 (**Table 3.3**). The minimal changes in DTW between the scenarios emphasized the high dependence of the aquifer on the WWR for recharge, especially within Zone 1 if the minimum ISFs are maintained in the WWR. This observation was consistent across the basin for most of the other zones when the number of MAR sites were reduced in the individual scenarios including S5, S7, and S8 for Zones 2 and 4. Zone 5 recorded the maximum declines (between 4.9 and 7.8 m) in DTW in all reduced MAR site scenarios compared to the base-case (**Table 3.3**). The DTW generally declined in the reduced MAR scenarios across the basin with S6 resulting in some increases in DTW in the upgradient (e.g., within Zones 2 and 5) the simulated area (**Fig. 3.5**). The results from the reduced MAR scenarios indicate that all water users across the basin would not benefit from increased aquifer levels if the number of sites were reduced.

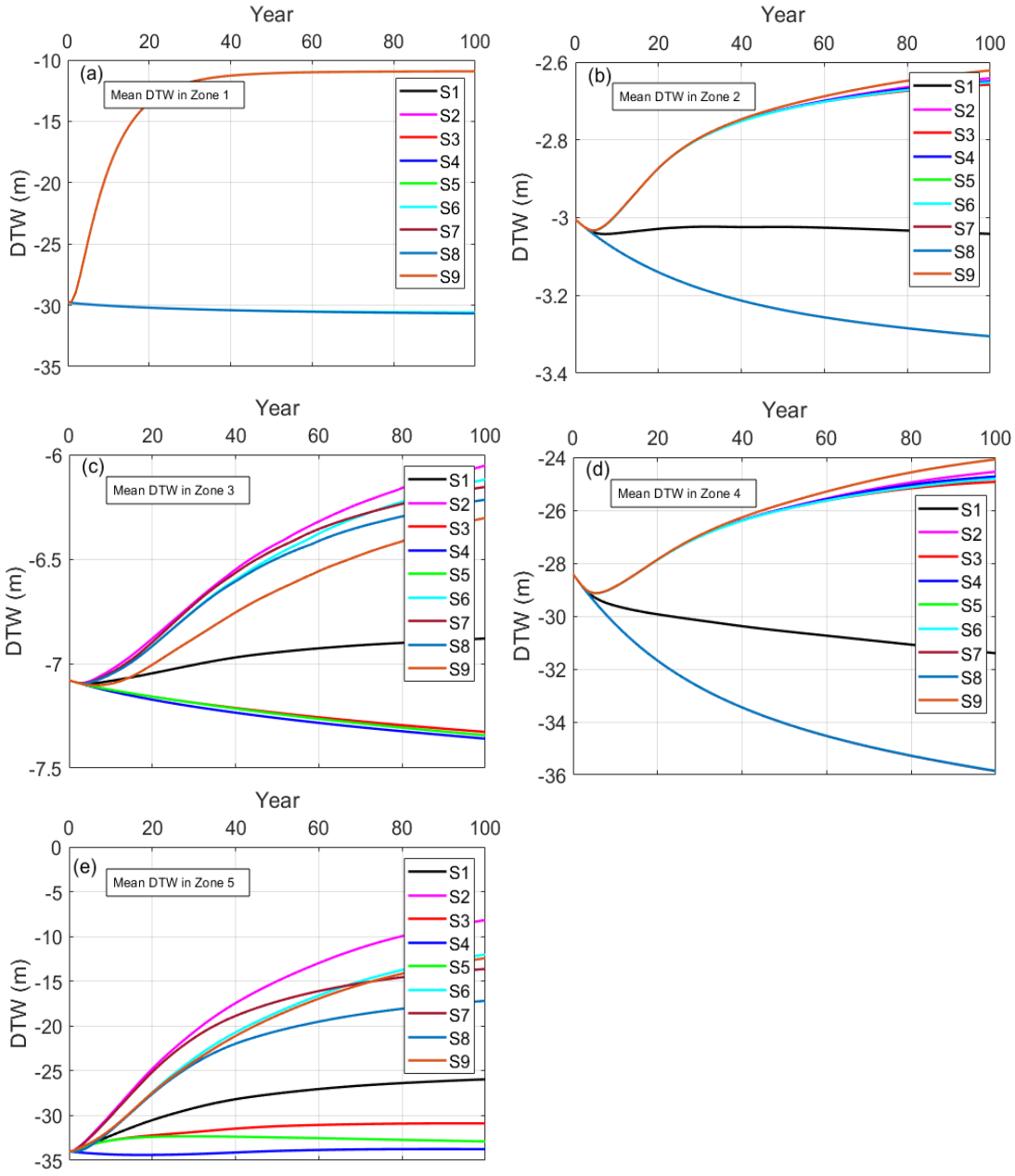

Fig. 3.5: Mean depths to groundwater table (DTW) within each zone over the 100-year simulation periods. Note that the graphs only show mean DTW in the zones across the basin and not making comparisons between zones. The plots show that S9 resulted in rises in mean DTW in all the zones

indicating that S9 presented a more balanced benefits to all users across the basin relative to the other scenarios. In Fig. 3.5(a), all scenarios apart from S9 showed similar declining DTW making them appear to be on the same line.

3.4.4 Scenario (S9)

River fluxes calculated for S9 with the same MAR recharge volumes as S2 indicate that the WWR would become gaining, but the volume gained decreased slightly relative to S2 (**Fig. 3.4**) by about 5%. The difference between the S9 and S2 was that two MAR sites including Anspach, and Fruitvale were moved from the upgradient i.e., Zones 3 and 5 to create S9A and S9B sites downgradient (Zone 1) the simulated area. It is likely that the reduced volume of water was lost through groundwater pumping within the Gardena Farms Irrigation District (Zone 1) which had since been supported solely by losses from the WWR, but the applied water directly became available to pumping when the sites were relocated to the area. The added benefit was that relocating the two MAR sites to Zone 1 led to increases in DTW in all zones across the basin (**Fig. 3.5**).

Scenario 9 resulted in a mean increase of DTW of about 19.6 m relative to the base-case (S1) (**Table 3.3**) in Zone 1. Introducing MAR at the downgradient (Zone 1) region reduced the impacts of groundwater pumping on aquifer levels and the ISFs in the WWR. The DTW increased in all the other zones under S9 relative to S1 (**Fig. 3.5**). Zones 2, 3, 4, and 5 saw increases in DTW under S9 by 0.4, 0.5, 7.4, and 13.5 m, respectively relative to S1. Relocating the Fruitvale and

Anspach sites only resulted in slight declines in their respective areas but was still able to stabilize DTW within Zones 3 and 5, relative to S2. The DTW declined by 0.2 and 4 m in S9 relative to S2 in Zones 3 and 5, respectively, but these were significantly smaller declines than under S1. The highest increases in DTW for S9 were in Zones 1, 2, and 4, relative to S2 and all the other scenarios (**Fig 3.5**). For example, the DTW increased by 19.6, 0.5, and 0.05 m in S9 relative to S2 for Zones 1, 2, and 4, respectively. This suggests that the aquifer levels would stabilize or increase in mean DTW across the basin i.e., in all zones if MAR would be spatially distributed as shown in S9 and the minimum ISFs are maintained in the WWR.

Generally, all model scenarios (except the base-case) showed increases in river flux within the first 5 years of the simulations signifying trend of movement of water into the WWR i.e., the WWR started to gain water at the initial stages of the simulation (**Fig. 3.4**). These were due to the initial sudden response of the system to high volumes of water provided by the MAR systems, which were instantly turned on and full volume. Recharge from the MAR pushed water back into the WWR at the early times (0-5 years), but the fluxes generally stabilized in response to impacts from groundwater withdrawals. In reality, the changes to MAR volumes would likely be more gradual and this would push the timetable back, but ultimately the same steady-state flux would be achieved given these recharge volumes.

3.5 Discussions and Conclusion

Numerical simulations were performed in this study to test the response of the aquifer system of the WWRB to supplemental MAR scenarios, given required minimum ISFs in the WWR over a 100-year period. The simulations addressed the key problem faced by the WWRB pertaining how minimum ISFs requirements could be maintained year-round while providing adequate recharge through MAR to stop or reverse aquifer declines across the basin. The specific questions included how much water need to be imported into the system, and where the water should be applied that would cause increases in aquifer levels across the basin and improve ISFs in the WWR. MAR scenarios were simulated that test options of adding water to the system through MAR, giving a river stage that meets minimum ISFs requirement in the WWR.

The results suggest that merely maintaining minimum ISFs in the WWR would support the groundwater system even with current MAR operations. However, such an approach would still require a net import of water into the basin to supplement the WWR flows, and it would not provide water to all users across the basin. River flow loss was highest under the current MAR conditions which signify that the WWR would continue to remain a losing stream under the current MAR conditions and, since river flows are not currently being supplemented, its frequency of going dry would likely increase. As a consequence, recharge would decrease, and users would need to drill deeper wells, but the aquifer's decline would continue. Such changes would permanently impact all activities in the WWRB and would also be detrimental to aquatic fauna and biota.

The objective of the reduced MAR sites scenarios was to find alternative schemes for achieving a sustainable groundwater system that maintains minimum ISFs and balances MAR benefits to

users across the basin. The results indicate that, without intervention, the WWR will largely continue to be a losing stream and any long-term conditions without MAR could have significant adverse impacts on users in the basin away from the WWR. Water users especially those within Zone 1 such as the Gardena Farms Irrigation District (GFID) may be at disadvantage if the reduced MAR site scenarios were implemented as currently designed. The downgradient portion of the simulated region (Zone 1) currently has no active MAR sites, and the topography and flow paths in the basin (see **Fig. 3.1**) indicate that the area is hydraulically disconnected from any benefits from the current MAR system. Consequently, the water users or farmers within Zone 1 would continue to rely on recharge or losses from the WWR to meet their crop water demands which are woefully inadequate.

One sure way to boost aquifer recharge across the basin could be to increase the amount of water used for MAR while keeping constant flows in the WWR. However, the simulation results suggest that where that water is applied in the basin is very important in achieving "balanced benefits" for all users. The maximum recharge scenario (S2) distributed recharge at all current MAR sites at their maximum historic or observed volumes, but the resultant effect was that aquifer levels kept declining downgradient (Zone 1) the simulated region and increased at the upgradient where most sites were located. This re-enforces that the current MAR sites as designed may not offer equal benefits to users across the basin, even with increased recharge volumes and minimum ISFs in the WWR, all year round. As a result, a more rational approach would be to relocate some of the MAR sites to supplement the recharge or losses from the WWR preferably at the downgradient region.

The WWR became a gaining stream under S2, S6, and S9 and a losing stream under all the other scenarios. The WWR gaining from the groundwater system was important for maintaining ISFs in the WWR and preventing the WWR from drying up. Conversely, increased flow in the WWR could become a vital recharge to the aquifer during dry years or when pumping exceeds recharge as seen under S3, S4, S5, S7, and S8. The WWR losing excess water to the aquifer could result in low ISFs which would be damaging to aquatic habitat, if S3, S4, S5, S7, and S8 were implemented. Scenarios S2, S6, and S9 yielded net rises in DTW relative to the base case, but only S9 stabilized the aquifer levels and offered balanced benefits to all users within the basin. The basin-wide stabilization of the aquifer levels provided by S9 would be crucial to farmers within the irrigation districts across the basin because it would mean existing wells could continue to be used if S9 is implemented. For successful implementation of any of the scenarios in the basin, water would have to be imported, but S9 suggests that equitable distribution of recharge would be realistic only if basin-wide MAR (relocation of some MAR sites) with maximum recharge volumes and the minimum ISFs in the WWR are prioritized. The challenge of meeting the needed volumes of water to be added to the WWR to maintain minimum ISFs or applied at MAR sites remain a hurdle to water users and managers.

The study incorporated many assumptions about the model simulations. The most important ones were the assumptions of constant mountain block recharge and projected net surface recharge, and lateral and vertical homogeneity of the aquifer layers. It was assumed that other sources of inflows or recharge into the groundwater system such as net surface recharge and mountain block recharge remain constant. These recharge assumptions are limitations because climate change over 100 years is uncertain in this region but is likely to include more winter precipitation as rain at the

cost of snowpack. Obviously, the natural recharge conditions are not likely to remain unchanged over the long-term. But the assumptions are that the recharge estimates represent the average conditions in the basin. The model domain consisted of five aquifer units and each unit was assumed to be laterally and vertically homogeneous. These simplifying assumptions of the aquifer units did not account for discontinuities that could slow down flow and prolong the time needed to reach equilibrium. The limitations and assumptions considered in this study do not in any way lessen the usefulness of the research but provide the appropriate perspective for interpretations of the results.

In a complex flow system such as the WWRB where there is a great dependence of the aquifer on the WWR, effective management of both surface water and groundwater systems need to be done by not only looking at the net mass balance of the system but with consideration of all the flow paths across the basin. For example, computation of a complete water balance of the basin is necessary to quantify the groundwater and surface water fluxes to identify the flux from the WWR. Understanding the contributions and direction of flow of the various components of the water balance would be vital to assess the impacts of any added water or inputs from the MAR system and where the added water need to be placed for the benefit of all. As MAR develops in the WWRB, a more effective strategy would be to prioritize both the MAR systems and the surface water or river flows that could help sustain river-aquifer exchanges to improve water availability in the WWR and distribute the applied or recharge water that will benefit all users across the basin.

CHAPTER FOUR

SIMULATION OF REGIONAL GROUNDWATER FLOW DYNAMICS IN THE MOSCOW-PULLMAN BASIN AND ITS RESPONSE TO ALTERNATIVE MANAGEMENT SCHEMES

Benjamin N. O. Kuffour[1*] and Nicholas B. Engdahl[1]

Abstract

Groundwater is the principal water supply for the Moscow-Pullman basin, southeastern Washington, and north-central Idaho. Over the last four decades, water levels within the basin have been dropping due to excessive pumping. Water conservation efforts have not been able to stop the declining water levels. Long-term solution requires a better understanding of the hydrogeologic characteristics of the region, which can be tested using groundwater flow models. However, no active groundwater flow model exists today that characterizes current aquifer conditions. In this study, a three-dimensional groundwater flow model was developed using MODFLOW-2005 for the basin. The model was calibrated with measured data and estimated parameters and used to evaluate response of the aquifers to eight future pumping scenarios: 100, 90, 80, 50, 25, 10, 2, and 0 percent of historic pumping records 1983-2018. Results indicate that basin-wide volume of groundwater could decline but the rate of decline is dependent on the rate of pumping. Aquifer levels in Pullman and Moscow could decline on average of 0.05 and 0.1 m per year, respectively between 2018 and 2053 if pumping remains equal to historic rates. Pumping at 90 percent of historic rates could lead to average water level declines of 0.04 and 0.09 m per year in Pullman and Moscow, respectively. Pumping 80 percent of historic rates could result in average water level decline of 0.02 and 0.08 m per year in Pullman and Moscow, respectively. Reducing pumping by 50 percent could lead to average drawdowns of 0.01 and 0.06 m per year in Pullman and Moscow, respectively. Pumping less than 25 percent could stabilize the aquifer levels in Pullman, with less than 0.02 m per year decline in Moscow area. Water levels could rise by 0.1 and 0.09 m per year in Pullman and Moscow, respectively, if pumping was halted. The model and findings from the

scenarios improve understanding of the hydrogeologic characteristics of the system and guides planning of water management options, however, the findings should not be used in isolation of the limitations, assumptions and uncertainties associated with model geometry and parameterization.

4.1 Introduction

Groundwater is the sole source of municipal water in the Moscow-Pullman region of southeastern Washington and north-central Idaho. The Moscow-Pullman Basin is home to over 60,000 native residents of Moscow, Pullman, and Colfax in addition to populations of University of Idaho and Washington State University [*Candel et al.*, 2016; *Dhungel and Fiedler*, 2016]. Groundwater availability in the region is a key water resource management issue because of high municipal water demands. Groundwater level trends along the Moscow-Pullman corridor i.e., within the South Fork Palouse Basin (SFPB) aquifer system have shown gradual declines over the last century due to excessive pumping [*Stevens*, 1960; *Candel et al.*, 2016; *Folnagy and Osiensky*, 2016]. According to the Palouse Basin Aquifer Committee (PBAC), an estimate of 11 million m^3 of water is being pumped from the SFPB aquifer system annually to meet water demands in the basin. Groundwater pumping is expected to increase to meet the growing water demands in the region and this is likely to lead to accelerating declines in aquifer levels. Previous water conservation or preservation practices such as wastewater reuse, changes in landscape irrigation practices, and water use efficiency measures have reduced groundwater pumping slightly but have not been able to halt the decline as demand continues to increase [*PBAC*, 2017]. As a result, long-term solutions are needed to maximize water use and retain water in the aquifer system. However, developing a long-term plan is currently inhibited by lack of a planning model for the basin because there are no modern hydrogeologic or groundwater flow models of the basin today that represents the system. This deficiency means there are limited tools available to evaluate water supply options or assess water level dynamics within the Pullman-Moscow corridor.

There have been numerous studies over the last decade that characterized hydrogeologic conditions of the basin [*Dijksma et al.*, 2011; *Moran*, 2011; *Folnagy*, 2012; *Candel et al.*, 2016; *Folnagy and Osiensky*, 2016]. However, little has been reported about numerical groundwater modeling efforts that assesses the response of the aquifer system to hydraulic stresses such as groundwater pumping, that can help maximize water use and water management within the SFPB. For example, a groundwater flow model can be created to simulate changes in water surface elevations to various pumping rates that may be used to develop management strategies that would help sustain the aquifers [*Barker*, 1979; *Smoot and Ralston*, 1987; *Lum et al.*, 1990; *Johnson et al.*, 1996]. Groundwater pumping in the basin is projected to increase on an annual average of 1 percent due to estimated increases in regional water demand over the next four decades [*Anchor QEA*, 2017]. Increases in water demand could mean increased exploitation of the aquifers, so the groundwater flow system needs to be studied to find ways to boost long-term water availability in the basin. This is important because continual exploitation of the aquifer without efforts to sustain the aquifers will eventually deplete the groundwater resources. The main goal of the study is to simulate groundwater flow dynamics in the Moscow-Pullman region and its response to alternative management schemes. The conceptual model of the flow system and the findings from this study are intended to serve as a guide to water managers (i.e., the Palouse Basin Aquifer Committee) and users in regulating pumping or water use in the region and also to serve as a knowledge base for future researchers in the basin.

4.1.1 Purpose and Objectives of the Study

The primary objective of this study is to produce functioning conceptual and numerical (groundwater flow) models that represent the descriptions of the hydrogeologic characteristics of the SFPB. The study provides a framework for simulation of future flow dynamics and can serve as a physically-based tool for decision-making support within the SFPB. The specific objectives of the study are to: 1) develop a three-dimensional conceptual model based on the conceptual structure of the aquifer system or hydrogeologic framework of the SFPB, 2) develop from the conceptual model, a three-dimensional, distributed model of the groundwater flow system for the SFPB, 3) calibrate the numerical model parameters based on historic data such as groundwater pumping, observation well heads, and on previous studies in the basin, and 4) use the calibrated numerical framework in a comparative analysis of future water use scenarios to support decision making for groundwater management in the basin. These objectives were accomplished using the groundwater flow simulation platform MODFLOW-2005 [*Harbaugh*, 2005].

The model development process of the conceptual and numerical models is presented and described. These include descriptions to the simulation platform and groundwater flow equation solver, spatial and temporal discretization of the aquifer system, storage, and hydraulic properties of the hydrogeologic units that constitute the aquifers of the basin, stresses, and hydrologic boundaries of the simulated region. Conditions of the basin between periods of 1983 and 2018 were simulated to provide an understanding of the hydrogeologic characteristics in the study area. The aquifer conditions in 2018 were then used as a starting point to simulate alternative management scenarios that would help manage groundwater pumping or water use in the basin.

Model calibration processes, calibrated results, and observations used to calibrate the model are documented. The results from the application of the numerical model for eight management scenarios (pumping scenarios) are presented, which were selected based on outcomes proposed by the Palouse Basin Aquifer Committee, and the results are described focusing on the most stressed locations of the aquifer system. Model assumptions, uncertainties, and limitations are documented to provide better perspective for interpretation of the model results.

4.2 Study Background

Groundwater in the Moscow-Pullman region mainly occurs in the Columbia River Basalt Group (CRBG) and the Latah Formation with interbedded sediments [*Reidel et al.*, 1989; *Reidel and Tolan,* 2013]. The CRBG basically consist of two water bearing units: the Wanapum and Grande Ronde formations. Recent well data show that groundwater levels within the Grande Ronde formation decline on average of 0.3 m/year in response to groundwater pumping within the Moscow-Pullman region. Groundwater levels in the Wanapum unit for the most part have not shown significant declines over the past decade because most wells in the region are not completed within the Wanapum [*Beall et al.*, 2011]. Continuous declines in municipal groundwater monitoring wells show that the system has been in overdraft for the past several decades and this is a major concern for water managers within the Moscow-Pullman corridor where most of the population exists. The aquifers of the SFPB are largely recharged by precipitation and snow-melt

from the adjacent mountains including the Kamiack Butte to the north, Moscow Mountains to the northeast, and the Palouse Range to the south of the SFPB. [*Owsley*, 2003; *PBAC*, 2017].

Most of the recent research in the greater Palouse region focused more on the physical factors controlling the groundwater flow system. Typical projects focused on the evaluation and quantification of recharge into the basalt aquifers using numerous recharge estimation methods (see **Table 4.1**). Subsurface recharge in the Moscow-Pullman Basin is believed to occur mainly through the surficial loess sediments near streams, and infiltration of precipitation (rainfall and snow-melts) near Moscow Mountain [*Lum et al.*, 1990; *O'Geen et al.*, 2005; *Dijksma et al.*, 2011]. Flow of water in the unconsolidated loess sediment are largely controlled by water demands from dry-land agricultural activities (e.g., wheat and chickpeas lands) and seasonal changes in precipitation. Most recharge to the loess occurs during periods of high precipitation and low evapotranspiration in late fall, winter, and spring months, but short duration and high-intensity precipitation events may provide considerable recharge in parts of the year. Large amounts of recharge through the loess sediments occurs in lowlands between the rolling hills composed of loess. Spring snowmelt from the high elevations produce runoffs and accumulation of below ground lateral flows [*Lum et al.*, 1990; *Ely et al.*, 2014]. Recharge to the Wanapum and the Grande Ronde formations within the Pullman-Moscow region has been studied in the past through various surface-aquifer recharge estimation techniques [*Reeves*, 2009; *Dijksma et al.*, 2011]. **Table 4.1** provides detailed summary of previous studies that estimated recharge into the shallow aquifers of the CRBG in the Palouse basin.

Table 4.1: Studies that estimated recharge into surficial loess and shallow aquifers of the Palouse Basin.

Study	**Method of Estimation**	**Recharge Rate (mm/year)**
Stevens [1960]	Water Budget	30.5
Foxworthy and Washburn, [1963]	Water Budget	22.9
Barker [1979]	Darcy's Law	23.8
Smoot and Ralston, [1987]	USGS Daily Deep Percolation Model	91.4
Bauer and Vaccaro, [1990]	USGS Deep Percolation Model	69.8 – 100.1
Johnson, G. E., [1991]	Vadose sampling and one-dimensional infiltration model (LEACHM)	106.7
Muniz, [1991]	Vadose sampling and one-dimensional infiltration model (LEACHM)	53.3
Baines [1992]	Hill method and zero change method	26.9
O'Brien et al., [1996]	Environmental Tracer method (Chloride mass balance)	24.9 – 101.6
O'Geen et al., [2005]	Isotope Tracer (Chloride mass balance)	4.3
Reeves [2009]	Bayesian Model Averaging (Storage Equation)	121.9
Dijksma et al. [2011]	Soil Moisture Routing Model (Water Balance model)	68.6 (at eastside of basin)
Dhungel and Fiedler [2016]	Water Balance	45.7
Duckett et al. [2019]	Hydrogeochemical (Isotopic discrimination)	>39.9 (at eastside of basin)

Despite the previous attempts to identify and estimate pathways of recharge into the Wanapum and Grande Ronde formations no conclusive evidence regarding specific locations where recharge does or does not occur exists, so the current estimates are all laterally extensive and uniform across large regions. The lack of knowledge or resolution on the recharge zones and mean annual recharge in the area remain a concern because it is a significant source of uncertainty, and may also be a significant source of error since there is geological evidence that recharge is likely concentrated between Moscow and Moscow Mountain [*Bush, et al.*, 2016].

Groundwater flow modeling studies in the larger Palouse Basin generally began in the early 1970's. Early modeling works were done by [*Jones, R.W., and Ross*, 1972], who produced a mathematical model to predict water resources in the basin by delineating the aquifers and determining the hydraulic interconnections between them, then determined the directions of movement of groundwater and hydraulic properties of the aquifers. The mathematical model identified only a small degree of connection between the aquifers and did not attempt to estimate recharge into the aquifers because the mathematical model assumed no recharge occurred in the area. In 1979, Barker constructed the first computer simulation and geohydrology model of the basalt aquifer system (i.e., numerical groundwater flow model in the Grande Ronde basalt formation) in the Pullman-Moscow basin [*Barker*, 1979]. The finite difference model simulated historical water level declines in response to pumping between 1971 and 1975 in the Pullman area and identified vertical leakage from the aquifers as the most important source of recharge to the Grande Ronde basalt aquifer system. Baker's two-dimensional groundwater model was later evaluated and modified by *Smoot, J. L., and Ralston* [1987] to increase the complexity of the model by incorporating additional hydrogeologic parameters such as the use of deep percolation recharge

model developed by the United States Geological Survey (USGS), and also by increasing the model's geologic layers from one to three. The USGS recharge model simulated the physical processes of evaporation of intercepted moisture, plant transpiration, surface runoff, the accumulation and melting of snow, soil moisture accumulation, and evaporation from the soil. [*Smoot and Ralston*, 1987]. *Smoot, J. L., and Ralston*, [1987] constructed a three-dimensional (3-D) numerical groundwater flow model that incorporated the Grande Ronde basalt, Wanapum basalt, and an overlying surficial loess unit to form the three-layer model. The model approximated the solution of a partial differential equation that describes groundwater flow using the finite difference technique. The time-dependent model was calibrated by matching simulated with historic measured data. The calibrated model was used to predict general trends in groundwater levels in the region. Model results suggested that the aquifer levels in the basin would continue to drop with increase in groundwater pumping.

The next known model update of the Pullman-Moscow region was done by *Lum et al.* [1990] using data from a USGS study in the 1970's and observed data to construct a three-dimensional (3-D) numerical model of the groundwater flow system to provide understanding of the geohydrology of the basin. The *Smoot and Ralston* [1987] model was updated in the *Lum et al.* [1990] model by including a delineated thickness of the basalt in the basin taken from magnetotelluric geophysical survey conducted by USGS. The USGS modular groundwater flow program Modflow-77, created by *McDonald and Harbaugh* [1988] was used to construct the updated model. The 3-D groundwater flow model incorporated three layers: an overlying surficial loess (top), Wanapum basalt, and Grande Ronde basalt layers. The USGS recharge estimation model used by *Smoot and Ralston* [1987] was applied to estimate recharge rates of the groundwater

flow system. The groundwater flow model was used to calculate future groundwater levels changes under different groundwater pumping levels. Results from the study suggested that groundwater level declines would persist if pumping continued unabated. The recommendations were that groundwater recharge, movement, and discharge in the basin needed to be investigated to improve model's accuracy in predicting aquifer stress (e.g., pumping) responses in the future.

Johnson, et al. [1996] expanded the numerical model described by *Lum et al.* [1990] to predict the impact of future groundwater withdrawals on aquifer water levels in the Pullman-Moscow area. The study revised the *Lum et al.* [1990] into five-layer model that subdivided the aquifer in the Grande Ronde basalt into three layers, but did not recalibrate the revised model due to inadequate information on aquifer water levels. The simulation results indicated that the five-layered groundwater flow model reproduced nearly the same results in predicting the changes in groundwater levels as the prior 3-layered models such as the *Lum et al.* [1990] model. The various 3-D numerical or groundwater flow models developed for the basin in the past have not been reevaluated since the mid-1990s to include or capture current conditions of the flow systems in the region. However, the greater challenge is that these models are no longer available in any format so they cannot be re-run or updated; as such, a new modeling framework for the basin is needed.

4.3 Study Area

4.3.1 Location and Land Use

The South Fork Palouse River Basin covers approximately 290 km^2 located on the eastern margin of the Columbia Plateau, at the border between the states of Idaho and Washington. The basin is bounded towards the east by the Moscow Mountains, to the southeast by the Palouse Range, and northeast by the low permeability rocks of the Precambrian basement of the Kamiak Butte (**Fig. 4.1**). The Palouse region is characterized by rolling, dune-shaped hills consisting of wind-transported silty loam deposits [*Owsley*, 2003]. The basin's rolling dry land is notable for supporting its rich dryland farming or agriculture practices (including winter and spring wheat, legumes, and other crops). The vegetation types in the region vary depending on precipitation and surface altitudes. The natural vegetation ranges from grasslands and impervious residential and urban area (in the lowlands) to forest and barren rocks at the mountain ranges where precipitation (snowfall) is highest [*Ely et al.*, 2014]. The low elevations are composed largely of dryland grain production with interspersed portions of perennial grasslands [*Dijksma et al.*, 2011].

4.3.2 Climate

The climate of the SFPB is semi-arid. Mean annual precipitation within the region varies directly with elevation, and ranges from average values of 457.2 mm per year at the lowest to 1,016 mm per year at the highest elevations. The average annual precipitation at western portions of the basin (within low elevation regions) ranges from 457.2 mm to 660.4 mm and the eastern

portions, where elevations are high gets above 660.4 mm of precipitation per year. The Pullman-Moscow area gets an annual average of 584.2 mm of precipitation [*Larson et al.*, 2000; *Dijksma et al.*, 2011]. Precipitation mainly falls as snow in the adjacent mountains between November and April months. Precipitation occur as rainfall during the late summer months [*Lum et al.*, 1990; *Owsley*, 2003; *Dhungel and Fiedler*, 2016]. The major surface water sources in the basin are the South Fork Palouse River and its two tributaries: Paradise Creek and Missouri Flat Creek, which are supported by flows from the adjacent highlands and seasonal precipitation. Flow of water in the basin is topographically driven from the east to the northwest [*Leek*, 2006].

The average annual daytime temperature in the region is about 7.7^{o}C. Warm season occur during the relatively hot and dry summer months with highest temperature of 35^{o}C [*Dhungel and Fiedler*, 2016]. Lowest of temperatures in the Palouse region are recorded between the months of November and April. A typical coldest day in the winter occur with an average low of -3.9°C and high of 1.1°C. Over the course of the year, the daily temperatures typically varies from -3.9°C to 86°F and is rarely fall below -11.6°C at night or above 35°C during the day [*Dijksma et al.*, 2011].

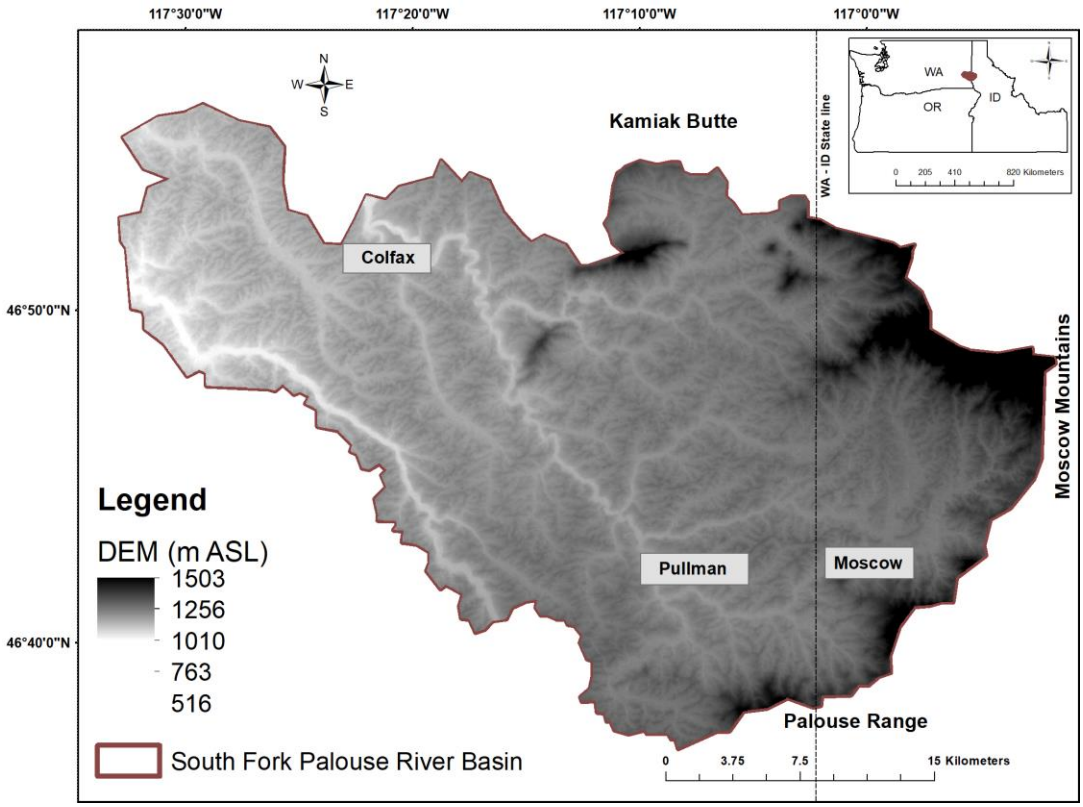

Fig. 4.1: Map of South Fork Palouse River Basin within the northeast Idaho and southeast Washington.

4.3.3 Geologic Setting

The Moscow-Pullman basin is geologically characterized by an igneous-metamorphic basement of Palaeo-Mesozoic age overlain uncomfortably by the interlayered Miocene sequence of the Columbia River Basalt Group (Grande Ronde, Wanapum, and saddle mountains basalts) and interbedded sediments [*Larson, et al.*, 2000; *Beall et al.*, 2011]. The Columbia River Basalt Group (CRBG) was formed between ca 16.7 Ma and 5.5 Ma [*Bush et al.*, 2016]. The CRBG

sequence can be up to approximately 750 m thick and is overlain by the Quaternary aeolian deposits of the Loess in the basin (including Pleistocene loess in the Pullman area overlain by Pleistocene loess in the Moscow area) [*Lum et al.*, 1990; *Leek*, 2006]. The volcanic geological group is divided in to two main units the "Grande Ronde" and the "Wanapum" formations in the basin, each of which has numerous members from specific extrusive events. The interbedded sediments of fluvial origin are part of the Latah Formation, which is organized into four members: the Sediments of Boville, Vantage, Shallow and Deep Sediments of Moscow. The stratigraphic scheme is illustrated in **Table 4.2** with specification of thickness of aeolian, fluvial, volcanic units, and the lithotype that characterize the South Fork Palouse River Basin.

Table 4.2: Hydro-stratigraphy within the basin with detail of the lithologies for the deposits of the Palouse and Latah (L) formations (LF) and the Columbia River Basalt Group (CRBG).

Hydro-stratigraphic units	**Epoch**	**Thickness (m)**	**Lithotype**
Loess Formation (L)	Holocene - Pleistocene	1 - 8	Clay, silt
Sediments of Boville (LF)	Pliocene	0 - 20	Clay, sand silt
Wanapum Basalt Formation (CRBG)	Miocene	40 - 70	Basalt
Vantage Member (LF)		2 - 10	Clay, sand silt
Upper Grande Ronde (CRBG)		50 - 80	Basalt
Shallow Sediment of Moscow (LF)		0 - 10	Clay, sand silt
Intermediate Grande Ronde (CRBG)		160 - 220	Basalt
Lower Grande Ronde (CRBG)		20 - 80	Basalt
Deep Sediment of Moscow (LF)		0- 25	Clay, sand silt

The Grande Ronde formation consists of fine-grained to very fine-grained aphyric flows [*Reidel et al.,* 1989; *Reidel and Tolan,* 2013]. The eruptive period for the Grande Ronde formation was 16.0 – 15.6 Ma [*Bush et al.,* 2016]. The unit is the most extensive of the Columbia River Basalt Group (CRBG) occupying nearly 90 percent of the total CRBG, by estimated volume, within the Columbia River Plateau [*Owsley,* 2003]. The Grande Ronde basalt covers large part of the entire Moscow-Pullman region. The Grande Ronde Formation consists of numerous lava flows that are separated by narrow layers of interbedded sediments of the Latah Formation called the Vantage member unit [*Leek,* 2006]. No surface exposures of the Grande Ronde formation occur

within the Moscow-Pullman region, but the formation is present beneath the Wanapum flow in depths below 100 meters deep in much of the Moscow-Pullman basin [*Reidel et al.*, 1989; *Bush et al.*, 2000].

The Wanapum unit forms the uppermost basalt over most of the basin and consists of medium to coarse-grained basalt containing olivine in a groundmass of intergranular pyroxine, micro-phenocrysts of plagioclase, and devitrified glass. The age date for the top of Wanapum unit is estimated ca. 15 Ma [*Bush et al.*, 2016]. The unit is spatially extensive and exposed at many roadcuts throughout the basin [*Bush et al.*, 2000]. The basalt of the Wanapum unit is thick in the Moscow region and decreases in thickness in the Pullman area. The Wanapum unit is small in thickness compared to the Grande Ronde Formation and makes up about 6 percent of the entire Columbia River Basalt Group [*Owsley*, 2003]. Both the Grande Ronde and the Wanapum contain the dominant aquifers of the basin [*Fairley, et al.*, 2006].

The older Asotin Member and the younger Weissenfels Ridge Member of the Saddle Mountains basalt are seldom available in the Moscow-Pullman Basin. The basalt represents the diminishing phases of eruption of the CRBG. Flows of the older Asotin Member have been mapped west and southwest of Pullman, on the Palouse Slope and in channels that erodes into the Wanapum basalt. The ages of the younger Weissenfels Ridge and the older Asotin Members are placed between 13.5 and 13 Ma [*Bush et al.*, 2016].

Overlying the basalt flows are the unconsolidated sediments of the Latah Formation (the Sediments of Boville, Vantage, Shallow and Deep Sediments of Moscow). The Latah Formation sediments also occur as interbed sediments between the individual basalt flows. The sediments of

Boville consists of clay, sand, silt, and gravel deposits that is laterally equivalent and mostly overlies the CRBG [*Bush et al.*, 2000]. The clay matrix is rich in kaolinite and mainly appears white, yellow, red, and brown with poorly sorted sand and gravels. The Boville sediments estimated to be deposited for more than 10,000,000 years are rarely exposed, but they are visible beneath thin loess sediments in places within the region [*Thurlow and Swanson*, 1987]. The Vantage member of the Latah Formation consists of interlayered sand, silt, and clay with wood fragments in some areas. The sand layers are poorly sorted with coarse grains of quartz and high clay content. The Vantage sediments are found between the Wanapum and uppermost Grande Ronde formations in the Moscow-Pullman area. The estimated depositional time for the Vantage sediments exceeds 400, 000 years. The Moscow sediments are mainly interbeds of sand, silt, and clay between the Grande Ronde flows and the prebasalt rocks of Moscow. Several discontinuities exist in the interbed sediments within the subsurface of Moscow. The sand content and grain size increases in the Moscow area and the interbeds thin out to less than few meters toward Pullman The estimated time for deposition of Moscow sediments is approximately 400,000 years [*Brown*, 1976; *Bush et al.*, 2016].

The Quaternary aeolian or surficial deposits of the Loess overlies the unconsolidated sediments of the Latah Formation. In places within the Moscow-Pullman region, the Sediments of Boville overlain by a sequence of Pleistocene loess deposits and interbedded clays of the Palouse Formation, although the loess deposits generally thin to the east over the Sediments of Boville [*Fairley et al.*, 2006]. The surficial deposits consists of alluvium and colluvium (stream deposits, slope-wash deposits derived from the loess-covered hills, and debris-flow deposits) [*Bush et al.*,

2000]. The dominant compositions are stream deposits that blend laterally into loess of the Palouse Formation.

Crystalline rocks older than the CRBG are visible around the edges of the basalt in the Moscow-Pullman basin. Granitic rocks arise steeply in elevation on the north, east, and south of Moscow [*Bush et al.*, 2000; *Holom*, 2006; *Folnagy*, 2012; *Bush et al.*, 2016]. The Kamiak Butte, Smoot Hill, and Angel Butte of the Precambrian-Cambrian quartzite form a discontinuous ring in Washington area, which defines portions of the north and northwestern margins of the Moscow-Pullman Basin. The CRBG extends out of Pullman area and between Angel Buttes and Kamiak on the north [*Bush et al.*, 2016].

4.3.4 Groundwater hydrology

Groundwater occurs in most of the geologic formations in the basin, but the CRBG (the Grande Ronde and the Wanapum formations) forms the most productive aquifers in the region. The interbedded sediments of the Latah Formation (the Vantage units) have comparatively little water, but they do have significant influence on the overall flow of water in the aquifer system because they control movement of water between the basalts in areas within the basin [*Owsley*, 2003]. The igneous-metamorphic basement of Palaeo-Mesozoic age that forms the pre-basalt formation also produces very little water. This basement has very low hydraulic conductivities and low porosity, which limit movement of groundwater, and there are likely few pathways for juvenile water to reach these rocks [*Smoot and Ralston*, 1987].

Groundwater exists in the Grande Ronde formation in sedimentary interbeds, fractures, and vesicles, which are subjected under high pressures. Aquifer tests indicated that the Grande Ronde basalt produces the largest volumes of municipal water for the area, with pumping wells supplying nearly 3,000 gallons per minute [*Smoot and Ralston*, 1987; *Owsley*, 2003]. The Grande Ronde formation supplies about 90 percent of the total water demand within the Palouse region. The Wanapum unit is also productive, at close to 5.7 m^3 per minute in some domestic wells in the past, and this supplies most of the balance for demand. These pumping rates are transient and believed to have changed over time [*Dhungel and Fiedler*, 2016].

The ground water basin within the Moscow area is bounded to the north, east and south by outcrop exposures of both igneous and metamorphic formations that consist of tightly interlocked grains of the Palouse Range, Bald Butte, Tomer Butte, Paradise Ridge, and many smaller unnamed hills, which creates a horseshoe-like flow region [*Owsley*, 2003]. In the Pullman area, the ground water flow system is bounded to the northwest by igneous and metamorphic formations of Smoot Hill, and to the north by igneous and metamorphic formations of Kamiak Butte [*Foxworthy and Washburn*, 1963; *Holom*, 2006].

4.4 Methods

The modeling approach used in this study started with the development of the conceptual model based on the structure of the aquifer system, followed by the translation of conceptual model into 3-D distributed, numerical model of the groundwater flow system. The groundwater flow model was calibrated using historic observed data and data from previous studies. The calibrated numerical model was then used to simulate the response of the aquifer system (changes in water surface elevations and aquifer drawdown) to different pumping scenarios. Details of the simulation platform and the modeling process are described in this section.

4.4.1 Simulation Platform and Groundwater Flow Equation Solver

MODFLOW is the U.S. Geological Survey (USGS) modular finite-difference flow model that solves the groundwater flow equation. Since the development of the code in the early 1980s, the USGS has released several versions of the code such as MODFLOW-88, -96, -2000, and -2005. The version used to develop the conceptual and groundwater flow models was MODFLOW-2005 [*Harbaugh*, 2005]. MODFLOW-2005 is a version of the USGS's, world standard, finite-difference groundwater flow model that incorporate different approach for managing internal data such as introduction of new subroutines and packages [*Harbaugh, ,* 2000]. A package is the part of the program that deals with a single aspect of simulation, hence the modular nature of the code. Several packages are used in MODFLOW-2005 to perform different tasks in a groundwater flow model but the core one is the Basic package. The Basic package handles various administrative tasks including specifying the locations of active, inactive, and head cells, reads initial heads in cells and track heads throughout time, calculates overall water budget and controls model output

according to user specifications. Other categories of packages are Hydrologic (e.g., Well, Recharge, and River Package) and Solver (e.g., Strongly Implicit Procedure and Preconditioned Conjugate Gradient Packages). The Hydrologic Packages formulate the coefficients that describe internal terms or external/boundary flows. Solver Packages implement algorithms for solving systems of finite-difference equations [*Harbaugh*, 2005].

MODFLOW-NWT is a program for solving the three-dimensional groundwater flow equation. MODFLOW-NWT employs Newton solution method, asymmetric matrix solvers to compute groundwater head [*Knoll and Keyes*, 2004]. The MODFLOW-NWT was created to work with the updated flow package, Upstream Weighting (UPW), which is used for computing intercell conductance based on different assumptions that older packages like the Hydrogeologic-Unit Flow (HUF), Block-Centered Flow (BCF), and Layer Property Flow (LPF). The UPW Package handles nonlinearities of cell drying and rewetting by use of a continuous function of groundwater head, rather than the discrete approach of drying and rewetting that is used by the HUF, BCF, and LPF Packages. A cell goes dry if the head is below the bottom of the cell, and such a cell is said to have no water in storage. The Newton method requires storage coefficient to transition smoothly with continuous derivatives. However, smoothing the storage coefficient creates the chance to produce mass-balance errors because the storage parameter is nonlinear for cell drying/rewetting, The UPW Package produced by *Niswonger* [2011] was used in this study to achieve numerical stability in the solution of the groundwater flow equation. [*Harbaugh*, 2005; *Niswonger*, 2011]. The Newton method for solving nonlinear equations (e.g., the multiphase-flow and variably saturated flow equations) [*Niswonger*, 2011; *Harbaugh*, 2005] was used to solve the groundwater flow equation in this study. Newton method has advantage over other nonlinear solvers such as the Picard

method. One advantage is that the Newton method has high convergence rates compared to the Picard method [*McDonald and Harbaugh*, 1988]. In addition, drying and subsequent wetting of cells can produce convergence failure of the groundwater flow equation when using the Picard method with the rewetting algorithms of the BCF, LPF, and HUF Packages [*Doherty et al.*, 2010]. A detailed description of the Newton solver implemented in MODFLOW-2005 and newer versions are presented in [*Niswonger*, 2011].

4.4.2 Conceptual Model for Groundwater System

The hydrogeology of the SFPB was classified into 9-hydrofacies that represent the major geological sequences. The objective of the conceptual model was to create a reasonable three-dimensional, representation of the locations of the geobodies that represent each hydro-facies unit based on borehole data. A three-dimensional geological model was first created based on the nine geologic units that depicts the Columbia River Basalts and the interbed sediments of the SFPB (as presented in **Fig. 4.2**) in MODFLOW-2005. The geological framework was built from 525 core logs provided by PBAC that define the surfaces of the nine geologic units. A mesh of lateral and vertical points for each geological units was imported into MODFLOW-2005 and inverse distance weighting (IDW) interpolation method was used to interpolate each unit's logs data into a laterally continuous surface. IDW was used instead of semivariogram-based or other geostatistical methods because the dataset is large, well-distributed throughout the basin, and the units were generally laterally extensive. No manual corrections were applied to the IDW field so some suspected hydrogeologic features may not be well represented, but this is a required uncertainty tradeoff.

Qualitative information could be used to update the geobodies or basin geometry to reflect subjective interpretations of the system, but for now the philosophy is for the model to be driven by hard data in the interest of uncertainty management.

Due to high levels of uncertainty associated with the complex geologic framework of the basin, the relatively limited distribution of monitoring wells in most of the hydrogeologic units, and also to reduce computational runtime of the groundwater flow model, the 9-units geologic framework was modified into a simplified version. The upper four units collectively form the "Wanapum" unit, the next three comprise an "Grande Ronde" formation, and the bottom two cover the "deeper sediments", which have much smaller permeabilities than the top seven units, creating a 3-unit model. The 3-units geologic model was converted into the groundwater flow model and eventually used in evaluating the comparative pumping scenarios. **Figure 4.2** illustrates the overall structure of the 9-geologic units and how the units were represented in the 3-units simplified version of the model for the groundwater flow model. Both the 9-unit and the 3-unit conceptual hydrogeologic models are presented in **Fig. 4.3a** and **b**, respectively.

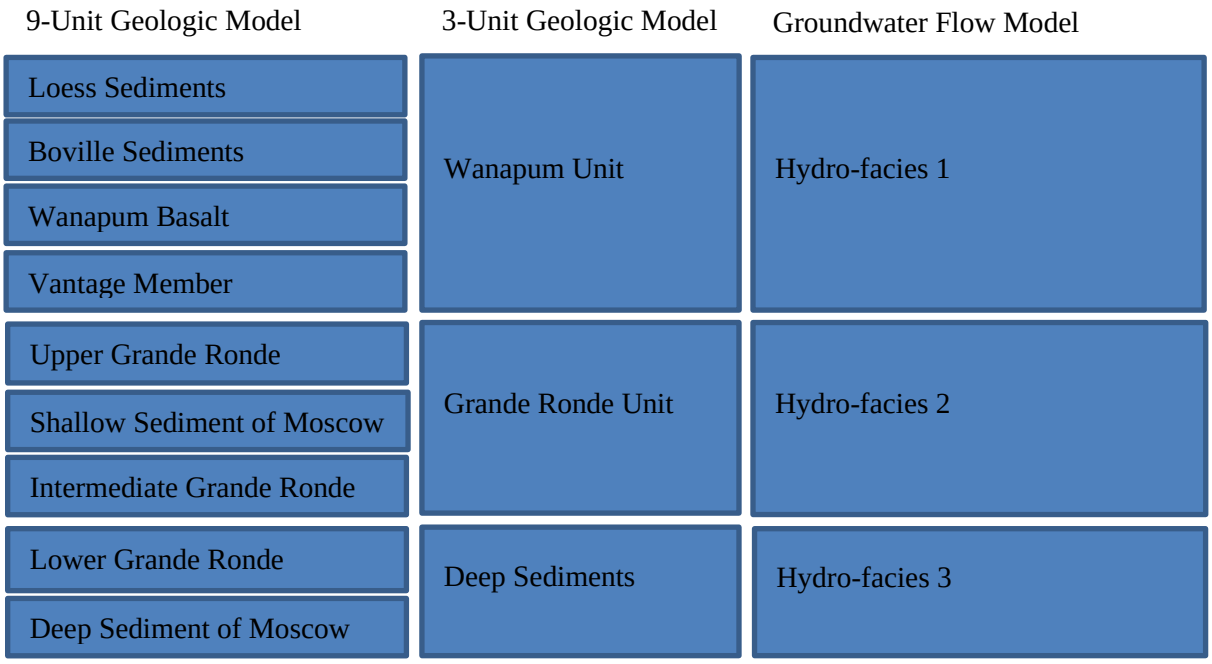

Fig. 4.2: Representation of the relationship between the structures of the 9-geologic units and the 3-units simplified version of the geological models, and the groundwater flow model. The upper four units were collectively called the "Wanapum" unit, the next three formed the "Grande Ronde" formation, and the bottom two covered the "deeper sediments" that sits on the bedrock.

Groundwater flow in the basin is controlled by the spatial distribution of natural recharge or inflows, outflows (e.g., aquifer boundary discharge), the geometry of the CRBG, the areal distribution of hydraulic conductivity, and groundwater pumping. Groundwater in the basin generally moves from higher elevations (in the east) toward the low elevation drainage area in the northwest. Groundwater relatively moves faster laterally compared to vertical flows in the CRBG deposits. Lateral hydraulic conductivities of the conceptual model of the aquifer system were

assumed to be highest in the upper aquifer units i.e., Wanapum and Grande Ronde units because of aquifers characteristics such as vesicles and the likely compaction of interbeds at depth.

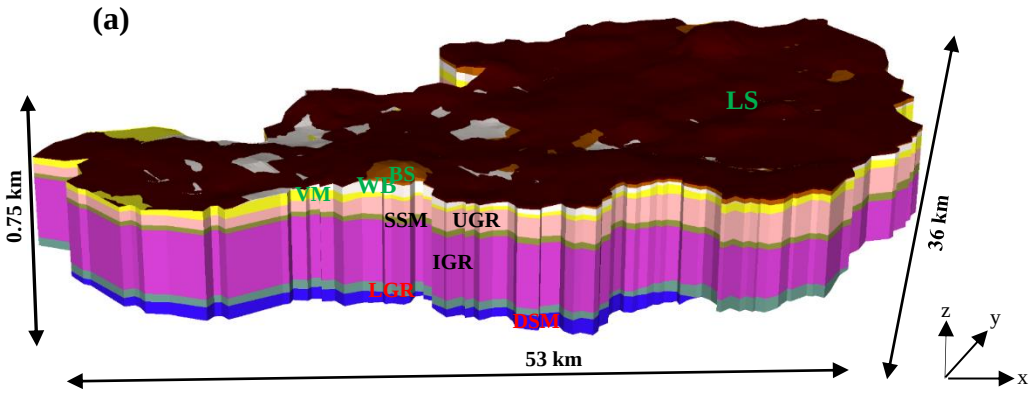

LS: Loess Sediment**; BS**: Boville Sediments; **WB**: Wanapum Basalt; **VM**: Vantage Member; **UGR**: Upper Grande Ronde**; SSM:** Shallow Sediment of Moscow; **IGR**: Intermediate Grande Ronde; **LGR**: Lower Grande Ronde; **DSM**: Deep Sediments of Moscow

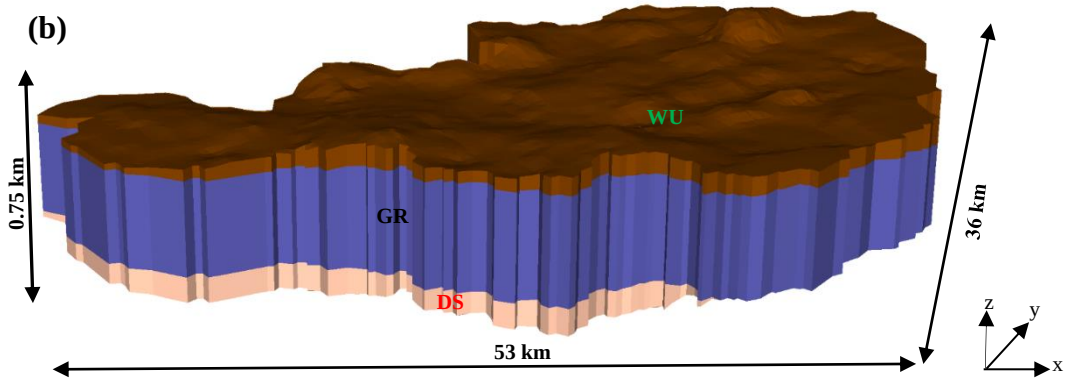

WU: Wanapum Unit; **GR**: Grande Ronde Unit**; DS**: Deep Sediments

Fig. 4.3: (a): The overall structure of the 9-unit geologic model of the model area generated from MODFLOW. (b): The 3-units simplified version of the geological model of the model area generated from MODFLOW.

4.4.3 Numerical Simulation of Groundwater Flow

Details of the simulation procedure for the groundwater flow model are presented below including spatial and temporal discretization, hydraulic and storage properties, pumping data, hydrologic boundaries, model calibration, and pumping scenario testing.

4.4.3.1 Groundwater Flow Equation

The partial differential equation of groundwater flow used in MODFLOW-2005 is:

$$\frac{\partial}{\partial x}\left(K_{xx}\frac{\partial h}{\partial x}\right)+\frac{\partial}{\partial y}\left(K_{yy}\frac{\partial h}{\partial y}\right)+\frac{\partial}{\partial z}\left(K_{zz}\frac{\partial h}{\partial z}\right)+W=S_s\frac{\partial h}{\partial t}, \qquad (4.1)$$

where K_{xx}, K_{yy}, and K_{zz} $\left[\frac{\mathrm{L}}{\mathrm{T}}\right]$ are values of hydraulic conductivity along the x, y, and z coordinate axes, which are assumed to be parallel to the major axes of hydraulic conductivity, h [L], is the hydraulic head, S_s $\left[\frac{1}{\mathrm{L}}\right]$ is the specific storage, t [T] is time, W $\left[\frac{1}{\mathrm{T}}\right]$ is the volumetric flux per unit volume representing sources and/or sinks of water, with positive volumetric flux for inflows into the model domain, and negative volumetric flux for outflow, [*Harbaugh*, 2005]. Equation (4.1) defines groundwater flow under non-equilibrium or transient conditions in a heterogeneous and anisotropic medium, given that the axes of hydraulic conductivity are aligned with the directions of the coordinates.

4.4.3.2 Spatial and Temporal Discretization

The MODFLOW-NWT model allows for arbitrary gridding of the domain into cells/grids in the vertical and horizontal directions. The SFPB model domain was subdivided into horizontal grids of 126 rows and 161 columns using a semi-uniform mesh with a constant lateral grid cell size of 300 m. The layer thicknesses varied spatially and also by layer to capture the changing thickness of the aquifer. The model domain was made up of 3 layers, which extended vertically up to 750 m at the thickest part of the active domain with an area of approximately 290 km^2. Each of the 3-geologic units was discretized vertically to represent the individual layers in the model domain, and also preserve the appropriate local-scale connectivity of each of the aquifers with hydrologic characteristics.

Temporal discretization occurs in the simulation process in two parts: time-steps and stress periods. Stress periods normally corresponds to the changes in external stresses such as groundwater pumping and recharge rates and a stress period may be applied for an arbitrary length of time. The MODFLOW solvers applies any changed at the beginning of a stress period then assumes that all properties and external forcings on the model remain constant during that stress period. Time-steps determine the time intervals at which the groundwater flow equations are solved and there may be multiple time steps within a stress period. Essentially, the time steps sub-divide the stress period to provide greater accuracy, which comes at the cost of additional solver calls; the solver must be called for each time step in each stress period. In the groundwater flow simulation, the first or initial stress period represent the steady-state predevelopment conditions, and this is because the steady-state model creates time-independent solution since all data inputs such as pumping are constant. Monthly time-step was selected for the simulation to better represent the changes of the transient flow field. MODFLOW automatically merges all of the different time

period data defined for each pumping well and boundary condition and use that to set the stress period for the simulation, so users do not set the stress period. A yearly stress period was specified by MODFLOW based on the different time period data defined in the model.

4.4.3.3 Hydraulic Properties

The individual geologic units were assumed to be locally homogenous and vertically anisotropic. Lateral hydraulic conductivity (K_h) in each of the geologic units was higher than the corresponding vertical hydraulic conductivity (K_v). The system was simulated as laterally or locally homogeneous because the geologic units generally are large volumes of basalts and are with or without very thin layers of sedimentary interbeds and each basalt unit is made up of common lithotype, but that varies vertically among the units. A single initial K_h was set for each of the geologic units. However, the K_h value for each of the geologic units was varied during parameter estimation process. The initial K_h values were defined based on estimated values for the basalt units from previous studies in the region such as *Lum et al.,* [1990] and *Hansen et al.,* [1994]. Since the previous work agglomerated field data and involved some calibrated models, the estimates from these studies provide a reasonable starting point for the hydraulic conductivity values prior to calibration. Previous estimates of K_h for the basalt aquifers generally decreased in depth, and that was attributed to long-term effects of pressure and secondary mineralization, that have caused reduction in pore space with depth. The role of reduced K_h with depth has been examined and used in groundwater flow modeling studies in deep aquifer systems and within the Columbia plateau [*Lum et al.,* 1990; *Hansen et al.,* 1994; *Ely et al.,* 2014].

Vertical movement of water through the aquifers (i.e., the 3-geologic units) are represented by the bulk K_v. The basalt aquifers (Wanapum and Grande Ronde formations) are thick, and water flow through the system is dominated by the thick flow interior of the basalts, the system may exhibit greater amount of heterogeneity vertically. As was the case of K_h, the K_v for the individual geologic units assumed lateral or local homogeneity. The initial (K_v) values were estimated based on the anisotropic ratios from the previous groundwater flow modeling studies in the basin [*Lum et al.*, 1990; *Hansen et al.*, 1994; *Ely et al.*, 2014].

4.4.3.4 Storage Properties

Aquifer storage properties for the groundwater flow model were based on the estimates from previous aquifer modeling studies within the Palouse region and in the Columbia basin including *Bauer and Vaccaro*, 1990; *Lum et al.*, 1990; *Hansen et al.*, 1994; *Ely et al.*, 2011; *Kahle et al.*, 2011; *Vaccaro et al.*, 2015. Values of specific storage S_s (1.0×10^{-4} m^{-1}) for the geologic units, and a bulk specific yield of $S_y = 0.2$ (dimensionless) were used as the initial values in the model and were consistent with the reported values from the prior studies. Values of porosity appropriate for basalt aquifers and consistent with the previous studies were used for the geologic units.

4.4.3.5 Hydrologic Boundaries

Three types of model boundaries were defined in the groundwater flow model: (1). No-Flow boundaries (zero-flux), (2) General head boundary (GHB), and (3) specified flux boundary, which accounted for the net surface recharge into the shallow aquifers. These represent physical

or topographic barriers to groundwater flow, groundwater flow out of the basin, and surface recharge, respectively.

The South Fork Palouse River Basin is bounded towards the east, south, and northeast by the low permeability rocks of the Meso-Cenozoic basement of Moscow Mountains, Palouse Range, and Kamiak Butte, respectively. These natural features at the east, south, and northeast served as hydraulic boundaries with nearly no groundwater flow across the boundary into or out of the simulation domain. As a result, these boundaries were set as "No-Flow" boundaries for all the geologic units in the model.

Groundwater discharge to the Palouse River occur along the northwest side of the Palouse Basin. However, the discharge may not be regional due to the size of the Palouse River [*Smoot and Ralston*, 1987]. The northwestern boundary was defined as a General-Head Boundary (GHB) at a boundary distance away from the model domain. The GHB is a head-dependent flux boundary, where flow into or out of a cell from an external source provided is proportional to the difference between the head in the cell and the reference head assigned to the external source/sink. The GHB are typically used to represent heads in a model that is influenced by large surface water sources away from the model area or to simply "pad" the domain from the influence of a boundary. The boundary conductance $C\ \left[\frac{\mathrm{L}^2}{\mathrm{T}}\right]$ term represents the resistance to flow between the cell or model domain (the aquifer) and the external source boundary head is:

$$C = \frac{(L \times W) \times K}{D}, \qquad (4.2)$$

where $(L \times W)$ $[\mathrm{L}^2]$ is the surface area of the cell face exchanging flow with the external source or sink, K $\left[\frac{\mathrm{L}}{\mathrm{T}}\right]$ is the average hydraulic conductivity of the aquifer material that separates the model cell from the external source or sink, and D [L] is the distance from the model cell to the external source [*Harbaugh*, 2005; *Niswonger*, 2011].

The basement rock of the Palouse region is believed to be made up of Precambrian Belt Supergroup metamorphic rocks, Cambrian metamorphic rocks, and Cretaceous granite associated with the Idaho Batholith [*Hernandez*, 2007]. These crystalline rocks are impermeable at the contact of the basalt units, so the bottom of the model was defined as a "No-Flow" boundary.

The top boundary was specified as net recharge flux to capture precipitation, evapotranspiration, and snowmelt effects on the shallow aquifer. Shallow aquifer recharge mainly occurs through the surficial loess which are responsive to seasonal precipitation, snowmelt, and little evapotranspiration. Generally, high intensity precipitation and snowmelt provide maximum recharge through the loess especially at the low-lying areas and these recharge eventually ends up in the deeper aquifers in places of high hydraulic connectivity [*Smoot and Ralston*, 1987; *Lum et al.*,, 1990; *Johnson, G. E.*, 1991; *Johnson et al.*, 1996; *Candel et al.*, 2016; *Duckett et al.*, 2019]. Recharge to the groundwater system in the Palouse region have been studied extensively in the past decades and different values of net recharge to the loess and shallow aquifers have been estimated (see Table 1). Recharge to the shallow aquifer was based on previous recharge estimates. The model domain was divided into two zones which were characterized by different natural net recharge rates into the shallow aquifer: Recharge Zone 1 and Recharge Zone 2 (**Fig. 4.4**). These zones are somewhat arbitrarily because of the uncertainty about specific recharge pathways, but

the boundaries are based on the general understanding of the recharge entering the shallow aquifer from previous studies. The western zone (Recharge Zone 1) was given a distributed average recharge value of 25 mm per year. The eastern zone (Recharge Zone 2) was characterized by higher (approximately 45 mm per year) recharge distributed over the area. The higher recharge rates at the eastern area of the basin is intended to account for snowmelt from the adjacent highlands [*Duckett et al.*, 2019]. Note that values applied to each are aerially integrated averages and that the actual distribution of recharge in specific places could be significantly higher or lower than the large-scale average.

4.4.3.6 Groundwater Pumping

Groundwater pumping wells in the basin primarily exist near Pullman and Moscow (**Fig. 4.4.**). Historic groundwater pumping data over the last four decades from 20 pumping wells within the model domain were supplied by Palouse Basin Aquifer Committee (PBAC). The pumping records spanned from 1983-2018 with intermittent periods of no records. Periods where no data existed, the average pumping was estimated using data from closest periods. For example, if no data exists for periods between 1990 and 1992, the average of records from 1990 and 1992 were used for the no-data period (i.e., 1991). Figure **Fig. 4.5** represents the total pumping rates within Moscow, University of Idaho (UI), Pullman, and Washington State University (WSU) areas between periods of 1983-2018 used in the model.

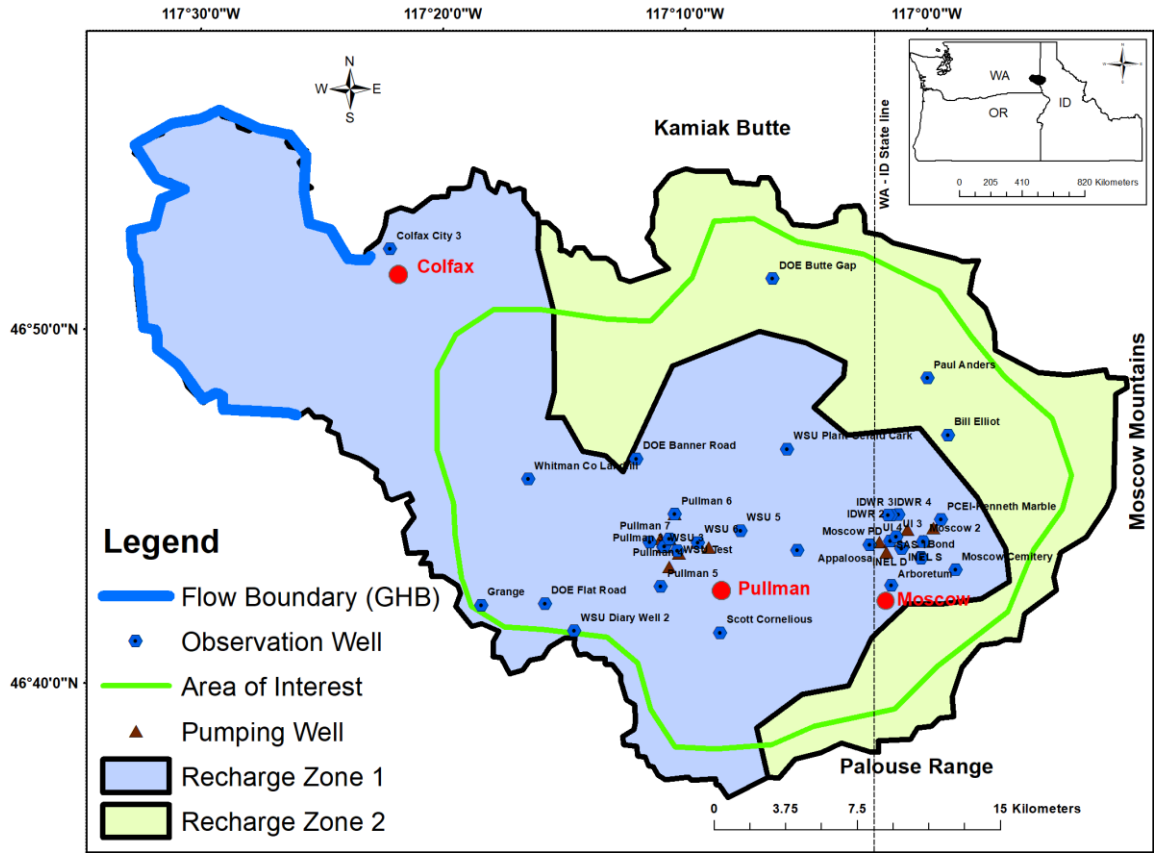

Fig. 4.4: Map showing locations of the flow boundary, observation wells, groundwater pumping wells, and net surface recharge locations within the SFPB. The "area of interest" in **Fig. 4.4** represents the portion of the model used in the analysis and indicates the region with the greatest water level changes over time. The westside of the "area of interest" is included to basically diminish the impacts of the uncertain boundary on the western edge. This is because there exists a sharp slope variation in the derivative of pumping tests near the western boundary indicating a further flow barrier. This flow barrier has been interpreted as a bulge in the basement or swarms of volcanic dykes which forms the Smoot Hill, west of the area of interest [*Lum et al.*, 1990].

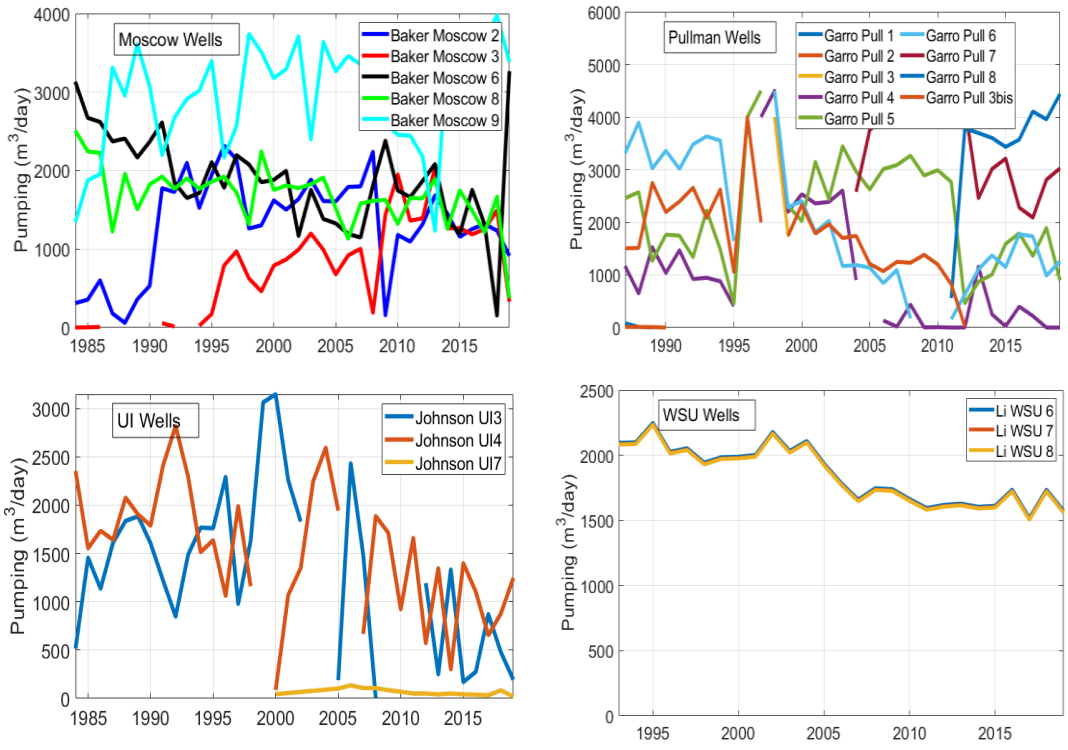

Fig. 4.5: Total groundwater pumping rates within Moscow, University of Idaho (UI), Pullman, and Washington State University (WSU) areas between periods of 1983-2018 as supplied by PBAC. All three WSU wells recorded equal pumping rates. These graphs only show the pumping rates in each of the specified areas and not for the purpose of comparison. A break in the graph indicates lack of data within that specific period of time.

4.4.3.7 Model Calibration

Two models were developed to simulate the groundwater flow in the SFPB: (a) a steady-state predevelopment model and (b) a time-dependent transient model The steady-state predevelopment

simulation represents the groundwater flow system prior to introduction of full-scale pumping and is used to initialize the transient simulation. The time-dependent, transient model simulated the calibration period of 1983 to 2018, which is then used as the starting point for comparative scenarios. Calibrations were done iteratively for both the predevelopment steady-state and time-dependent transient models starting with simulation of the predevelopment steady-state model. The initial parameters used in the predevelopment calibration such as hydraulic conductivity and specific storage were taken from previous studies [*Lum et al.*, 1990; *Hansen et al.*, 1994; *Johnson et al.*, 1996; *Ely et al.*, 2014]. The previous works used field data and also involved calibrated models, so estimates from these studies provided a suitable starting point for the calibration process. Parameter-estimated values (e.g., the hydraulic heads and lateral, and vertical hydraulic conductivity) from the steady-state model were used as starting parameter values and initial conditions in the time-dependent transient state model simulations. After evaluating each transient simulation, changes were made to the predevelopment steady-state model. For example, changes to the general head boundary value, recharge rates, and hydraulic conductivity were made in the steady-state model, and then used the estimated parameter values to start-off another transient model. The changes made to the steady-state model were done using a sequential update, trial and error method of calibration since the model ran very quickly. The transient state models were calibrated using both a non-automated parameter estimation approach and the built-in parameter estimation tool (PEST) package in MODFLOW-2005 [*Doherty et al.*, 2010]. The non-automated parameter estimation approach was used first to find reasonable initial values, then PEST was run to improve parameter estimations.

PEST allows model-independent parameter estimation and parameter/predictive-uncertainty analysis [*Doherty and Hunt,* 2010]. PEST uses a nonlinear least-squares regression to determine the parameter values that reduces a weighted sum-of- squared-errors objective function. Parameter adjustments made in the calibration process were done so parameter estimates agreed with the general understanding of the aquifer system, based on previously documented parameters such as the hydraulic conductivity and recharge estimates.

Data used in the calibration of the models such as measured hydraulic heads were provided by PBAC (Data availability and request should directed to PBAC). Monthly hydraulic head measurements from 40 observation wells were provided that spanned from 1983-2018 were divided and used for the time-dependent model calibration. The wells were divided based on those in and around Pullman-Moscow area where the aquifers are believed to be stressed due to pumping, and wells expected to be outside the influence of external stresses such as near Colfax and at the northeast boundary of the model area. The hydraulic head observations used for the transient calibration were 31 and were those near or within Moscow-Pullman areas. The other 8 observation wells were used separately to verify or assess the model behavior in those areas but were not used to determine model confidence. Two observation wells located in Moscow were screened within the Lower Grande Ronde. Seventeen well head observations were in the Upper Grande Ronde, and Twenty-one within the Wanapum unit. For calibration of the predevelopment steady-state model, a total number of 37 well head observation points for the year 1983 were used. A total number of 59,578 of mainly monthly head observation points were used for the transient model calibration. All observations targets were equally weighted.

4.4.3.7.1 Best Parameter Estimates

One-time parameter estimations were done for the predevelopment steady-state model, and the estimated parameters were used to initialize the transient model calibration. For the predevelopment steady-state model calibration, estimated model parameters were lateral and vertical hydraulic conductivity, specific storage, and hydraulic heads. K_h, K_v, and storage parameters each for the 3-layers (geologic units) were estimated from the steady-state model. The K_h was highest in the shallow Wanapum unit where basalt flows are heavy and thickest, and generally decreased slightly with depth into the lower Grande Ronde. The Wanapum unit was grouped with the overlying loess sediments and the Vantage unit of the Latah formation. The values of K_v generally increased slightly moving from the Wanapum to the lower Grande Ronde. The predevelopment steady-state model was only used to initialize the transient model calibration, so no analysis of its results is included.

The transient model calibration refined, and improved model by modifying each parameter including lateral and vertical hydraulic conductivity, surface recharge, and specific storage. **Figure 4.6** shows the plots of simulated versus measured hydraulic heads estimated in the transient model.

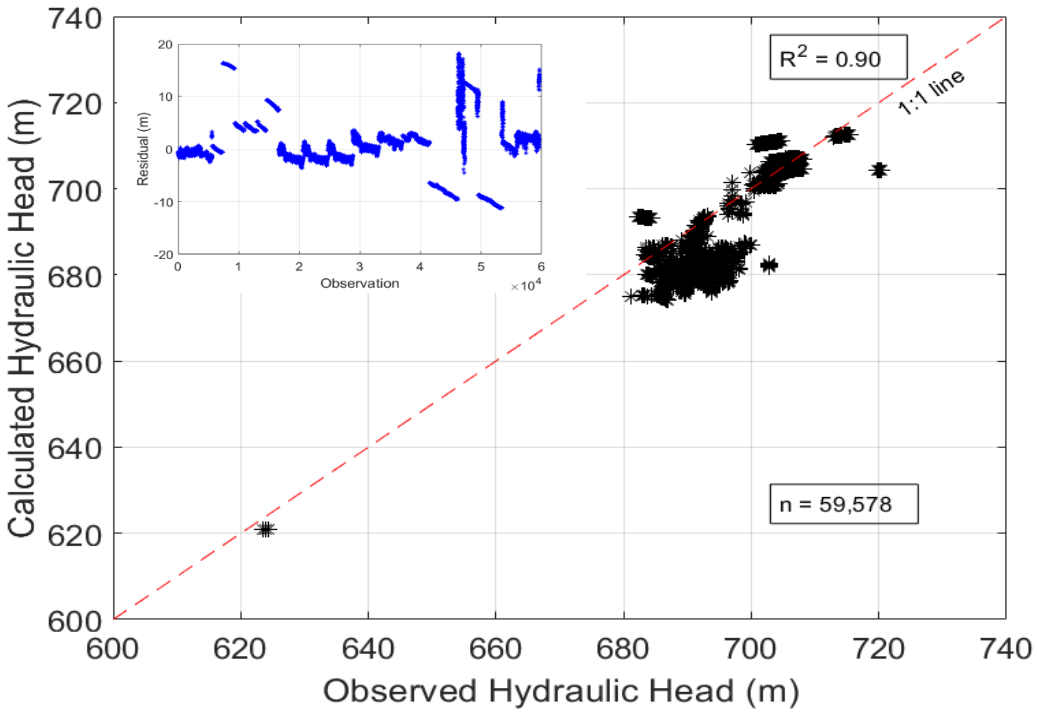

Fig. 4.6: Plot of simulated versus observed hydraulic heads for the transient calibration between 1983-2018. Insert shows plot of the residuals. There were total of 59,578 observed hydraulic heads in the model area.

Several statistical measures were used to evaluate modeling results. The average hydraulic head residual for the transient model was 1.4 m. The minimum and maximum residuals were 5.20×10^{-5} and 16.3 m found in wells located in Moscow and southeast of Pullman, respectively. The correlation coefficient R, which indicates the linear relationship between the simulated and observation data points was estimated. The computed R value of the model was approximately 0.95. The calibration outcomes with $R > 0.7$ are arbitrarily regarded as "acceptable" in hydrological practice [*Jian et al.*, 2017]. The standard error of the model estimated hydraulic heads was 0.0025 m. The final calibrated parameter values for the model domain are presented in

Table 4.3. Note that these represent layer (block) averages and that actual, local values of hydraulic conductivity in the field could be significantly higher or lower. Also note the high lateral to vertical anisotropy ratio, which may partially be an artifact since the model does not explicitly represent the connected flow paths that dominate groundwater movement.

Table 4.3: Calibrated model parameters for the South Fork Palouse River Basin used for the pumping scenarios.

Geologic Unit	**Lateral Hydraulic Conductivity (m/day)**	**Vertical Hydraulic Conductivity (m/day)**	**Specific Storage (1/m)**
Wanapum	3.5	0.003	1.0E-04
Grande Ronde	3.0	0.005	1.0E-04
Deep Sediments	2.5	0.007	1.0E-04

The mean and median difference between the simulated and observed hydraulic head data points (residuals) for the time-dependent transient model were -0.68 and 0.45 m, respectively. The residuals indicate that 54 percent of the simulated hydraulic heads were greater than the observed hydraulic heads and 46 percent were less than the observed hydraulic heads. Simulated hydraulic heads were generally less than the observed hydraulic heads in the areas of Pullman and the WSU for over 90 percent of the time. The observed against simulated hydraulic heads plots in representative or selected wells show that the hydraulic head residuals for these locations were within 6 to 10 m (**Fig. 4.7**). These areas were generally under direct influence from pumping wells due to proximity of the observation wells (**Fig. 4.4**). The trends in observed against simulated hydraulic heads in Moscow and UI areas were such that the simulated were larger than the

observed. Observation heads that were distant from the pumping locations in Moscow recorded residuals less than 2 m.

These errors are reasonable considering the homogeneity of the model layers cannot capture the highly heterogeneous distribution of hydraulic conductivity nor any highly connected, preferential flow paths. Likewise, the patterns of underestimation and overestimation of the hydraulic heads in various locations across the basin are to be expected. Most wells in Pullman, WSU, UI, and Moscow areas showed the simulated hydraulic heads being less than the observed. However, these patterns vary by positions as few wells (e.g., PCEI-Kenneth Marble and UI wells) within Moscow had the simulated hydraulic head exceeding the observed.

The high residuals produced may also be related to areas of uncertainty associated with the model such as pumping records and net recharge to the shallow aquifer and structural errors, including homogenization of the layers. For example, the use of uniform distributed recharge to the shallow aquifer may not have been physically realistic but there is insufficient data available to specify a distributed recharge field. Moreover, uncertainties in groundwater pumping rates and or screened intervals could have a direct impact on the aquifer levels or hydraulic head fluctuations. Periods without pumping records also contribute to this uncertainty (**Fig. 4.5**).

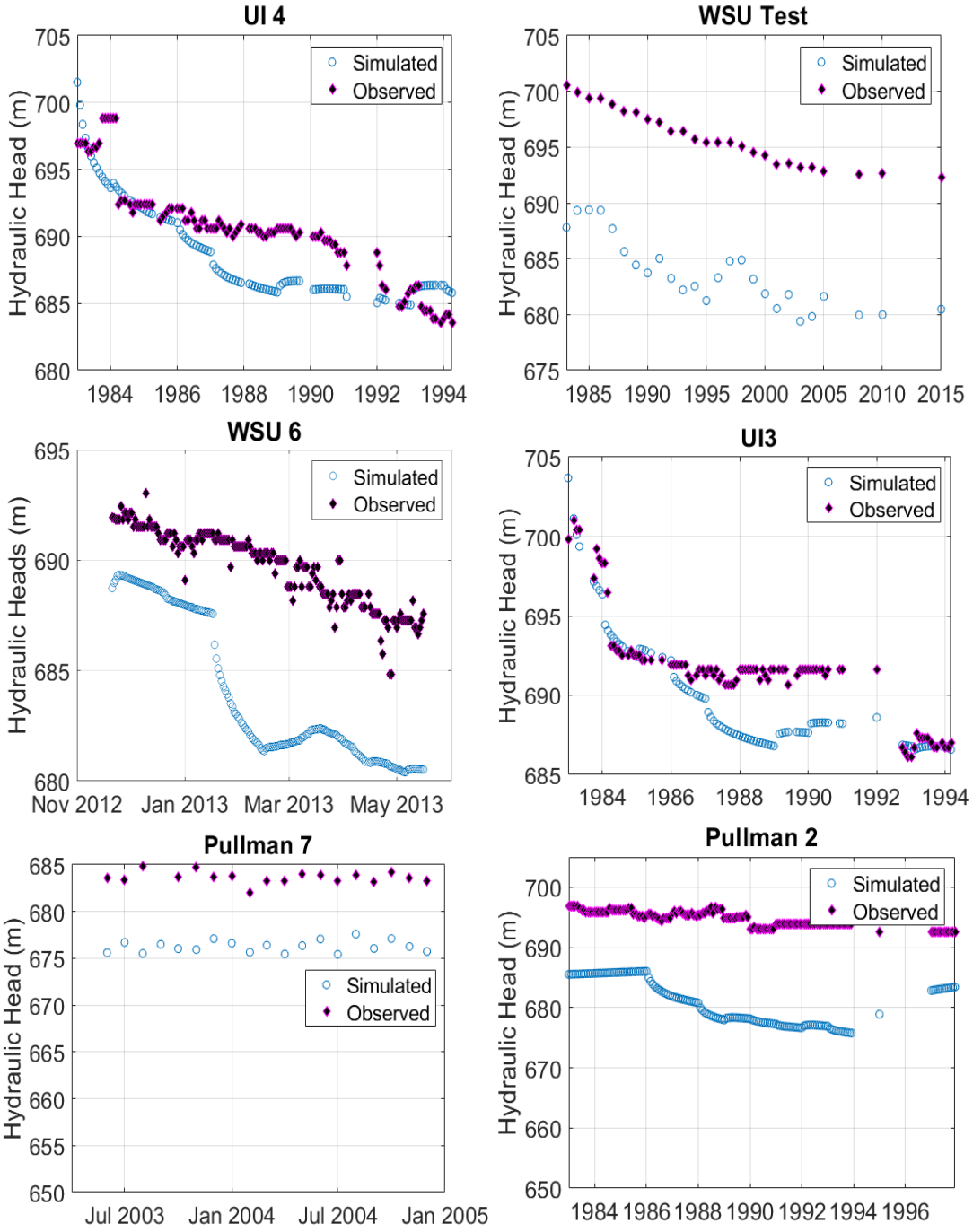

Fig. 4.7: Timeseries plots of simulated vs observed hydraulic heads in selected wells from Moscow, UI, WSU, and Pullman. These wells were arbitrarily selected as representation of the system in these areas.

4.4.4 Pumping Scenarios

The focus of the groundwater pumping scenarios were; 1) to apply the developed groundwater flow model to investigate the future response of the aquifer system to anticipated hydraulic stresses such as pumping and recharge (**Fig. 4. 8**), and 2) to determine if/how the aquifers can be revitalized with a combination of reduced pumping and supply use alternatives over the next four decades. That is, to quantify future water level changes under different pumping scenarios across the SFPB. This is important because, going into the future, an understanding of the rise of the water levels or drawdowns in responds to groundwater pumping is critical for making water management plans for the basin. For example, PBAC is currently exploring alternative ways to reduce groundwater pumping to help sustain the aquifers for the future including possible managed aquifer recharge.

Eight pumping scenarios were examined in order to evaluate aquifer response to different future pumping patterns. Since pumping patterns in the future are not known, the recorded pumping rates (as supplied by PBAC) between 1983 and 2018 were assumed to be similar to future pumping patterns; in other words, the same pumping time series from 1983-2018 was used for the future scenarios but were shifted to match the known pumping rates in 2018 (**Fig. 4.8**). The motivation for this choice was to base the future on known pumping histories; however, data are unlikely to accurately reflect future conditions. Future pumping rates will deviate from the historic rates due to population growth and any potential conservation measures (e.g., reuse of wastewater) in the basin and future climate changes could exacerbate these deviations. An alternative approach would be to use the average pumping rate in each well over the most recent 5-years of data and

apply this as the expected value for all future years, which might impact the scenarios but the long term mean of the hypothetical, future pumping rates (**Fig. 4.8**) is only slightly below the initial pumping rate so only small changes in overall behavior are expected when shifting to the mean value for future scenarios. Scenario 1 (**S1**) was based on stable pumping rates as recorded between 1983-2018 (i.e., 100 percent pumping). Scenarios 2, 3, 4, 5, 6, and 7 (**S2**, **S3**, **S4**, **S5**, **S6**, and **S7**) were based on 90, 80, 50, 25, 10, and 2 percent pumping, respectively relative to the historic pumping rates, and a no or zero-pumping scenario (**S8**) (**Fig. 4.8**). Each scenario was simulated starting off from the calibrated transient model using aquifer conditions in 2018 as reference year. The metrics to evaluate these scenarios were changes in water surface elevations (WSEL), basin-wide aquifer drawdowns, and total volume of water in the aquifer under each scenario over 35-year period.

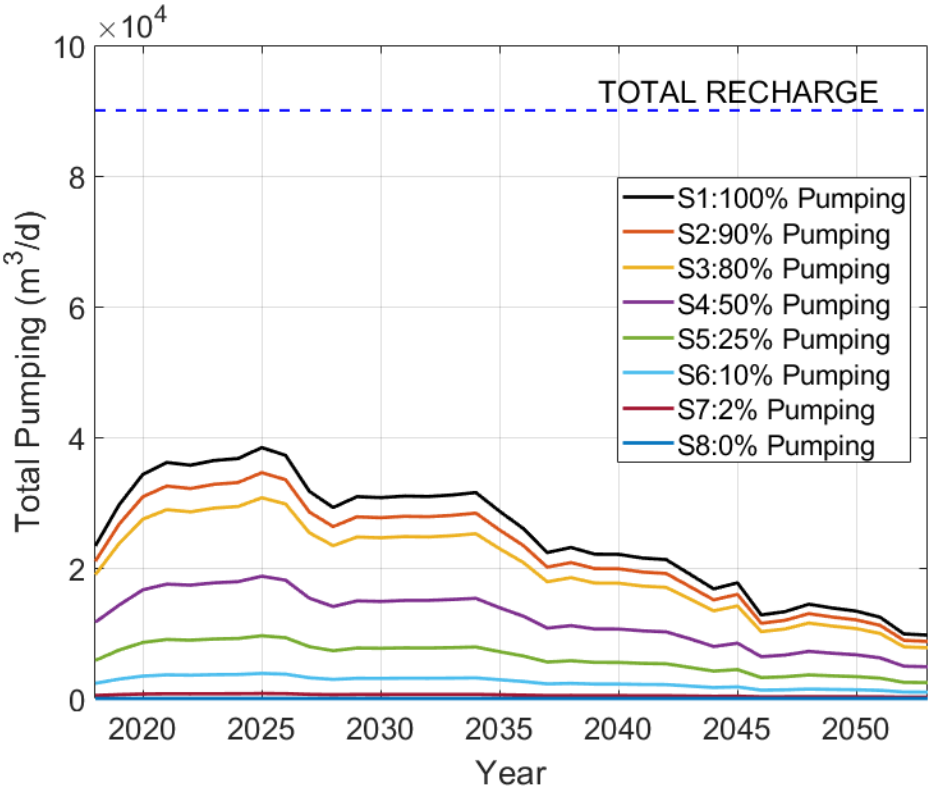

Fig. 4.8: Total groundwater pumping and shallow aquifer recharge used in each scenario.

4.5 Results and Discussions

The Pullman-Moscow aquifer responses to the impacts of different rates of groundwater pumping were investigated with the groundwater flow model. Results indicate that groundwater levels or elevations will generally decline within the area of interest (**Fig. 4.4**) if pumping remain unchanged (**S1**) into the future relative to the historic rates between 1983 and 2018 (**Figs. 4.9** and **4.10**). Conversely, groundwater levels generally could stabilize in Pullman area and improve

significantly in Moscow if pumping rates were reduced by at least 98 percent. Moreover, groundwater levels will stabilize or rise across the basin relative to the levels in 2018 (reference year) if pumping is halted. The aquifer or groundwater level is said to i) "stabilize" if the WSEL stays at or near the reference year, 2018 levels, ii) "rise or increase" if WSEL is above that of the reference year, and iii) "improve" if WSEL is above the water levels seen under **S1**. So, the WSEL could improve but still show a declining trend relative to the reference year's water level. The simulation results indicate that general trends in the depth and length of time of the decline, stabilization, or a rise in WSEL are dependent on the pumping rates. Likewise, the depth and length of time of the decline, stabilization, or a rise in WSEL were dependent on the locations of the pumping wells within the basin. Larger pumping rates increase the depth at which the WSEL stabilization or rise will occur, especially at the locations of the pumping wells (within the area of interest).

4.5.1 Scenario 1 (Pumping at 100 percent of 1983-2018 levels)

This scenario (**S1**) was simulated to assess if the aquifer levels would stabilize across the basin over a 35-year period (2018-2053) with no change in groundwater pumping relative to the pumping rates between 1983-2018. The results indicate that groundwater levels would generally decline but in a similar trend as were seen between 1983-2018. For the selected wells from Pullman and WSU areas, the groundwater levels declined on average 0.5 m within the first 10 years (i.e., by 2028) in "DOE Banner Road" and "WSU Plant Gerald Clark" wells but an average of less than 0.5 m drawdown was seen within the same period in "Pullman 5" and "DOE Flat Road" wells

relative to groundwater level in 2018 (**Fig. 4.9**). The wells then experienced additional average drawdown of about a meter in the following 25 years between 2028 and 2053. The trend in WSEL or aquifer drawdown in the selected wells were similar to other wells from the WSU and Pullman region (**Fig. 4.9**).

The simulated changes in WSEL show that groundwater levels within the Moscow and UI areas will continue to experience drawdowns if pumping continues at the same rates as seen between 1983 and 2018 (**Fig. 4.10**). The WSEL seen in the selected wells "IDWR 4", "UI 4", and "Moscow Cemetery 2" wells indicated that groundwater levels generally could decline by average of 1.0 and 4 m over the next 10 and 35 years, respectively in Moscow area relative to the WSEL in the reference year 2018. Aquifer drawdown of less than 3 m would be seen between the next 20 to 30 years under the 100 percent or historic pumping rates in the Moscow area. Moreover, the "PCEI-Kenneth Marble well" within east of Moscow showed similar declining trend in groundwater levels as were the case of other Moscow wells (**Fig. 4.10**). It must be emphasized that the selected wells were located within the area of interest and around heavily pumped regions in UI and Moscow areas but were distant from the pumping wells to avoid bias in the results (**Fig. 4.4**).

The significance of the results for the "do nothing only pump" or 100 percent pumping scenario is that there are virtually little or no chance for groundwater levels to improve or stabilize over the next 35 years in the Pullman-Moscow region especially within the area of interest. The declines in aquifer levels will persist through to the end of the 35 years. The implication of the simulation results is that stabilization of the aquifer levels may occur, but it could take quite a long time before

that happens, probably close to a century if groundwater pumping continues unabated or at a rate equal to the recent (1983-2018) pumping rates. The results showed that some areas within the basin could experience rises in groundwater levels with 100 percent pumping conditions, but these areas were seen to be far from the pumping wells i.e., outside the area of interest (see 35-year basin-wide drawdown plots in **Appendix Fig. A1**). As a result, those regions were not captured within the cone of depression of the pumping wells yielding the rises or stabilization of the groundwater levels.

4.5.2 Reduced Pumping Scenarios (**S2-S7**)

The reduced pumping scenarios were designed to simulate the response of the groundwater flow system in terms of changes in WSEL and aquifer drawdowns under the condition that groundwater pumping across the basin were reduced by 10, 20, 50, 75, 90, or 98 percent with reference to the historic pumping rates (1983-2018). The simulation results showed that reducing groundwater pumping could generally lead to improved aquifer levels in locations within the area of interest (**Figs 4.9** and **4.10**). Groundwater level stabilization at certain locations and to some extent rises in the aquifer levels were seen at the margins of the area of interest and outside the area of interest (**Appendix Figs. A2-A7**), but the stabilization or rises in the aquifer levels depend on the magnitude of the reduction in pumping. Generally, larger reduction in pumping resulted in greater declines in aquifer drawdown. With exception of **S6** and **S7** (10 and 2 percent pumping) where the WSEL increased in Pullman area, the general trends in WSEL and aquifer drawdown were relatively similar to **S1** (100 percent pumping) where the aquifer levels declined within the

area of interest. Reducing pumping by either 10, 20, 50, or 75 percent could generally lead to improved aquifer levels but showed a declining trend when the system is considered on a long term i.e., 35 years.

In the 10 percent pumping reduction scenario (**S2**), the initial 10 years (2018-2028) saw little improvement in WSEL (approximately 0.05 m relative to **S1**) within the Pullman and WSU areas. The difference between **S1** and **S2** drawdown was approximately 0.2 m in the selected wells from Pullman and WSU over the last 25 years of the simulation. The aquifer levels in Pullman and WSU wells (e.g., DOE Banner Road, DOE Flat Road, WSU Plant Gerald Clark, and WSU Dairy well 2) declined by an average of 1.2 m, relative to the water level simulated in 2018 in the last 25 years of the simulation when groundwater pumping was reduced by 10 percent. An average of 1.5 m drawdown was seen in wells from WSU and Pullman areas relative to 2018 water levels over the 35-year period. Less than 0.1 m drawdown occurred between **S1** and **S2** in the first 10 years in Moscow wells (IDWR 4, Moscow Cemetery 2, and PCI-Kenneth Marble wells) (**Fig. 4.10**). Aquifer levels in most of the wells in UI and Moscow only declined by 0.5 m within the first 10 years, relative to the water levels seen in the reference year 2018. The difference between **S1** and **S2** drawdown was approximately 0.1 m in wells from UI and Moscow over the last 25 years. Overall, the aquifer under **S2** declined on average of 3.5 m in UI and Moscow areas relative to water level in the reference year, 2018. This indicate that reducing groundwater pumping by 10 percent would be slightly better in improving the aquifer levels and these changes could be significant over time giving the fact that the drawdown shown were close to aquifer stressed zones i.e., within the area of interest where significant pumping occur in the basin.

Results of **S3** (20 percent reduction in groundwater pumping) were generally similar to that of **S2**, such that the aquifer levels continue to decline, but with little improvement in WSEL relative to **S2**. The simulated WSEL for **S3** were slightly higher than **S1** and **S2** i.e., less drawdown occurred under **S3** (**Figs. 4.9** and **4.10**) in all wells from the various locations within the area of interest. **S3** indicated that reducing pumping by 20 percent could only improve the aquifer levels by 0.1 m in the next decade in Pullman and WSU areas compared to 100 percent pumping. The Moscow wells experienced about 0.2 m improvement in the aquifer levels within the first 10 years with respect to the **S1** groundwater levels. **S3** resulted in about 0.5 m and 1.0 m declines in aquifer drawdown in Pullman and Moscow areas, respectively relative to the drawdown simulated under 100 percent pumping scenario (**S1**). Moreover, the aquifer declined by an average of 1.0 m and 3.1 m in Pullman and Moscow regions, respectively relative to that of the reference year 2018 over the 35 years of the simulation.

Simulation of **S4** indicated that pumping at 50 percent relative to the historic pumping rates (1983-2018) may not stabilize the aquifer levels but likely lead to significant improvements in aquifer levels in most parts or locations of the areas of interest (**Figs. 4.9** and **4.10**). The region outside the area of interest could see stabilization of the aquifer levels (see **Appendix Fig. A4**). The flow path and the downward hydraulic gradient in the basin is such that groundwater that is not available for pumping would likely move to the region leading to stabilized aquifer levels. There were about 0.4 m improvement in aquifer levels in Pullman and WSU wells in the first 10 years of the simulation compared to **S1**. Aquifer drawdowns were reduced in Pullman and WSU areas by approximately 1.2 m over the 35-year period relative to the aquifer levels under **S1**. The

average aquifer decline in WSU and Pullman region under **S4** was 0.5 m relative to water level recorded in the reference year 2018. The simulated WSEL in **S4** indicated an average improvement in aquifer levels of 1.8 m over the simulation period in UI and Moscow areas relative to the aquifer levels under **S1**. However, the aquifers declined on average 2.2 m relative to the reference year 2018 in the region.

Results of **S5** indicate that pumping 75 percent less than the historic rates could generally lead to stabilized aquifer levels at locations in Pullman, and significant improvement in water levels in UI and Moscow areas. Pullman water levels increased by an average of 0.05 m in the first decade of the simulation relative to water level recorded in the reference year 2018. The aquifer levels increased by an average of 0.2 m relative to 2018 water level at the end of the 35-year period. Only "WSU Plant Gerald Clark" well recorded a water level decline of about 0.8 m in the first 10 years and 1.6 m at the end of the simulation relative to 2018 water level (**Fig. 4.9**). This well was close to the Moscow area. Insignificant water level declines (less than 0.001 m on average) occurred in UI and Moscow areas in the first 10 years of the simulation. Moreover, about 1.7 m drawdown was seen in the Moscow area at the end of the 35-year period relative to 2018 water levels.

The results indicate that pumping less than 10 percent (**S6** or **S7**) historic rates could likely lead to increased water levels at locations within the area of interest (e.g., Pullman) and improved aquifer levels in the Moscow areas. Reducing pumping by 90 or 98 percent could improve the water levels in UI and Moscow areas by an average of 3 m relative to the 100 percent pumping scenario (**S1**). The aquifer levels declined on average of 1.2 m relative to reference year 2018 water

levels in UI and Moscow areas if pumping occur at 2 percent of the historic pumping levels. Pullman aquifer levels increased by an average value of 1.0 m relative to 2018 water levels over the 35-year period if less than 10 percent pumping relative to historic levels were done. However, the aquifer levels Iin Pullman rose about 2.5 m relative to **S1**.

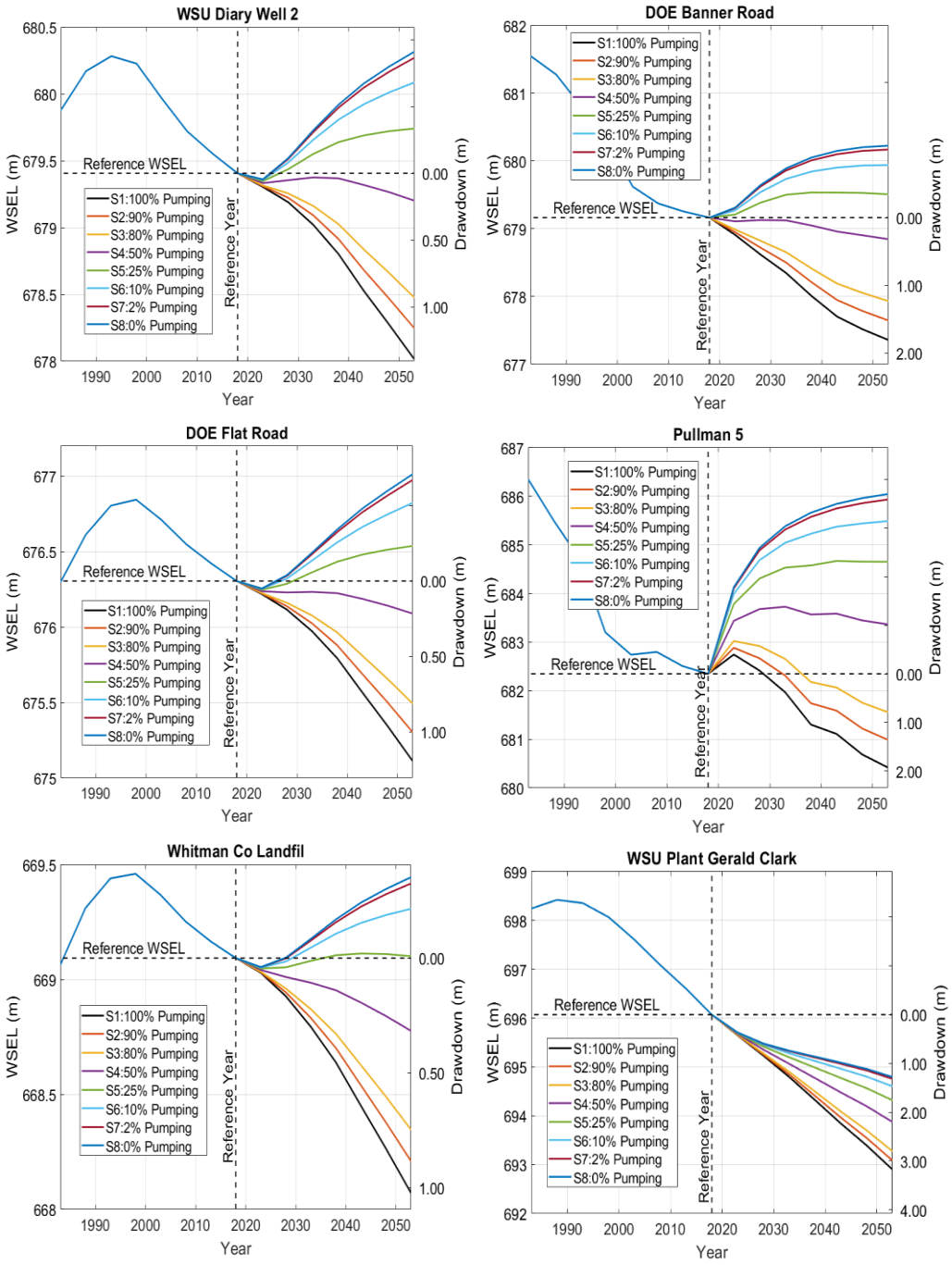

Fig. 4.9: Simulated aquifer drawdown in selected wells within Washington State University and Pullman region. The WSEL to the left of the "Reference year 2018" were periods used for model calibration or pre-scenario period and WSEL to the right are simulated under the scenarios. Below

the “Reference WSEL” shows the drawdowns (on the right y-axis) counting downward. The scenarios spanned from 2018-2053. These wells were all within the area of interest.

All the reduced pumping scenarios indicated that lowering groundwater pumping by 10, 20, 50, 75, 90, or 98 percent could reduce aquifer drawdown and may stabilize water levels (in the case of 90 or 98 reduction in pumping) in portions of the basin. The rate of declines in drawdown is directly proportional to the rate of reduction in groundwater pumping i.e., the greater the reduction in pumping the higher the decline in drawdown. This signifies that pumping has great impact on aquifer levels especially within the area of interest or heavily pumped regions in Pullman and Moscow areas. Groundwater pumping impacts on the system were much seen in the WSEL for Pullman area. For example, during the period 1996-1998, no pumping data were recorded (**Fig. 4.5**), as such aquifer levels were seen to improve in wells close to the area for that period. This does not in any way denigrate the significance of the results from this study but only identifies where some of the extremities seen in the results could be traced. Although, the groundwater flow model developed in this study used the best estimates of recharge to the shallow aquifers that were distributed uniformly to the arbitrary recharge zones, we believe more effort still need to be directed finding the controls of groundwater recharge in the area.

4.5.3 No Pumping Scenario (S8)

Scenario 8 simulates the aquifer system with zero groundwater pumping. The results showed that aquifer levels could likely stabilize and continue to increase with no possibility of

future declines. All wells within the area of interest showed rising aquifer levels throughout the simulation period. The average rise in WSEL within the first decade in WSU and Pullman areas was 1.2 m relative to water surface elevations recorded in the reference year 2018 (**Fig. 4.9**). The aquifer increased by an average of 3.5 m over the entire period in the WSU and Pullman areas compared to the water elevations in 2018. The WSEL in Moscow and UI areas showed average increase of 1.0 m relative to 2018 elevations in the first 10 years and that trend continued to about 3.2 m at the end of the simulation (**Fig. 4.10**). Scenario 8 produced the most suitable results in terms of always causing aquifer level stability or revitalization. However, implementation of this scenario by water managers (i.e., PBAC) may not be feasible because that could mean water users would have to stop pumping entirely over a period.

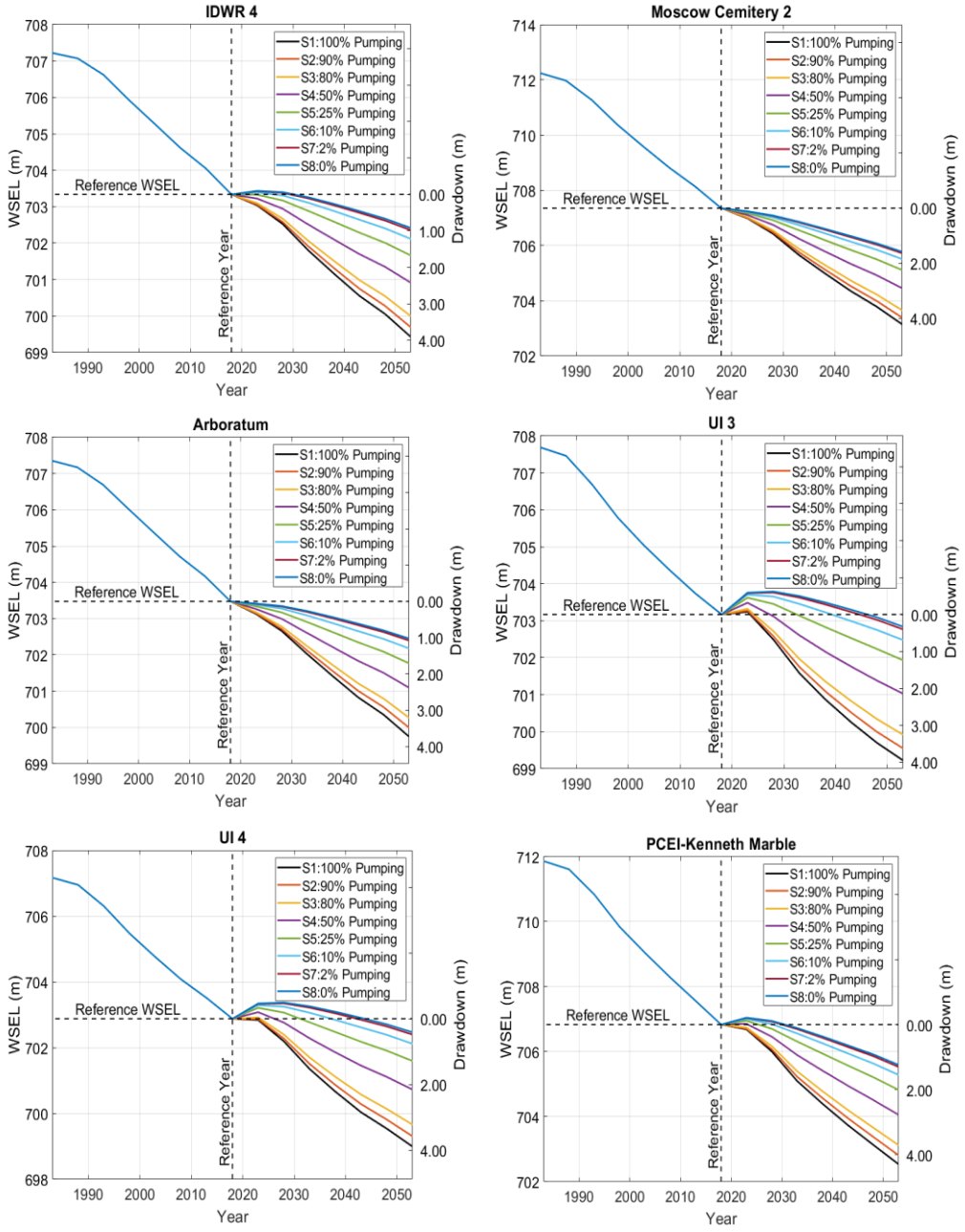

Fig. 4.10: Simulated aquifer drawdown in selected wells within University of Idaho and Moscow areas. The WSEL to the left of the "Reference year 2018" were periods used for model calibration or pre-scenario period and WSEL to the right are simulated under the scenarios. Below the

"Reference WSEL" shows the drawdowns (on the right y-axis) counting downward. The scenarios spanned from 2018-2053. All wells were within the area of interest.

Since groundwater is the sole municipal water supply source for the towns and cities within the Palouse region including Pullman, Moscow, and Colfax, and the populations of the WSU and the University of Idaho, it is important the aquifers remain as a reliable water source for future generations. One sure way to achieve groundwater availability in the foreseeable future is to reduce groundwater pumping significantly or preferably halt pumping for a period of time within the Moscow-Pullman corridor. The aquifer levels could be revitalized to a sustainable level where future drawdowns at locations within the basin are eliminated if pumping is reduced by at least 90 percent or completely halted, especially within regions of "greater importance" i.e., areas where groundwater is under the influence of pumping wells. Additional results suggest that the aquifer levels generally will continue to decline mostly near the pumping areas if groundwater pumping remain equal or even reduced by half or 75 percent of the historic pumping levels. The groundwater flow model developed in this study and the pumping scenarios evaluated (i.e., water level simulations) provide some guidance for regulating pumping within the Moscow-Pullman Basin. Specifically, the model will come as a useful decision-making tool to water managers and users including the Palouse Basin Aquifer Committee (PBAC) and the cities of Moscow and Pullman, and the two universities in evaluating future groundwater management options in the Moscow- Pullman region.

4.5.4 Total Aquifer Volume

Reducing groundwater pumping generally could lead to stabilized or improved water levels at locations across the basin, but the total volume of water in the aquifer system could decrease in response to pumping. Results of the total volume of water in the aquifer under each of the scenarios indicate that aquifer volume could generally decrease under each of the reduced pumping scenarios, relative to the aquifer volume estimated in the first year 1983 (**Fig. 4.11**). However, the rate of decline in the total volume of water in the aquifer is dependent on the rate of reduction in groundwater pumping. High pumping could likely lead to high reduction in the total volume of the aquifer. The results suggest that increase in total aquifer volume could persist under zero pumping conditions over the next four decades.

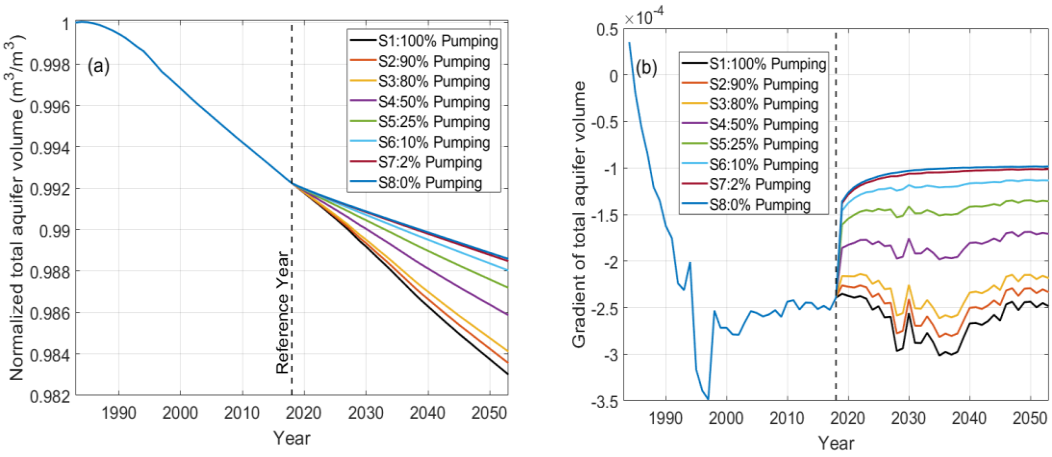

Fig. 4.11: (a) Estimated total aquifer volume under each scenario normalized with respect to 1983 total aquifer volume. (b) Time derivative of the total aquifer volume of the normalized curve in Fig. 4.11 (a). The gradient indicate that steady drawdown rate occurs in each of the scenarios based

on the averaged groundwater pumping.

The results of **S1** (100 percent pumping) indicate that approximately 70.4 billion m^3 of groundwater could remain in the basin. Close to 1.2 billion m^3 could likely be lost from the aquifers relative to the basin-wide aquifer volume in the first year (i.e., the simulated total volume of groundwater in the system in 1983 was approximately 71.6 billion m^3). Scenarios **2**, **3**, **4**, **5**, **6**, and **7** could result in total aquifer volumes of 704.5 billion m^3, 704.9 billion m^3, 706.2 billion m^3, 707.3 billion m^3, 707.9 billion m^3, and 708.2 billion m^3, respectively over the 35-year period. Moreover, the no-pumping scenario (**S8**) could yield a total aquifer volume of 72.2 billion m^3.

4.6 Model Uncertainty and Limitations

The three-dimensional groundwater flow model was developed to represent the complex aquifer system in the Moscow-Pullman region. There are inherent uncertainties and errors linked to the assumptions and parameter simplifications that were made to complete the model. Also, there were potential errors that can be associated with the hydrologic modeling process that include: i) representation of the hydrogeologic system (aquifer units) in the region, ii) input data including observation data points and groundwater pumping and recharge, and iii) model calibration. These collectively could limit the efficiency of the model in evaluating future management scenarios.

The model was designed to map the nine geologic units to represent the extent and thickness of each of the geologic units in the basin. Simplification of the nine-units version to

three-units eliminate details of the hydraulic properties including vertical and lateral hydraulic conductivity of individual basalt flows and the interbed sediments. This is a shortcoming of the model that may be a hinderance to the application of the model to simulate the real system.

The model relied on data on groundwater pumping and observation head points for the calibration process and model scenarios and it is important to note that there are uncertainties associated with the data too. For example, periods of no records were recorded for both observation head points and pumping wells. This means that there was a great deal of uncertainty in the predictions from the model for the periods when no data existed, since no comparisons could be made. Periods where few pumping wells in Pullman were estimated or generated from the available data likely led to greater uncertainty and inaccuracy. Also, the approach for specifying future pumping rates based on historic rates may not be reasonable for the forward simulations (i.e., future scenarios) for several reasons. First, the period of record from 1983 onward has a sharp change in drawdown that reflects conservation measures enacted by PBAC; it is not likely that the same gains could be made again. Second, as a consequence of the first reason, the time series of pumping rates decreases over time but population in the region is expected to grow by about 1% annually. This implies a small long-term gain might be more realistic past 2018. Third, the variability in the future pumping time series used herein is essentially arbitrary and may introduce uncertainty. The long-term mean of the signal is only slightly below the 2018 pumping rates, but a less-biased approach of applying the mean from 2013-2018 for any period beyond 2018 would likely impose less uncertainty. Future variability in annual pumping rates should be estimated based on a combination of anticipated population growth, changes in water usage, changes in climate, and then combined into a stochastic ensemble to assess the plausible ranged of uncertainty

about the anticipated mean behaviors.

Recharge to the shallower aquifer were based on estimates from previous studies in the Palouse region [e.g., *Barker*, 1979; *O'Brien et al.*, 1996; *O'Geen et al.*, 2005; *Reeves*, 2009; *Burns et al.*, 2011; *Dijksma et al.*, 2011; *Duckett et al.*, 2019]. The approach used in estimating recharge in this model development did not account for the inherent contributions from streams and creeks (e.g., the Paradise Creek) and other sources such as wastewater treatment plants in the region. Previous studies may have accounted for these potential recharge sources, but the uniform recharge distributed over the two defined zones did not capture the modern inflows to the shallow aquifers. This uncertainty associated with recharge estimates may have increased the limitations of the model in predicting hydrologic conditions of the region. These simplifications and assumptions or estimations used could substantially affect the outcomes of the model when used to evaluate future management scenarios without improvement in the data.

4.7. Summary and Recommendation

Three-dimensional groundwater flow model was created and calibrated to simulate the hydrogeologic conditions or aquifers of the South Fork of the Palouse River Basin. The model was used to evaluate the impacts of groundwater pumping on the aquifer levels and discover ways to regulate or control pumping, so the Moscow-Pullman aquifer system is sustained into the foreseeable future. The groundwater flow model was developed using the available hydrogeologic data and estimated parameters from previous studies within the Moscow-Pullman region such as

the stratigraphy or geologic units of the region that defines the aquifer layers, groundwater well data, hydraulic parameters, and shallow aquifer recharge estimates.

Key to the results was that all groundwater pumping scenarios could likely lead to decreasing basin-wide aquifer volume over the next four decades. However, the total volume of groundwater in the basin would increase over time with zero pumping across the basin. Simulation results of the various pumping scenarios suggest that groundwater levels would continue to decline if pumping rates were kept matching the historic levels between 1983 and 2018. The groundwater levels would decline on average by 0.1 and 0.05 m per year in Moscow and Pullman areas, respectively over the next four decades. Reducing groundwater pumping by over 90 percent of the rate recorded between 1983 and 2018 would stabilize or increase the aquifer levels in Pullman area. However, more than 90 percent reduction in pumping could still lead to slight declines in aquifer levels at locations in Moscow. It was found that Moscow region could experience average aquifer level declines of up to 0.01 m per year through 2053 if pumping occurs less than 10 percent of the historic levels. Future aquifer level stability and future aquifer revitalization within the area of interest could occur with less than 10 percent pumping but that could be achieved more "quickly" with near zero pumping. The aquifer levels could rise by 0.1 and 0.09 m per year in Pullman and Moscow regions, respectively if no pumping occur over the next four decades.

Clearly, the groundwater flow model and the findings and conclusions drawn from the pumping scenarios provide an understanding of the hydrogeologic characteristics or flow system of the Moscow-Pullman region. Much information has been provided by this study that could be helpful to water managers (i.e., PBAC) and users within the region in making plans to manage the

groundwater resources e.g., plans to regulate pumping in the region and even consider possibility of artificial recharge within the area of interest if pumping must continue unabated. Further, the groundwater flow model created could serve as a knowledge base to future investigations in the basin such as studying groundwater discharge sources which is vital to sustaining the aquifers. Groundwater models are developed and updated over time with modern data. We recommend that the model be updated in the future, not only by introducing modern information but real time data such as regularly collected groundwater pumping and observation heads data, and recharge. These could be useful to limiting assumptions and uncertainties associated with parameter estimations.

Model Availability: the model including MODFLOW input and output files for the calibration and scenario simulations would first be provided to the funding agency the Palouse Basin Aquifer Committee (PBAC) for possible public distribution. All request and concerns relating to model availability and use should be directed to the Palouse Basin Aquifer Committee. All measured data e.g., pumping and observation head points used can be accessed from PBAC.

REFERENCES

Abu-El-Sha'r, W. Y., and J. F. Rihani (2007), Application of the high performance computing techniques of parflow simulator to model groundwater flow at Azraq basin, *Water Resour. Manag.*, *21*(2), 409–425, doi:10.1007/s11269-006-9023-5.

Adelsman, H. (2003), Washington water acquisition program: Finding water to restore streams.

Ajami, H., M. F. McCabe, J. P. Evans, and S. Stisen (2014), Assessing the impact of model spin-up on surface water-groundwater interactions using an integrated hydrologic model, *Water Resour. Res.*, *50*(3), 1–21, doi:10.1002/2013WR014258.Received.

Ajami, H., M. F. McCabe, and J. P. Evans (2015), Impacts of model initialization on an integrated surface water-groundwater model, *Hydrol. Process.*, *29*(17), 3790–3801, doi:10.1002/hyp.10478.

Allievi, A., and S. M. Calisal (1992), Application of Bubnov-Galerkin formulation to orthogonal grid generation, *J. Comput. Phys.*, *98*(1), 163–173, doi:10.1016/0021-9991(92)90181-W.

Amdahl, G. M. (1967), Validity of the single processor approach to achieving large scale computing capabilities, in *spring joint computer conference*, vol. 37, pp. 256–9.

Anchor QEA, L. and H. E. I. (2017), Palouse Groundwater Basin Water Supply Alternatives Analysis.

Anyah, R. O., C. P. Weaver, G. Miguez-Macho, Y. Fan, and A. Robock (2008), Incorporating water table dynamics in climate modeling: 3. Simulated groundwater influence on coupled

land-atmosphere variability, *J. Geophys. Res. Atmos.*, *113*(7), 1–15, doi:10.1029/2007JD009087.

Ashby, Steven F. Falgout, R. D. (1996), A Parallel Multigrid Preconditioned Conjugate Gradient Algorithm for Groundwater Flow Simulations, *Nucl. Sci. Eng.*, *124*, 145–159.

Ashby, S. F., R. D. Falgout, S. G. Smith, and A. F. B. Tompson (1993), Modeling groundwater flow on MPPs, *Proc. Scalable Parallel Libr. Conf.*, 17–25, doi:10.1109/SPLC.1993.365586.

Ashby, S. F., R. Falgout, A. Tompson, and T. Fogwell (1994), Numerical simulation of groundwater flow on MPPs, , 17–25.

Ashby, S. F., R. D. Falgout, and A. F. B. Tompson (1997), A Scalable Approach to Modeling Groundwater Flow on Massively Parallel Computers, in *In Next Generation Environmental Models and Computational Methods*, vol. 87, p. 201.

Atchley, A. L., and R. M. Maxwell (2011), Influences of subsurface heterogeneity and vegetation cover on soil moisture, surface temperature and evapotranspiration at hillslope scales, *Hydrogeol. J.*, *19*(2), 289–305, doi:10.1007/s10040-010-0690-1.

Atchley, A. L., R. M. Maxwell, and A. K. Navarre-Sitchler (2013), Human health risk assessment of CO2 leakage into overlying aquifers using a stochastic, geochemical reactive transport approach, *Environ. Sci. Technol.*, *47*(11), 5954–5962, doi:10.1021/es400316c.

Baines, C. A., 1992 (1992), Determination of Sustained Yield for the Shallow Basalt Aquifer in the Moscow Area, Idaho, University of Idaho.

Baldauf, M., Seifert, A., Forstner, J., Majewski, D., and Raschendorfer, M. (2011), Operational Convective-Scale Numerical Weather Prediction with the COSMO Model : Description and Sensitivities, *Am. Meteorol. Soc.*, 3887–3905, doi:10.1175/MWR-D-10-05013.1.

Barber, M. E., A. Hossain, J. J. Covert, and G. J. Gregory (2009), Augmentation of seasonal low stream flows by artificial recharge in the Spokane Valley-Rathdrum Prairie aquifer of Idaho and Washington, USA, *Hydrogeol. J.*, *17*(6), 1459–1470, doi:10.1007/s10040-009-0467-6.

Barker, R. A. (1979a), Computer Simulation and Geohydrology of a Basalt Aquifer System in the Pullman-Moscow Basin, Washington and Idaho.

Barker, R. A. (1979b), Computer Simulation and Geohydrology of a Basalt Aquifer System in the Pullman-Moscow Basin, Washington and Idaho.

Bauer, H. H., and J. J. Vaccaro (1990), Estimates of ground-water recharge to the Columbia Plateau regional aquifer system, Washington, Oregon, and Idaho, for predevelopment and current land-use conditions / by H.H. Bauer and J.J. Vaccaro; a contribution of the Regional Aquifer-System Analyses [sic] Program, *Water-resources Investig. Rep.*

Beall, A., F. Fiedler, J. Boll, and B. Cosens (2011), Sustainable water resource management and participatory system dynamics. Case study: Developing the palouse basin participatory model, *Sustainability*, *3*(5), 720–742, doi:10.3390/su3050720.

Beisman, J. (2007), Development of a parallel reactive transport model with spatially variable nitrate reduction in a floodplain aquifer.

Beisman, J. J., R. M. Maxwell, A. K. Navarre-Sitchler, C. I. Steefel, and S. Molins (2015),

ParCrunchFlow : an efficient , parallel reactive transport simulation tool for physically and chemically heterogeneous saturated subsurface environments, *Comput. Geosci.*, *19*(2), 403–422, doi:10.1007/s10596-015-9475-x.

Bekele, E., S. Toze, B. Patterson, and S. Higginson (2011), Managed aquifer recharge of treated wastewater: Water quality changes resulting from infiltration through the vadose zone, *Water Res.*, *45*(17), 5764–5772, doi:10.1016/j.watres.2011.08.058.

Bell, J. B., C. N. Dawson, and G. R. Shubin (1988), An unsplit, higher order godunov method for scalar conservation laws in multiple dimensions, *J. Comput. Phys.*, *74*(1), 1–24, doi:10.1016/0021-9991(88)90065-4.

Benson, D. A., T. Aquino, D. Bolster, N. E. C, and D. F.-G. Christopher V. Henri (2017), A comparison of Eulerian and Lagrangian transport and non-linear reaction algorithms, *Adv. Water Resour.*, *99*, 15–37.

Bettems, J. M., Asensio, H., Bonafe, Duniec, G., Fuhrer, O., Helmert, J., Heret, C., Kazakova, E., Lange, Machulskaya, E., Mazur, A., De Morsier, G., Rianna, G., Rozinkina, I., Vieli, B., Vogel, G. (2015), The COSMO Priority Project “COLOBOC”: Final Technical Report No 27, , (No 27).

Beven, K. (2004), Robert E. Horton’s perceptual model of infiltration processes, *Hydrol. Process.*, *18*(17), 3447–3460, doi:10.1002/hyp.5740.

Bhaskar, A. S., C. Welty, R. M. Maxwell, and A. J. Miller (2015), Untangling the effects of urban development on subsurface storage in Baltimore, *Water Resour. Res.*, *51*(2), 1158–1181, doi:10.1002/2014WR016039.

Bixio, A. C., A. G. Gambolati, A. C. Paniconi, A. M. Putti, A. V. M. Shestopalov, V. N. Bublias, A. A. S. Bohuslavsky, A. N. B. Kasteltseva, and Y. F. Rudenko (2002), Modeling groundwater-surface water interactions including effects of morphogenetic depressions in the Chernobyl exclusion zone, *Environ. Geol.*, *42*(162–177), doi:10.1007/s00254-001-0486-7.

Bouwer, H. (2002), Artificial recharge of groundwater: Hydrogeology and engineering, *Hydrogeol. J.*, *10*(1), 121–142, doi:10.1007/s10040-001-0182-4.

Bower, B., and K. Lindsey (2010), Aquifer Recharge as a Water Management Tool: Hudson Bay Recharge Testing Site Report (2004-9).

Bower, R., M. Sc, B. Sc, and R. Bower (2011), Stabilizing and Restoring an Aquifer and Springs – Managed Aquifer Recharge in the Walla Walla Basin.

Briggs, W. L., V. E. Henson, and S. F. McCormick (2000), A Multigrid Tutorial, Second Edition, 2nd ed.

Brookfield, A. E., E. A. Sudicky, Y.-J. Park, and B. Conant (2009), Thermal transport modelling in a fully integrated surface/subsurface framework, *Hydrol. Process.*, *23*(15), 2150–2164, doi:10.1002/hyp.7282.

Brown, B. C. (1976), Well Construction and Stratigraphic Information: Pullman Test and Observation Well, Pullman, Washington, Pullman.

Brown, P. N., and Y. Saad (1990), Hybrid Krylov Methods for Nonlinear Systems of Equations, *SIAM J. Sci. Stat. Comput.*, *11*(3), 450–481, doi:10.1137/0911026.

Bruce LaVerne Foxworthy, R. L. W.- (1963), Ground Water in the Pullman Area, Whitman County, Washington.

Burns, E. R., D. S. Morgan, R. S. Peavler, and S. C. Kahle (2011), Three-Dimensional Model of the Geologic Framework for the Columbia Plateau Regional Aquifer System , Idaho , Oregon , and Washington, *U.S. Geol. Surv. Sci. Investig. Rep. 2010-5246*, 44.

Burstedde, C., J. A. Fonseca, and S. Kollet (2018), Enhancing speed and scalability of the ParFlow simulation code, *Comput. Geosci.*, *22*(1), 347–361, doi:10.1007/s10596-017-9696-2.

Bush, J. H., G. D. L. and D. P. (2016), Geology and geologic history of the Moscow-Pullman basin, Idaho and Washington, from late Grande Ronde to late Saddle Mountains time. Exploring the Geology of the Inland Northwest*; 151-174.*, edited by K. L. S. Reed S. Lewis, Geological Society of America.

Bush, J. H., J. L. Pierce, and G. N. Potter (2000), Bedrock geologic map of the Moscow East quadriangle, Latah County, Idaho.

Cahill, K., T. Walsh, M. Morgan, D. Mcfarlane, P. J. D. April, and J. Vanderzalm (2015), Managed Aquifer Recharge and RecyclingOptions : Understanding clogging processes and water quality impacts.

Camporese, M., C. Paniconi, M. Putti, and S. Orlandini (2010), Surface-subsurface flow modeling with path-based runoff routing, boundary condition-based coupling, and assimilation of multisource observation data, *Water Resour. Res.*, *46*(2), n/a-n/a, doi:10.1029/2008WR007536.

Candel, J., E. Brooks, R. Sánchez-Murillo, G. Grader, and R. Dijksma (2016), Identifying groundwater recharge connections in the Moscow (USA) sub-basin using isotopic tracers and a soil moisture routing model, *Hydrogeol. J.*, *24*(7), 1739–1751, doi:10.1007/s10040-016-1431-x.

Castronova, A. M., J. L. Goodall, and M. B. Ercan (2013), Integrated Modeling within a Hydrologic Information System: An OpenMI Based Approach, *Environ. Model. Softw.*, doi:10.1016/j.envsoft.

Celia, M. A., E. T. Bouloutas, and R. L. Zarba (1990), A general mass-conservative numerical solution for the unsaturated flow equation, *Water Resour. Res.*, *26*(7), 1483–1496, doi:10.1029/WR026i007p01483.

Cey, B. D., G. B. Hudson, J. E. Moran, and B. R. Scanlon (2008), Impact of artificial recharge on dissolved noble gases in groundwater in California, *Environ. Sci. Technol.*, *42*(4), 1017–1023, doi:10.1021/es0706044.

Chow, F. K., F. K. Chow, S. J. Kollet, S. J. Kollet, R. M. Maxwell, R. M. Maxwell, Q. Duan, and Q. Duan (2006), Effects of Soil Moisture Heterogeneity on Boundary Layer Flow with Coupled Groundwater, Land-Surface, and Mesoscale Atmospheric Modeling, *17th Symp. Bound. Laters Turbul.*, doi:10.1016/j.phrs.2010.10.003.

Collier, A. M., A. C. Hindmarsh, R. Serban, and C. S. Woodward (2015), User Documentation for kinsol v2.8.2 (SUNDIALS v2.6.2), , *1*, 120.

Condon, L. E., and R. M. Maxwell (2013), Implementation of a linear optimization water allocation algorithm into a fully integrated physical hydrology model, *Adv. Water Resour.*,

60(October 2013), 135–147, doi:10.1016/j.advwatres.2013.07.012.

Condon, L. E., and R. M. Maxwell (2014), Groundwater-fed irrigation impacts spatially distributed temporal scaling behavior of the natural system: a spatio-temporal framework for understanding water management impacts, *Environ. Res. Lett.*, *9*(3), 034009, doi:10.1088/1748-9326/9/3/034009.

Condon, L. E., and R. M. Maxwell (2015), Evaluating the relationship between topography and groundwater using outputs from a continental-scale integrated hydrology model, *Water Resour. Res.*, *51*(8), 6602–6621, doi:10.1002/2014WR016774.

Condon, L. E., R. M. Maxwell, and S. Gangopadhyay (2013), The impact of subsurface conceptualization on land energy fluxes, *Adv. Water Resour.*, *60*, 188–203, doi:10.1016/J.ADVWATRES.2013.08.001.

Condon, L. E., A. S. Hering, and R. M. Maxwell (2015), Quantitative assessment of groundwater controls across major US river basins using a multi-model regression algorithm, *Adv. Water Resour.*, *82*, 106–123, doi:10.1016/J.ADVWATRES.2015.04.008.

Cronin, A. E., L. B. Fowler, and I. Fee (2012), Water Banks Water Banks Limited.

Dai, Y. et al. (2003), The Common Land Model, *Bull. Am. Meteorol. Soc.*, *84*(8), 1013–1023, doi:10.1175/BAMS-84-8-1013.

Dembo, Ron S., Stanley C. Eisenstat, and T. S. (1982), Inexact newton methods, in *SIAM J. NUMER. ANAL.*, vol. 19, pp. 400–408.

Dennis Jr, John E., and R. B. S. (1996), Numerical Methods for Unconstrained Optimization and

Nonlinear Equations.

Dhungel, R., and F. Fiedler (2016), Water balance to recharge calculation: Implications for watershed management using systems dynamics approach, *Hydrology*, *3*(1), doi:10.3390/hydrology3010013.

Dijksma, R., E. S. Brooks, and J. Boll (2011), Groundwater recharge in Pleistocene sediments overlying basalt aquifers in the Palouse Basin, USA: Modeling of distributed recharge potential and identification of water pathways, *Hydrogeol. J.*, *19*(2), 489–500, doi:10.1007/s10040-010-0695-9.

Doherty, J., and R. Hunt (2010), Approaches to highly parameterized inversion: a guide to using PEST for groundwater-model calibration, *U. S. Geol. Surv. Sci. Investig. Rep. 2010-5169*, 70.

Doherty, J., R. Hunt, and M. Tonkin (2010), Approaches to Highly Parameterized Inversion : A Guide to Using PEST for Model-Parameter and Predictive-Uncertainty Analysis: *U.S. Geological Survey Scientific Investigations Report 2010 – 5211*.

Duckett, K. A., J. B. Langman, J. H. Bush, E. S. Brooks, P. Dunlap, and J. M. Welker (2019), Isotopic discrimination of aquifer recharge sources, subsystem connectivity and flow patterns in the South Fork Palouse River Basin, Idaho and Washington, USA, *Hydrology*, *6*(1), doi:10.3390/hydrology6010015.

Duniec, G., and A. Mazur (2011), COLOBOC - MOSAIC parameterization in COSMO model v. 4.8, , (11), 69–81.

Durbin, P. (2002), An Approach to Local Refinement of Structured Grids An Approach to Local Refinement of Structured Grids, *J. Comput. Phys.*, *181*(June 2017), 639–653, doi:10.1006/jcph.2002.7147.

Ebeling, E., Kearl, Z., Weaver, E., and Wentzel, N. (2019), Water Marketing : Literature Review.

Eca, L. (1996), 2D orthogonal grid generation with boundary point distribution control, *J. Comput. Phys.*, *125*(2), 440–453, doi:10.1006/jcph.1996.0106.

Eisenstat, S. C., and H. F. Walker (1996), Choosing the Forcing Terms in an Inexact Newton Method, *SIAM J. Sci. Comput.*, *17*(1), 16–32, doi:10.1137/0917003.

Ek, M. B., K. E. Mitchell, Y. Lin, E. Rogers, P. Grunmann, V. Koren, G. Gayno, and J. D. Tarpley (2003), Implementation of Noah land surface model advances in the National Centers for Environmental Prediction operational mesoscale Eta model, *J. Geophys. Res. Atmos.*, *108*(D22), 8851, doi:10.1029/2002JD003296.

Ely, D., M. Bachmann, and J. Vaccaro (2011), Numerical Simulation of Groundwater Flow for the Yakima River Basin Aquifer System , Washington, *U.S. Geol. Surv.*, (Scientific Investigations Report 5155), 102.

Ely, D. M., E. R. Burns, D. S. Morgan, and J. J. Vaccaro (2014), Numerical Simulation of Groundwater Flow in the Columbia Plateau Regional Aquifer System, Idaho, Oregon, and Washington, *U.S. Geol. Surv.*, (Scientific Investigations Report 2014-5127), 90.

Engdahl, N. B., and R. M. Maxwell (2015), Quantifying changes in age distributions and the

hydrologic balance of a high-mountain watershed from climate induced variations in recharge, *J. Hydrol.*, *522*(June 2016), 152–162, doi:10.1016/j.jhydrol.2014.12.032.

Engdahl, N. B., J. L. McCallum, and A. Massoudieh (2016), Transient age distributions in subsurface hydrologic systems, *J. Hydrol.*, *543*, 88–100, doi:10.1016/J.JHYDROL.2016.04.066.

Falgout, R. D., and U. M. Yang (2002), hypre: A Library of High Performance Preconditioners, in *International Conference on Computational Science.*, pp. 632–641, Springer, BerliN.

Falgout, R. D., C. Baldwin, W. Bosl, R. Hornung, D. Shumaker, S. Smith, C. Woodward, and A. F. B. Tompson (1999), Enabling Computational Technologies for Subsurface Simulations,

Ferguson, I. M., Jefferson, J. L., Maxwell, R. M., and Kollet, S. J. (2016), Effects of root water uptake formulation on simulated water and energy budgets at local and basin scales, *Env. Earth Sci*, *75*(316), doi:DOI 10.1007/s12665-015-5041-z.

Ferguson, I. M., and R. M. Maxwell (2010), Groundwater-Land Surface-Atmosphere Feedbacks: Impacts of Groundwater Pumping and Irrigation on Land-Atmosphere Interactions, *Proc. Xviii Int. Conf. Comput. Methods Water Resour.*, 722–729.

Ferguson, I. M., and R. M. Maxwell (2012), Human impacts on terrestrial hydrology: climate change versus pumping and irrigation, *Environ. Res. Lett.*, *7*(4), 044022, doi:10.1088/1748-9326/7/4/044022.

Folnagy, A. J. B. (2012), Long-Term Grande Ronde Aquifer Stress Testing to Delineate Aquifer Compartmentalization and Water Level Responses in the Palouse Groundwater Basin, ,

(June), doi:10.13140/RG.2.1.1798.8248.

Folnagy, A. J. B., and J. L. Osiensky (2016), Reevaluating Palouse Groundwater Basin Compartmentalization, , (October), doi:10.1130/abs/2016rm-273011.

Fontaine, M. M. (2007), Assessing Vulnerability to Natural Hazards: An Impact-Based Method and Application to Drought in Washington State Matthew.

Frei, S., J. H. H. Fleckenstein, S. J. J. Kollet, and R. M. M. Maxwell (2009), Patterns and dynamics of river-aquifer exchange with variably-saturated flow using a fully-coupled model, *J. Hydrol.*, *375*(3–4), 383–393, doi:10.1016/j.jhydrol.2009.06.038.

Gasper, F., K. Goergen, P. Shrestha, M. Sulis, J. Rihani, M. Geimer, and S. Kollet (2014), Implementation and scaling of the fully coupled Terrestrial Systems Modeling Platform (TerrSysMP v1.0) in a massively parallel supercomputing environment - A case study on JUQUEEN (IBM Blue Gene/Q), *Geosci. Model Dev.*, *7*(5), 2531–2543, doi:10.5194/gmd-7-2531-2014.

Gebler, S., S. Kollet, W. Qu, and H. Vereecken (2015), High resolution modelling of soil moisture patterns with ParFlow-CLM : Comparison with sensor network data, , *17*, 2015.

GeoSystems Analysis Inc. (2015), Walla Walla Basin Integrated Water Flow Model : Model Development and Calibration, Hood River.

Gibson, T. M. and Campana, M. E. (2014), A Desktop Suitability Assessment of Aquifer Storage and Recovery (ASR) in Washington State.

Gibson, M., M. Campana, and D. Nazy (2018), Estimating Aquifer Storage and Recovery (ASR)

Regional and Local Suitability: A Case Study in Washington State, USA, *Hydrology*, *5*(1), 7, doi:10.3390/hydrology5010007.

Gilbert, J. M., and R. M. Maxwell (2016), Examining regional groundwater-surface water dynamics using an integrated hydrologic model of the San Joaquin River basin, *Hydrol. Earth Syst. Sci. Discuss.*, (October), 1–39, doi:10.5194/hess-2016-488.

GSI Water Solutions, I. (2007), Geologic Setting of the Miocene (?) to Recent Suprabasalt Sediments of the Walla Walla Basin , Southeastern Washington and Northeastern Oregon, Walla Walla.

van der Gun, J. (2012), Groundwater and Global Change: Trends, Opportunities and Challenges.

Gustafson, J. L. (1988), Reevaluating amdahl's law, , *31*(5), 532–533.

Hansen, a J., J. J. Vaccaro, and H. H. Bauer (1994), Groundwater flow simulation of the Columbia Plateau regional aquifer system , *Washington , Oregon , and Idaho*.

Harbaugh, A.W., Banta, E. R., Hill, C. M., and McDonald, M. G. (2000), ModFlow-2000, The U.S. geological survey modular groundwater model-User guide to modularization concepts and the groundwater flow process.

Harbaugh, Arlen, W. (2005), MODFLOW-2005 , The U . S . Geological Survey Modular Ground-Water Model — the Ground-Water Flow Process, *U.S. Geol. Surv. Tech. Methods*, 253, doi:U.S. Geological Survey Techniques and Methods 6-A16.

Haussling, H. ., and R. . Coleman (1981), A method for generation of orthogonal and nearly orthogonal boundary-fitted coordinate systems, *J. Comput. Phys.*, *43*(2), 373–381,

doi:10.1016/0021-9991(81)90129-7.

HDR Engineering Inc., G. W. S. I. (2009), Hydrogeology Report: Asotin Creek and Alpowa Creek Sub-Basins.

Hernandez, H. P. (2007), Observations of Recharge to the Wanapum Aquifer System in the Moscow area, Latah County, Idaho., University of Idaho.

Hindmarsh, A. C., P. N. Brown, K. E. Grant, S. L. Lee, R. Serban, D. E. Shumaker, and C. S. Woodward (2005), SUNDIALS: Suite of nonlinear and differential/algebraic equation solvers, *ACM Trans. Math. Softw.*, *31*(3), 363–396, doi:10.1145/1089014.1089020.

Holom, D. (2006), Ground water flow conditions related to the pre-basalt basement geometry delineated by gravity measurements near Kamiak Butte, Eastern Washington.

Jefferson, J. L., and Maxwell, R. M. (2015), Evaluation of simple to complex parameterizations of bare ground evaporation, *J. Adv. Model. Earth Syst.*, *7*, 1075–1092, doi:10.1002/ 2014MS000398. Received.

Jefferson, J. L., J. M. Gilbert, P. G. Constantine, and R. M. Maxwell (2015), Active subspaces for sensitivity analysis and dimension reduction of an integrated hydrologic model, *Comput. Geosci.*, *83*, 127–138, doi:10.1016/j.cageo.2015.07.001.

Jefferson, J. L., R. M. Maxwell, and P. G. Constantine (2017), Exploring the Sensitivity of Photosynthesis and Stomatal Resistance Parameters in a Land Surface Model, *J. Hydrometeorol.*, *18*(3), 897–915, doi:10.1175/JHM-D-16-0053.1.

Jerry P. Fairley, Mark D. Solomon, Jennifer J. Hinds, George W. Grader, John H. Bush, and A.

L. R. (2006), Latah County hydrologic characterization project final report, Moscow.

Jian, J., D. Ryu, J. F. Costelloe, and C. H. Su (2017), Towards hydrological model calibration using river level measurements, *J. Hydrol. Reg. Stud.*, *10*, 95–109, doi:10.1016/j.ejrh.2016.12.085.

Jiang, X., G. Y. Niu, and Z. L. Yang (2009), Impacts of vegetation and groundwater dynamics on warm season precipitation over the Central United States, *J. Geophys. Res. Atmos.*, *114*(6), 1–15, doi:10.1029/2008JD010756.

Johnson, G. E. (1991), Estimating Groundwater recharge beneath different slope positions in the Palouse formation using a numerical unsaturated flow model, Washington State University.

Johnson, G.S., Bloomsburg, G., and Ralston, D. R. (1996), Evaluation and Modification of the Pullman-Moscow Groundwater Flow Model, Moscow, Idaho.

Johnson, G. S., G. Bloomsburg, and D. R. Ralston (1996), Evaluation and modification of the Pullman-Moscow groundwater flow model, Moscow, Idaho.

Jones, R.W., and Ross, S. H. (1969), Detailed Ground Water Investigation of the Moscow Basin., Moscow, Idaho.

Jones, J. E., and C. S. Woodward (2000), Preconditioning Newton- Krylov Methods for Variably Saturated Flow, in *13th International Conference on Computational Methods in Water Resources*, Calgary, Alberta, Canada.

Jones, J. E., and C. S. Woodward (2001), Newton-Krylov-multigrid solvers for large-scale, highly heterogeneous, variably saturated flow problems, *Adv. Water Resour.*, *24*(7), 763–

774, doi:10.1016/S0309-1708(00)00075-0.

Kahle, S. C., D. S. Morgan, W. B. Welch, D. M. Ely, S. R. Hinkle, J. J. Vaccaro, and L. L. Orzol (2011), Hydrogeologic framework and hydrologic budget components of the Columbia Plateau regional aquifer system, *Washington, Oregon, and Idaho*.

Keune, J., F. Gasper, K. Goergen, A. Hense, P. Shrestha, M. Sulis, and S. Kollet (2016), Studying the influence of groundwater representations on land surface-atmosphere feedbacks during the European heat wave in 2003, *J. Geophys. Res.*, *121*(22), 13,301-13,325, doi:10.1002/2016JD025426.

Khorsandi, E., S. Kollet, V. Venema, and C. Simmer (2014), Investigating the effect of bottom boundary condition placement on ground heat storage in climate time scale simulations using ParflowE, *Geophys. Res.*, *16*(4), 2014, doi:10.1029/2006GL028546.

Kirkner, D. J., and Reeves, H. (1988), Multicomponent Mass Transport With Homogeneous and Heterogeneous Chemical Reactions' Effect of the Chemistry on the Choice of Numerical Algorithm 1. Theory, *Water Resour. Res.*, *24*(10), 1719–1729.

Knoll, D. A., and D. E. Keyes (2004), Jacobian-free Newton-Krylov methods: A survey of approaches and applications, *J. Comput. Phys.*, *193*(2), 357–397, doi:10.1016/j.jcp.2003.08.010.

Koch, J., T. Cornelissen, Z. Fang, H. Bogena, B. Diekkrüger, S. Kollet, and S. Stisen (2016), Inter-comparison of three distributed hydrological models with respect to seasonal variability of soil moisture patterns at a small forested catchment, *J. Hydrol.*, *533*, 234–249, doi:10.1016/j.jhydrol.2015.12.002.

Kollet, S., Mauro Sulis, Reed M. Maxwell, Claudio Paniconi, Mario, Mario Putti, Giacomo Bertoldi, Ethan T. Coon, Emanuele Cordano, Stefano Endrizzi, Evgeny Kikinzon, Emmanuel Mouche, Claude Mugler, Young-Jin Park, Jens C. Refsgaard, Stisen Simo, and E. S. (2017), The integrated hydrologic model intercomparison project,IH-MIP2: A second set of benchmark results to diagnoseintegrated hydrology and feedbacks, *Water Resour. Res.*, *52*(1), 1–20, doi:10.1002/2014WR015716.

Kollet, S. J. (2009), Influence of soil heterogeneity on evapotranspiration under shallow water table conditions: transient, stochastic simulations, *Environ. Res. Lett.*, *4*, 035007, doi:10.1088/1748-9326/4/3/035007.

Kollet, S. J. (2015), Optimality and inference in hydrology from entropy production considerations: synthetic hillslope numerical experiments., *Hydrol. Earth Syst. Sci.*, *12*, 5123–5149.

Kollet, S. J., and R. M. Maxwell (2006), Integrated surface-groundwater flow modeling: A free-surface overland flow boundary condition in a parallel groundwater flow model, *Adv. Water Resour.*, *29*(7), 945–958, doi:10.1016/j.advwatres.2005.08.006.

Kollet, S. J., and R. M. Maxwell (2008a), Capturing the influence of groundwater dynamics on land surface processes using an integrated, distributed watershed model, *Water Resour. Res.*, *44*(2), 1–18, doi:10.1029/2007WR006004.

Kollet, S. J., and R. M. Maxwell (2008b), Demonstrating fractal scaling of baseflow residence time distributions using a fully-coupled groundwater and land surface model, *Geophys. Res. Lett.*, *35*(7), 1–6, doi:10.1029/2008GL033215.

Kollet, S. J., I. Cvijanovic, D. Schüttemeyer, R. M. Maxwell, A. F. Moene, and P. Bayer (2009), The Influence of Rain Sensible Heat and Subsurface Energy Transport on the Energy Balance at the Land Surface, *Vadose Zo. J.*, *8*(4), 846, doi:10.2136/vzj2009.0005.

Kollet, S. J., R. M. Maxwell, C. S. Woodward, S. Smith, J. Vanderborght, H. Vereecken, and C. Simmer (2010), Proof of concept of regional scale hydrologic simulations at hydrologic resolution utilizing massively parallel computer resources, *Water Resour. Res.*, *46*(4), 1–7, doi:10.1029/2009WR008730.

Konikow, L. F. (2011), Contribution of global groundwater depletion since 1900 to sea-level rise, *Geophys. Res. Lett.*, *38*(17), 1–5, doi:10.1029/2011GL048604.

Kuffour, B. N., N. Engdahl, C. Woodward, L. Condon, S. Kollet, and R. Maxwell (2020), Simulating Coupled Surface-Subsurface Flows with ParFlow v3.5.0: Capabilities, applications, and ongoing developmentof an open-source, massively parallel, integrated hydrologic model, *Geosci. Model Dev. Discuss.*, *13*(3), 1–66, doi:10.5194/gmd-2019-190.

Kumar, M., C. J. Duffy, and K. M. Salvage (2009), A second-order accurate, finite volume–based, integrated hydrologic modeling (FIHM) framework for simulation of surface and subsurface flow, *Vadose Zo. J.*, *8*(4), 873, doi:10.2136/vzj2009.0014.

LaBolle, E. M., A. A. Ahmed, and G. E. Fogg (2003), Review of the Integrated Groundwater and Surface-Water Model (IGSM), *Ground Water*, *41*(2), 238–246, doi:10.1111/j.1745-6584.2003.tb02587.x.

Larson, K.R., Keller, C.K., Larson, P.B. Allen-King, R. M. (2000), Water resource implications 18O and 2H distributions in a basalt aquifer system, *Groundwater*, *38*(6), 947–953.

Leek, F. (2006), Hydrogeological Characterization of the Palouse Basin Basalt Aquifer System, Washington and Idaho.

Levis, S., and E. B. Jaeger (2011), COSMO-CLM2 : a new version of the COSMO- CLM model coupled to the Community Land Model coupled to the Community Land Model, *Clim. Dyn.*, *37*(November), 1889–1907, doi:10.1007/s00382-011-1019-z.

Li, L., S. C. I. K. M. B. E. A. H. (2010), Effects of physical and geochemical heterogeneities on mineral transformation and biomass accumulation during uranium bioremediation at Rifle, Colorado, *J. Contam. Hydrol.*, *11*, 45–63.

Li, L., C. I. Steefel, and L. Yang (2007), Scale dependence of mineral dissolution rates within single pores and fractures, *Geochim. Cosmochim. Acta*, *72*, 360–377, doi:10.1016/j.gca.2007.10.027.

Lindsey, K. (1996), The Miocene to Pliocene Ringold Formation and Associated Deposits of the Ancestral Columbia River System, South-central Washington and North-central Oregon.

Lindsey, K. (2007), Results of the First Season of Shallow Aquifer Recharge Testing at the Locher Road Site, Walla Walla County, Washington.

Lum II, W. E., Smoot, J. L., and Ralston, D. R. (1990), Geohydrology and numerical model analysis of groundwater flow in the Pullman-Moscow area, Washington and Idaho, Tacoma, Washington.

Mahoney, B. D., G. Mendel, Lambert, M., Trump, J., Bronson, P., Gembala, M., and Gallinat, M. (2009), The Walla Walla Subbasin collaborative Salmonid monitoring and evaluation

project: 2007 and 2008 Annual Report.

Markstrom, S. L., R. G. Niswonger, R. S. Regan, D. E. Prudic, and P. M. Barlow (2008), GSFLOW—Coupled Ground-Water and Surface-Water Flow Model Based on the Integration of the Precipitation-Runoff Modeling System (PRMS) and the Modular Ground-Water Flow Model (MODFLOW-2005), *U.S. Geol. Surv.*, (Techniques and Methods 6-D1), 240.

Mary, B., and J. Coombs (2002), Threats to Water Quality in the Deep Basalt Aquifer , City of Walla Walla , Washington.

Maxwell, R., and N. L. Miller (2005a), Development of a Coupled Land Surface and Groundwater Model, *J. Hydrometeorol.*, *6*, 233–247, doi:10.1175/JHM422.1.

Maxwell, R. M. (2010), Infiltration in Arid Environments: Spatial Patterns between Subsurface Heterogeneity and Water-Energy Balances, *Vadose Zo. J.*, *9*(4), 970, doi:10.2136/vzj2010.0014.

Maxwell, R. M. (2013), A terrain-following grid transform and preconditioner for parallel, large-scale, integrated hydrologic modeling, *Adv. Water Resour.*, *53*, 109–117, doi:10.1016/j.advwatres.2012.10.001.

Maxwell, R. M., and N. . Miller (2005b), Development of a Coupled Land Surface and Groundwater Model, *J. Hydrometeo*, *6*, 233–247, doi:10.1175/2010MWR3392.1.

Maxwell, R. M., C. Welty, and A. F. B. Tompson (2003), Streamline-based simulation of virus transport resulting from long term artificial recharge in a heterogeneous aquifer, *Adv. Water*

Resour., *26*(10), 1075–1096, doi:10.1016/S0309-1708(03)00074-5.

Maxwell, R. M., F. K. Chow, and S. J. Kollet (2007), The groundwater–land-surface–atmosphere connection: Soil moisture effects on the atmospheric boundary layer in fully-coupled simulations, *Adv. Water Resour.*, *30*(12), 2447–2466, doi:10.1016/j.advwatres.2007.05.018.

Maxwell, R. M., J. K. Lundquist, J. D. Mirocha, S. G. Smith, C. S. Woodward, and A. F. B. Tompson (2011), Development of a Coupled Groundwater–Atmosphere Model, *Mon. Weather Rev.*, *139*(1), 96–116, doi:10.1175/2010MWR3392.1.

Maxwell, R. M., L. E. Condon, and S. J. Kollet (2015), A high-resolution simulation of groundwater and surface water over most of the continental US with the integrated hydrologic model ParFlow v3, *Geosci. Model Dev*, 923–937, doi:10.5194/gmd-8-923-2015.

Maxwell, R. M. et al. (2016), ParFlow User ' s Manual,

McDonald, M. G., and A. W. Harbaugh (1988), A modular three-dimensional finite difference ground-water flow model, *Tech. Water-Resources Investig. B. 6*, 588, doi:10.1016/0022-1694(70)90079-X.

Meehl, G. A., C. Covey, B. McAvaney, M. Latif, and R. J. Stouffer (2005), Overview of the coupled model intercomparison project, *Bull. Am. Meteorol. Soc.*, *86*(1), 89–93, doi:10.1175/BAMS-86-1-89.

Mendel, G., J. Trump, and M. Gembala (2005), Assessment of salmonids and their habitat conditions in the Walla Walla River basin within Washington. *Annual report 2003-2004.*

Meyerhoff, S. B., and R. M. Maxwell (2010), Using an integrated surface-subsurface model to

simulate runoff from heterogeneous hillslopes, in *XVIII International Conference on Water Resources*, CIMNE, Barcelona.

Michalakes, J., J. Dudhia, D. Gill, J. Klemp, and W. Skamarock (1999), Design of a next-generation regional weather research and forecast model, *Towar. Teracomputing*.

Michalakes, J., S. Chen, J. Dudhia, L. Hart, J. Klemp, J. Middlecoff, and W. Skamarock (2001), Development of a next-generation regional weather research and forecast model, *Towar. Teracomputing*.

Mikkelson, K. M., R. M. Maxwell, I. Ferguson, J. D. Stednick, J. E. Mccray, and J. O. Sharp (2013), Mountain pine beetle infestation impacts: Modeling water and energy budgets at the hill-slope scale, *Ecohydrology*, *6*(1), 64–72, doi:10.1002/eco.278.

Mirlas, V., V. Antonenko, V. Kulagin, and E. Kuldeeva (2015), Assessing Artificial Groundwater Recharge on Irrigated Land Using the MODFLOW Model A Case Study from Karatal Agricultural Area , Kazakhstan, *Earth Sci. Res.*, *4*(2), doi:10.5539/esr.v4n2p16.

Mironov, D., E. Heise, E. Kourzeneva, and B. Ritter (2010), Implementation of the lake parameterisation scheme FLake into the numerical weather prediction model COSMO, *Boreal Environ. Res.*, *6095*(April), 218–230.

Mobley, C. D., and R. J. Stewart (1980), On the numerical generation of boundary-fitted orthogonal curvilinear coordinate systems, *J. Comput. Phys.*, *34*(1), 124–135, doi:10.1016/0021-9991(80)90117-5.

Molders, N., and Ruhaak, W. (2002), On the impact of explicitly predicted runoff on the

simulated atmospheric response to small-scale land-use changes—an integrated modeling approach, *Atmos. Res.*, *63*.

Moran, K. (2011), Interpretation of Long-Term Grande Ronde Aquifer Testing in the Palouse Basin of Idaho and Washington, *Methodology*, (August).

Morris, A. A. (1956), Washington Law Review Washington Water Rights — A Sketch, , *31*(3).

Muniz, H. R. (1991), Computer Modeling of Vadose Zone Groundwater Flux at a Hazardous Wast Site, Washington State University.

Navarre-Sitchler, A., Steefel, C. I., Sak, P. B., and Brantley, S. L. (2011), A reactive-transport model for weathering rind formation on basalt, *Geochim. Cosmochim. Acta*, *75*, 7644–7667, doi:10.1016/j.gca.2011.09.033.

Niswonger, R. G. (2011), *MODFLOW-NWT ,* A Newton Formulation for MODFLOW-2005.

O'Brien, R., Keller, C. K., and Smith, J. L. (1996), Multiple tracers of shallow groundwater flow and recharge in Hilly Loess.

O'Geen, A. T., P. A. McDaniel, J. Boll, and C. K. Keller (2005), Paleosols as deep regolith: Implications for ground-water recharge across a loessial climosequence, *Geoderma*, *126*(1-2 SPEC. ISS.), 85–99, doi:10.1016/j.geoderma.2004.11.008.

Oleson, K. W. et al. (2008), Improvements to the Community Land Model and their impact on the hydrological cycle, *J. Geophys. Res. Biogeosciences*, *113*(G1), n/a-n/a, doi:10.1029/2007JG000563.

Osei-Kuffuor, D., R. M. Maxwell, and C. S. Woodward (2014), Improved numerical solvers for implicit coupling of subsurface and overland flow, *Adv. Water Resour.*, *74*, doi:10.1016/j.advwatres.2014.09.006.

Owsley, D. (2003), Characterization of Grande Ronde Aquifers in the Palouse Basin using large scale aquifer tests.

Pagel, M. (2016), Oregon ' s Umatilla Basin Aquifer Recharge and Basalt bank.

Panday, S., and P. S. Huyakorn (2004), A fully coupled physically-based spatially-distributed model for evaluating surface/subsurface flow, *Adv. Water Resour.*, *27*(4), 361–382, doi:10.1016/j.advwatres.2004.02.016.

Patten, S. (2014), Water Year 2013 Oregon Walla Walla Basin Aquifer Recharge Report, Walla Walla.

Patten, S. (2017), Walla Walla Basin Aquifer Recharge Annual Report Water Year 2017.

Petrides, A. (2008), Modeling Surface Water and Groundwater Interactions near Milton-Freewater, Oregon, *MS thesis*.

Petrides, A. (2012), Managed Artificial Aquifer Recharge and Hydrological Studies in the Walla Walla Basin to Improve River and Aquifer Conditions.

Petrides, A. C., M. Asce, ; R Stewart, R. Bower, R. H. Cuenca, and B. Wolcott (2015), Case Study: Scaling Recharge Rates from Pilot Projects of Managed Artificial Aquifer Recharge in the Walla Walla Basin, Oregon, , *20*(8), 3–8, doi:10.1061/(ASCE)HE.1943-5584.0001102.

Price, E. C. (1960), Artificial Recharge of a Well Tapping Basalt Aquifers , Walla Walla Area, Washington.

Racz, A. J., A. T. Fisher, C. M. Schmidt, B. S. Lockwood, and M. L. Huertos (2012), Spatial and Temporal Infiltration Dynamics During Managed Aquifer Recharge, *Ground Water*, *50*(4), 562–570, doi:10.1111/j.1745-6584.2011.00875.x.

Rahman, M., M. Sulis, and S. J. Kollet (2016), Evaluating the dual-boundary forcing concept in subsurface-land surface interactions of the hydrological cycle, *Hydrol. Process.*, *30*(10), 1563–1573, doi:10.1002/hyp.10702.

Reeves, M. (2009), Estimating Recharge Uncertainty using Bayesian Model Averaging and Expert Elicitation with Social Implications.

Reidel, S. P., and T. L. Tolan (2013), The Grande ronde basalt, Columbia River basalt group, *Spec. Pap. Geol. Soc. Am.*, *497*(05), 117–153, doi:10.1130/2013.2497(05).

Reidel, S. P., T. L. Tolan, P. R. Hooper, M. H. Beeson, K. R. Fecht, R. D. Bentley, and J. L. Anderson (1989), The Grande ronde basalt, Columbia River basalt group; Stratigraphic descriptions and correlations in Washington, Oregon, and Idaho, *Spec. Pap. Geol. Soc. Am.*, *239*(March), 21–53, doi:10.1130/SPE239-p21.

Ren, D., and M. Xue (2004), A revised force–restore model for land surface modeling, *Am. Meteorol. Soc.*

Reyes, B., R. M. Maxwell, and T. S. Hogue (2016), Impact of lateral flow and spatial scaling on the simulation of semi-arid urban land surfaces in an integrated hydrologic and land surface

model, *Hydrol. Process.*, *30*(8), 1192–1207, doi:10.1002/hyp.10683.

Richards, L. A. (1931), Capillary conduction of liquids through porous mediums, *J. Appl. Phys.*, *1*(5), 318–333, doi:10.1063/1.1745010.

Rihani, Jehan F., Chow, Fotini K., and Maxwell, R. M. (2015), Isolating effects of terrain and soil moisture heterogeneity on the atmospheric boundary layer: Idealized simulations to diagnose land-atmosphere feedbacks, *J. Adv. Model. Earth Syst.*, *6*, 513–526, doi:10.1002/2014MS000371.Received.

Rihani, J. F., R. M. Maxwell, and F. K. Chow (2010), Coupling groundwater and land surface processes: Idealized simulations to identify effects of terrain and subsurface heterogeneity on land surface energy fluxes, *Water Resour. Res.*, *46*(12), 1–14, doi:10.1029/2010WR009111.

Robinson, T. (2016), Revisiting Many Waters : An Evaluation of the Walla Walla Water Management Initiative.

Roderick, M. L., F. Sun, W. H. Lim, and G. D. Farquhar (2014), A general framework for understanding the response of the water cycle to global warming over land and ocean, *Hydrol. Earth Syst. Sci.*, *18*, 1575–1589, doi:10.5194/hess-18-1575-2014.

Russo, T. A., and U. Lall (2017), Depletion and response of deep groundwater to climate-induced pumping variability, *Nat. Geosci.*, *10*(2), 105–108, doi:10.1038/ngeo2883.

Ryskin, G., and L. . Leal (1983), Orthogonal mapping, *J. Comput. Phys.*, *50*(1), 71–100, doi:10.1016/0021-9991(83)90042-6.

Saad, Y., and M. H. Schultz (1986), GMRES: A Generalized Minimal Residual Algorithm for Solving Nonsymmetric Linear Systems, *SIAM J. Sci. Stat. Comput.*, *7*(3), 856–869, doi:10.1137/0907058.

Scherberg, J., Baker, T., Selker, J. S., Henry, R. (2005), Design of Managed Aquifer Recharge for Agricultural and Ecological Water Supply Assessed Through Numerical Modeling, , 1–22.

Scherberg, J., T. Baker, J. S. Selker, and R. Henry (2014), Design of Managed Aquifer Recharge for Agricultural and Ecological Water Supply Assessed Through Numerical Modeling, *Water Resour. Manag.*, *28*(14), 4971–4984, doi:10.1007/s11269-014-0780-2.

Scherberg, J., J. Keller, S. Patten, T. Baker, and M. Milczarek (2018), Modeling the impact of aquifer recharge, in-stream water savings, and canal lining on water resources in the Walla Walla Basin, *Sustain. Water Resour. Manag.*, *4*(2), 275–289, doi:10.1007/s40899-018-0215-y.

Scherberg, J. N. (2012), The Development of a Hydrological Model of the Walla Walla Basin Using Integrated Water Flow Model, , 164.

Schwarzenegger, A. (2005), Sedimentary Basin Database for Washington and Oregon States for the Geologic Carbon Dioxide Assessment.

Seck, A., C. Welty, and R. Maxwell (2015), Spin-up behavior and effects of initial conditions for an integrated hydrologicmodel Alimatou, *Water Resour. Res.*, *51*, 2188–2210, doi:10.1002/2014WR016371.Received.

Seuffert, G., P. Gross, A. C. Simmer, and E. F. Wood (2002), The Influence of Hydrologic Modeling on the Predicted Local Weather: Two-Way Coupling of a Mesoscale Weather Prediction Model and a Land Surface Hydrologic Model, *J. Hydrometeorol.*, *3*.

Shen, C., and M. S. Phanikumar (2010), A process-based, distributed hydrologic model based on a large-scale method for surface-subsurface coupling, *Adv. Water Resour.*, *33*(12), 1524–1541, doi:10.1016/j.advwatres.2010.09.002.

Shi, Y., K. J. Davis, F. Zhang, and C. J. Duffy (2014), Evaluation of the Parameter Sensitivities of a Coupled Land Surface Hydrologic Model at a Critical Zone Observatory, *J. Hydrometeorol.*, *15*(1), 279–299, doi:10.1175/JHM-D-12-0177.1.

Shrestha, P., M. Sulis, M. Masbou, S. Kollet, and C. Simmer (2014), A Scale-Consistent Terrestrial Systems Modeling Platform Based on COSMO, CLM, and ParFlow, *Mon. Weather Rev.*, *142*, doi:10.1175/MWR-D-14-00029.1.

Shrestha, P., M. Sulis, C. Simmer, and S. Kollet (2015), Impacts of grid resolution on surface energy fluxes simulated with an integrated surface-groundwater flow model, *Hydrol. Earth Syst. Sci*, *19*, 4317–4326, doi:10.5194/hess-19-4317-2015.

Simmer, C. et al. (2015), Monitoring and modeling the terrestrial system from pores to catchments: The transregional collaborative research center on patterns in the soil-vegetation-atmosphere system, *Bull. Am. Meteorol. Soc.*, *96*(10), 1765–1787, doi:10.1175/BAMS-D-13-00134.1.

Skamarock, W. C., and J. B. Klemp (2007), A Time-Split Nonhydrostatic AtmosphericModel forWeather Research and Forecasting Applications, , (001), 1–43.

Skamarock, W. C., J. B. Klemp, J. Dudhia, D. O. Gill, D. M. Barker, W. Wang, and J. G. Powers (2005), *A description of the advanced research WRF Version 2*.

Smith, S. G., SF Ashby RD Falgout SG, and A. F. B. T. (1995), The parallel performance of a groundwater flow code on the CRAY T3D. In Proceedings of the Seventh SIAM Conference on Parallel Processing for Scientific Computing, p. 131.

Smoot, J. L., Ralston, D. R. (1987), Hydrogeology and a Mathematical Model of Groundwater Flow in the Pullman-Moscow Region, Washington and Idaho, Moscow, ID, Idaho.

Smoot, J. L., and D. R. Ralston (1987), Hydrogeology and a mathematical model of ground-water flow in the Pullman-Moscow region, Washington and Idaho.

Srivastava, V., W. Graham, R. Muñoz-Carpena, and R. M. Maxwell (2014), Insights on geologic and vegetative controls over hydrologic behavior of a large complex basin – Global Sensitivity Analysis of an integrated parallel hydrologic model, *J. Hydrol.*, *519*, 2238–2257, doi:10.1016/J.JHYDROL.2014.10.020.

Steefel, C., and S. SB Yabusaki (1996), OS3D/GIMRT software for modeling multicomponent-multidimensional reactive transport, Richland, WA.

Steefel, C. I. (2009), CrunchFlow Software for Modeling Multicomponent Reactive Flow and Transport User's Manual,

Steefel, C. I., and P. Van Cappellen (1990), A new kinetic approach to modeling water-rock interaction: The role of nucleation, precursors, and Ostwald ripening, *Geochim. Cosmochim. Acta*, *54*(10), 2657–2677, doi:10.1016/0016-7037(90)90003-4.

Steefel, C. I., and A. C. Lasaga (1994), A coupled model for transport of multiple chemical species and kinetic precipitation/dissolution reactions with application to reactive flow in single phase hydrothermal systems, *Am. J. Sci.*, *294*(5), 529–592, doi:10.2475/ajs.294.5.529.

Steefel, C. I. et al. (2015), Reactive transport codes for subsurface environmental simulation, *Comput. Geosci.*, *19*(3), 445–478, doi:10.1007/s10596-014-9443-x.

Steiner, A. L., J. S. Pal, F. Giorgi, R. E. Dickinson, and W. L. Chameides (2005), The coupling of the Common Land Model (CLM0) to a regional climate model (RegCM), *Theor. Appl. Climatol.*, *82*(3–4), 225–243, doi:10.1007/s00704-005-0132-5.

Steiner, A. L., J. S. Pal, S. A. Rauscher, J. L. Bell, N. S. Diffenbaugh, A. Boone, L. C. Sloan, and F. Giorgi (2009), Land surface coupling in regional climate simulations of the West African monsoon, *Clim. Dyn.*, *33*(6), 869–892, doi:10.1007/s00382-009-0543-6.

Stevens, P. R. (1960), Ground-Water Problems in the Vicinity of Moscow Latah County, Idaho, *Geol. Surv. water-supply Pap.*, *1460-H*.

Sudicky, E. A., J. P. Jones, Y. J. Park, A. E. Brookfield, and D. Colautti (2008), Simulating complex flow and transport dynamics in an integrated surface-subsurface modeling framework, *Geosci. J.*, *12*(2), 107–122, doi:10.1007/s12303-008-0013-x.

Sulis, M., S. B. Meyerhoff, C. Paniconi, R. M. Maxwell, M. Putti, and S. J. Kollet (2010), A comparison of two physics-based numerical models for simulating surface water-groundwater interactions, *Adv. Water Resour.*, *33*(4), 456–467, doi:10.1016/j.advwatres.2010.01.010.

Sulis, M., J. L. Williams, P. Shrestha, M. Diederich, C. Simmer, S. J. Kollet, and R. M. Maxwell (2017), Coupling Groundwater, Vegetation, and Atmospheric Processes: A Comparison of Two Integrated Models, *J. Hydrometeorol.*, *18*(5), 1489–1511, doi:10.1175/JHM-D-16-0159.1.

Teasdale, E.Eddy Teasdale, PG; Jim Zhang; and Liz Elliot, P., and E. (2010), Using General-Head Boundary Condition in Groundwater Flow Model, *Am. Geophys. Union, Fall Meet. 2010*.

Therrien, R and Sudicky, E. (1996), Three-dimensional analysis of variably-saturated flow and solute transport in discretely- fractured porous media, *J. Contam. Hydrol.*, *23*(95), 1–44, doi:10.1016/0169-7722(95)00088-7.

Thurlow, J., and E. Swanson (1987), Stratigraphy and structure of the Buchans Group, *Buchans Geol. ...*, *14*.

Tompson, A. F. B., R. Ababou, and L. W. Gelhar (1989), Implementation of the three-dimensional turning bands random field generator, *Water Resour. Res.*, *25*(10), 2227–2243, doi:10.1029/WR025i010p02227.

Tompson, A. F. B., S. F. Ashby, and R. D. Falgout (1994), Use of high performance computing to examine the effectiveness of aquifer remediation,

Tompson, A. F. B., R. D. Falgout, S. G. Smith, W. J. Bosl, and S. F. Ashby (1998), Analysis of subsurface contaminant migration and remediation using high performance computing, *Adv. Water Resour.*, *22*(3), 203–221, doi:10.1016/S0309-1708(98)00013-X.

Tompson, A. F. B., S. F. Carle, N. D. Rosenberg, and R. M. Maxwell (1999), Analysis of groundwater migration from artificial recharge in a large urban aquifer: A simulation perspective, *Water Resour. Res.*, *35*(10), 2981–2998, doi:10.1029/1999WR900175.

Vaccaro, J. J., S. C. Kahle, and D. S. Ely, D. M., Burns, E. R., Snyder, D. T., Haynes, J. V., Olsen, T. D., Welch, W. B., and Morgan (2015), Groundwater availability of the Columbia Plateau Regional Aquifer System, Washington, Oregon, and Idaho, Reston, Virginia.

Valcke, S. (2013), The OASIS3 coupler : a European climate modelling community software, *Geosci. Model Dev*, *6*, 373–388, doi:10.5194/gmd-6-373-2013.

Valcke, S., V. Balaji, P. Bentley, E. Guilyardi, B. Lawrence, and C. Pascoe (2009), Developing a Common Information Model for climate models and data, *Geophys. Res. Abstr.*, *11*, 10592.

Valcke, S., V. Balaji, A. Craig, C. Deluca, R. Dunlap, R. W. Ford, R. Jacob, J. Larson, and R. O. Kuinghttons (2012), Model Development Coupling technologies for Earth System Modelling, *Geosci. Model Dev.*, *5*, 1589–1596, doi:10.5194/gmd-5-1589-2012.

VanderKwaak, J. E. (1999), Numerical simulation of flow and chemical transport in integrated surface-subsurface hydrologic systems.

VanGenuchten, M. T. (1980), A Closed-form Equation for Predicting the Hydraulic Conductivity of Unsaturated Soils, *Soil Sci. Soc. Am. J.*, *44*, 892–898, doi:10.2136/sssaj1980.03615995004400050002x.

Visbal, M., and D. Knight (1982), Generation of orthogonal and nearly orthogonal coordinates with gridcontrol near boundaries, *AIAA J.*, *20*(3), 305–306, doi:10.2514/3.7915.

Vogel, B., H. Vogel, M. Bangert, K. Lundgren, R. Rinke, and T. Stanelle (2009), The comprehensive model system COSMO-ART – Radiative impact of aerosol on the state of the atmosphere on the regional scale, *Atmos. Chem. Phys.*, *9*, 8661–8680.

Volker, J. (1987), Multigrid Methods, , doi:10.1137/1.9781611971057.

Wagner, S., B. Fersch, F. Yuan, Z. Yu, and H. Kunstmann (2016), Fully coupled atmospheric-hydrological modeling at regional and long-term scales: Development, application, and analysis of WRF-HMS, *Water Resour. Res.*, *52*(4), 3187–3211, doi:10.1002/2015WR018185.

Weill, S., E. Mouche, and J. Patin (2009), A generalized Richards equation for surface/subsurface flow modelling, *J. Hydrol.*, *366*(1–4), 9–20, doi:10.1016/j.jhydrol.2008.12.007.

Weill, S., A. Mazzia, M. Putti, and C. Paniconi (2011), Coupling water flow and solute transport into a physically-based surface-subsurface hydrological model, *Adv. Water Resour.*, *34*(1), 128–136, doi:10.1016/j.advwatres.2010.10.001.

Williams, J. L., and R. M. Maxwell (2011), Propagating Subsurface Uncertainty to the Atmosphere Using Fully Coupled Stochastic Simulations, *J. Hydrometeorol.*, *12*(1994), 690–701, doi:10.1175/2011JHM1363.1.

Williams, J. L., R. M. Maxwell, and L. D. Monache (2013), Development and verification of a new wind speed forecasting system using an ensemble Kalman filter data assimilation technique in a fully coupled hydrologic and atmospheric model, *J. Adv. Model. Earth Syst.*, *5*(4), 785–800, doi:10.1002/jame.20051.

Wood, B. D. (2009), The role of scaling laws in upscaling, *Adv. Water Resour.*, *32*(5), 723–736, doi:10.1016/j.advwatres.2008.08.015.

Woodward, S. C. (1998), A Newton-Krylov-multigrid solver for variably saturated flow problems, Proceedings on the Twelfth International Conference on Computational Methods in Water Resources, in *Computational Mechanics Publications*, vol. 2, pp. 609–616.

Wozniak, K. (2007), Water use and recharge estimates in the Umatilla and Walla Walla drainage basins, Oregon.

Xanke, J., N. Goeppert, A. Sawarieh, T. Liesch, J. Kinger, W. Ali, H. Hötzl, K. Hadidi, and N. Goldscheider (2015), Impact of managed aquifer recharge on the chemical and isotopic composition of a karst aquifer, Wala reservoir, Jordan, *Hydrogeol. J.*, *23*(5), 1027–1040, doi:10.1007/s10040-015-1233-6.

Xu, L., Raman, S., and Madala, R. V. (1991), A review of non-hydrostatic numerical models for the atmosphere, *Math. Subj. Classif.*

Xue, M., K. K. Droegemeier, and V. Wong (2001), The Advanced Regional Prediction System (ARPS) - A multi-scale nonhydrostatic atmospheric simulation and prediction tool. Part II: Model dynamics and verification, *Meteorol. Atmos. Phys.*, *75*, 161–193, doi:10.1007/s007030170027.

Zhufeng Fang, Heye Bogena, Stefan Kollet, Julian Koch, H. V. (2015), Spatio-temporal validation of long-term 3D hydrological simulations of a forested catchment using empirical orthogonal functions and wavelet coherence analysis, *Hydrology*, *529*(1754–1767).

Zinn, B. A., and L. F. Konikow (2007), Potential effects of regional pumpage on groundwater age distribution, *Water Resour. Res.*, *43*(6), 1–17, doi:10.1029/2006WR004865.

APPENDIX

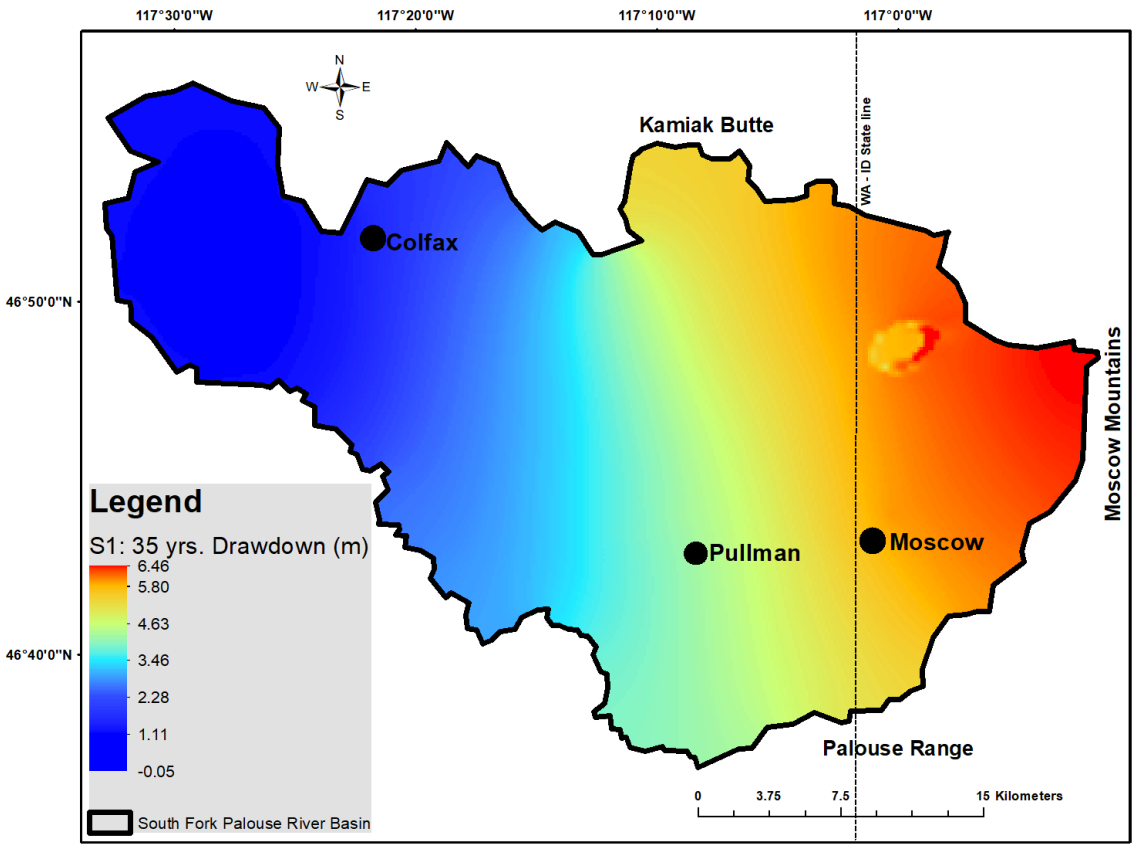

Fig. A1: Basin-wide aquifer drawdown after 35 years under 100 percent pumping scenario (**S1**). *Negative drawdown* or reversed drawdown means the aquifer level increased starting from or relative to the 2018 water levels.

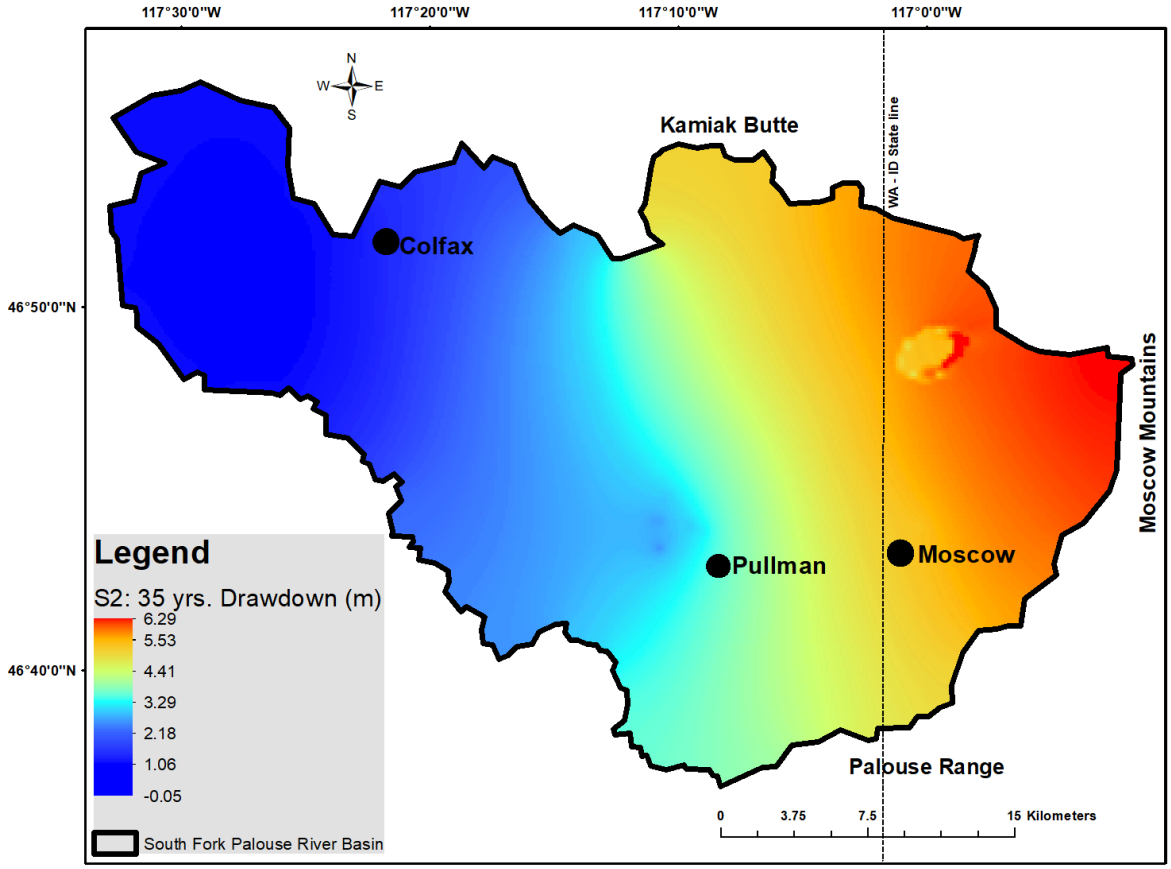

Fig. A2: Basin-wide aquifer drawdown after 35 years under 90 percent pumping scenario (**S2**). *Negative drawdown* or reversed drawdown means the aquifer level increased starting from or relative to the 2018 water levels.

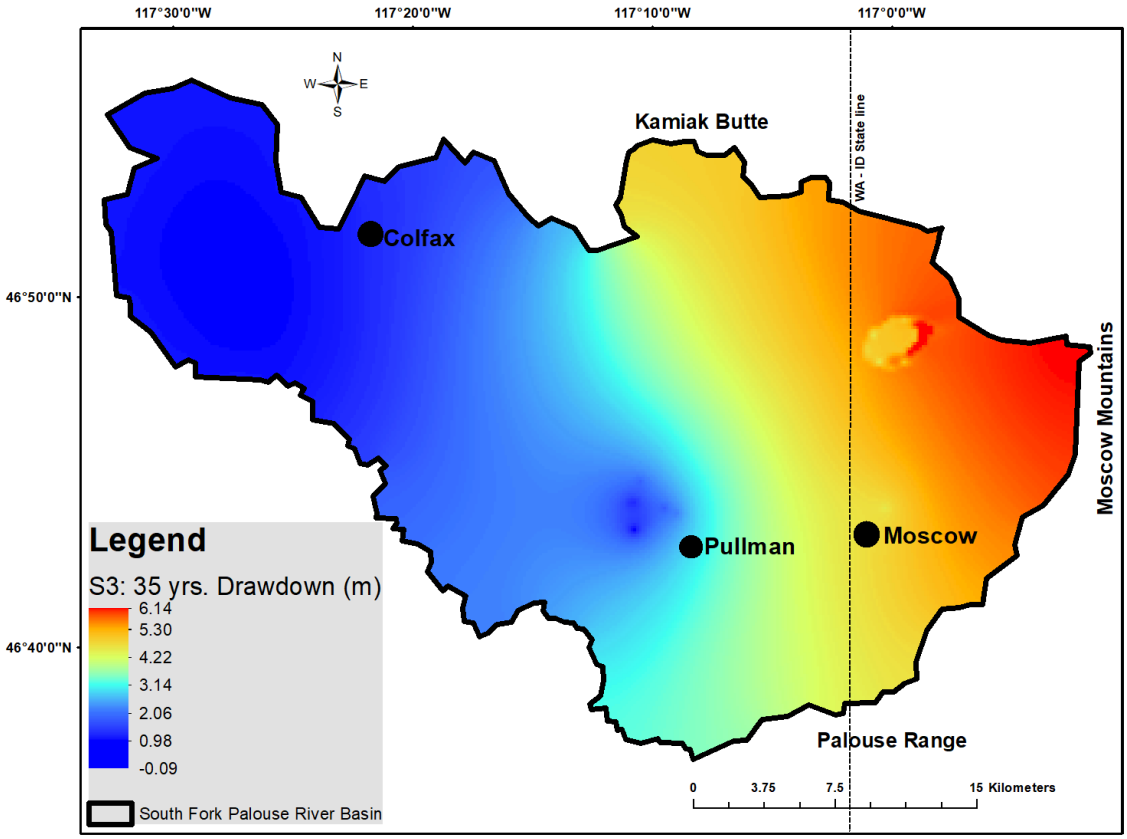

Fig. A3: Basin-wide aquifer drawdown after 35 years under 80 percent pumping scenario (**S3**). *Negative drawdown* or reversed drawdown means the aquifer level increased starting from or relative to the 2018 water levels.

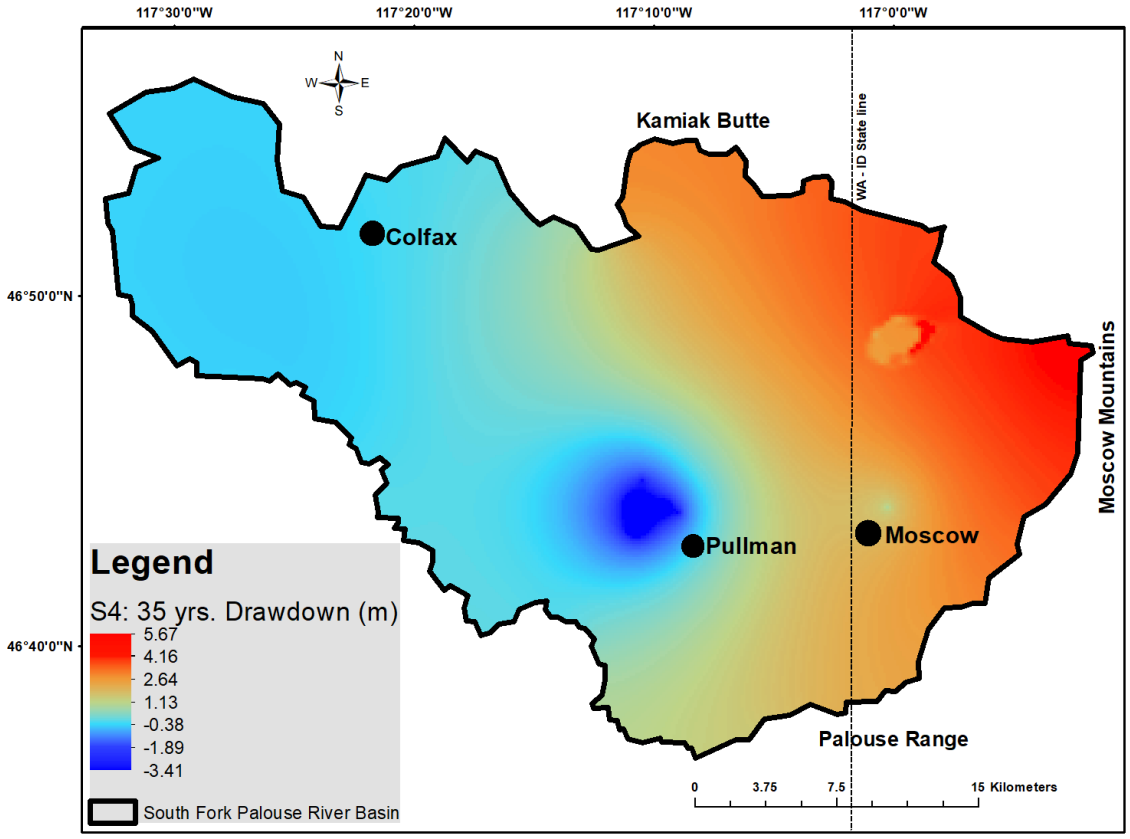

Fig. A4: Basin-wide aquifer drawdown after 35 years under 50 percent pumping scenario (**S4**). *Negative drawdown* or reversed drawdown means the aquifer level increased starting from or relative to the 2018 water levels.

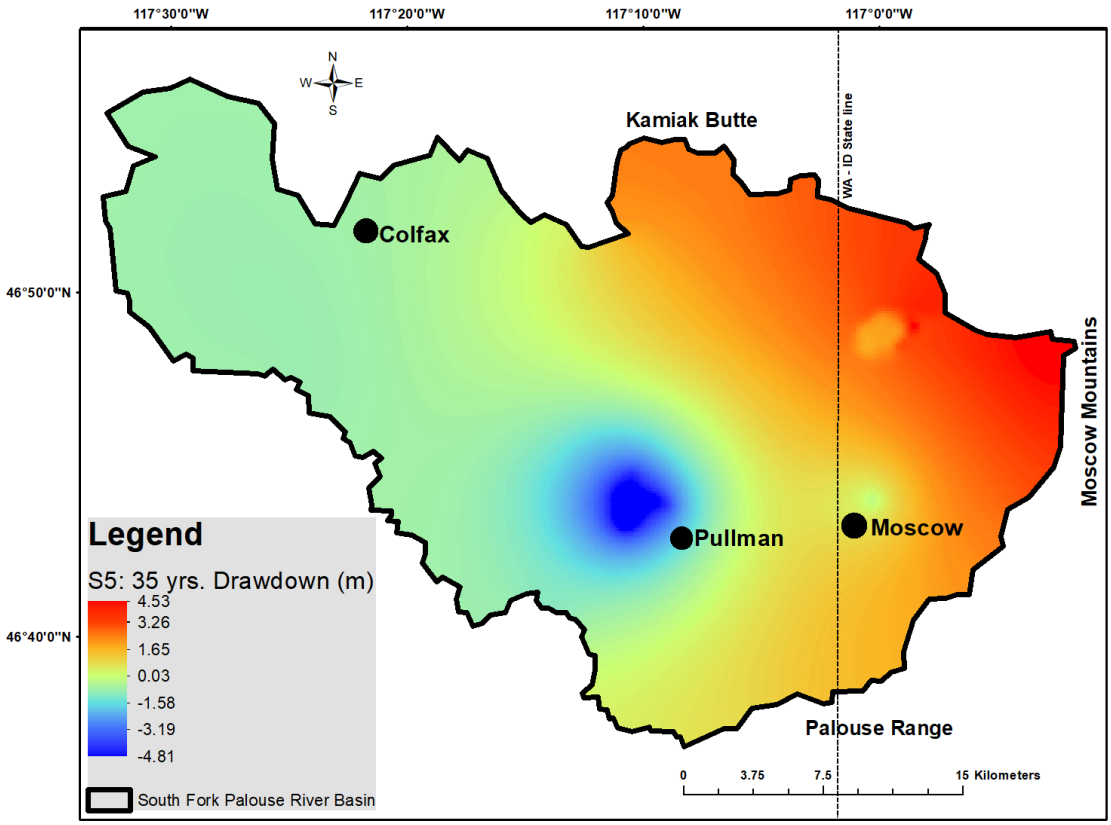

Fig. A5: Basin-wide aquifer drawdown after 35 years under 25 percent pumping scenario (**S5**). *Negative drawdown* or reversed drawdown means the aquifer level increased starting from or relative to the 2018 water levels.

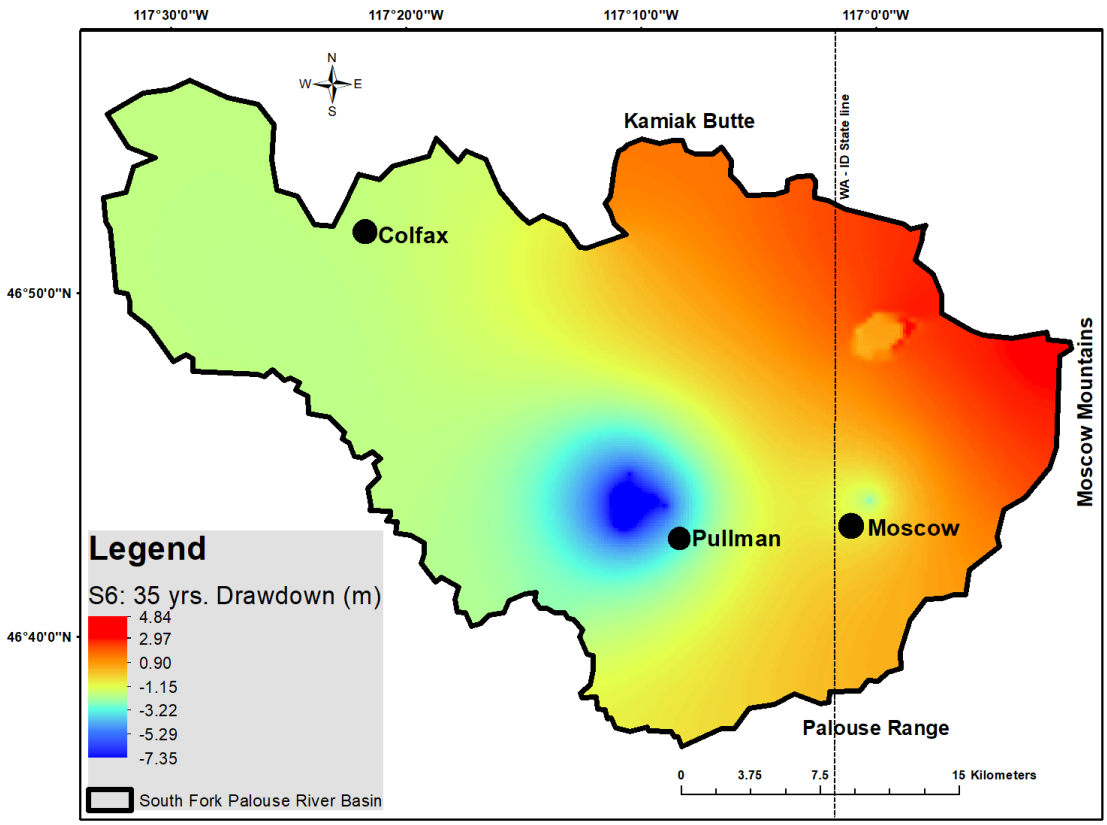

Fig. A6: Basin-wide aquifer drawdown after 35 years under 10 percent pumping scenario (**S6**). *Negative drawdown* or reversed drawdown means the aquifer level increased starting from or relative to the 2018 water levels.

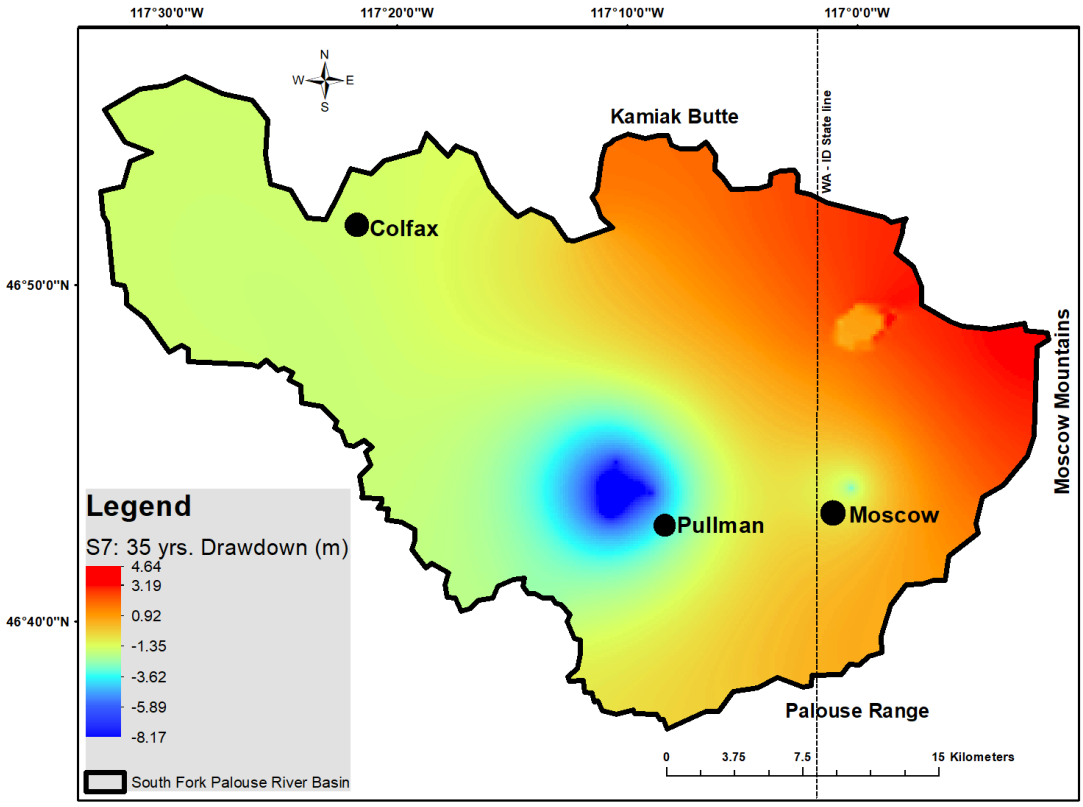

Fig. A7: Basin-wide aquifer drawdown after 35 years under 2 percent pumping scenario (**S7**). *Negative drawdown* or reversed drawdown means the aquifer level increased starting from or relative to the 2018 water levels.

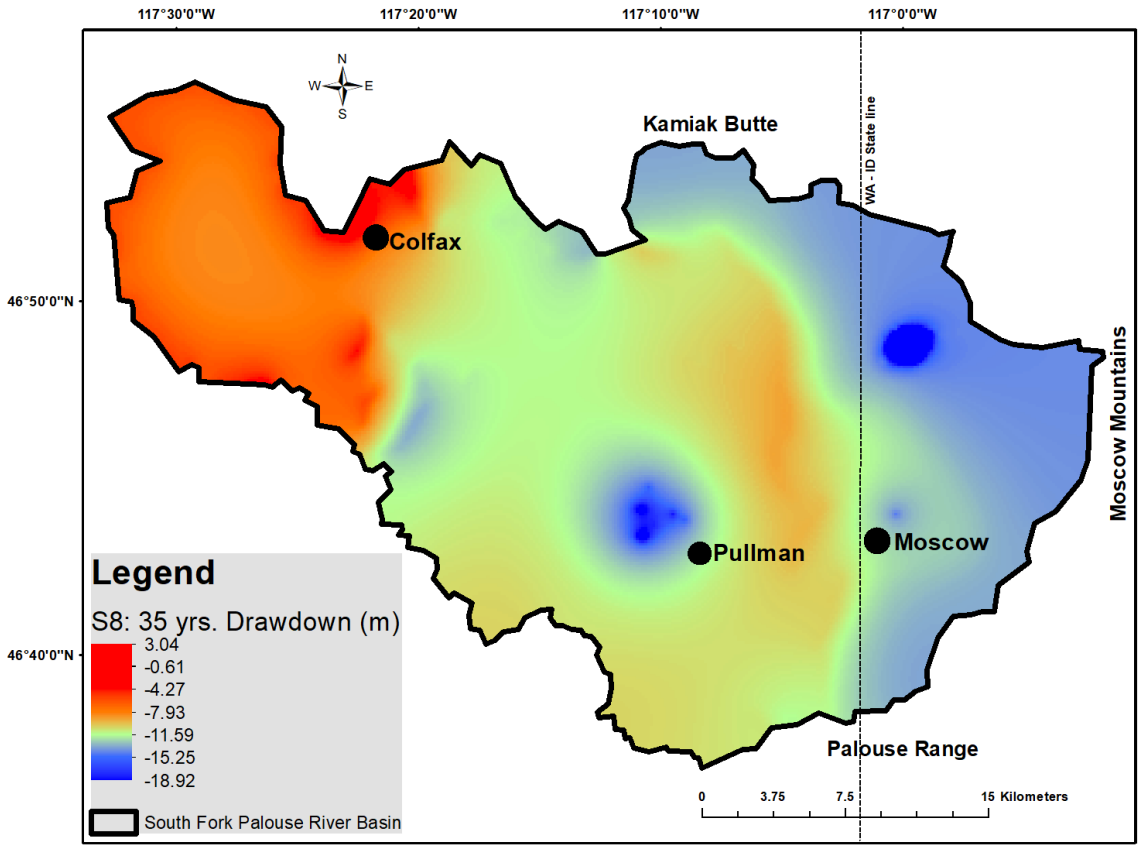

Fig. A8: Basin-wide aquifer drawdown after 35 years under zero pumping scenario (**S8**). *Negative drawdown* or reversed drawdown means the aquifer level increased starting from or relative to the 2018 water levels.